U.PORTO
FEUP FACULDADE DE ENGENHARIA
UNIVERSIDADE DO PORTO

U.PORTO
INSTITUTO DE CIÊNCIAS BIOMÉDICAS ABEL SALAZAR
UNIVERSIDADE DO PORTO

An advanced 3D in vitro model to study epithelial-fibroblastic cells crosstalk in breast tissue

Ricardo Jorge de Almeida Oliveira

Master Dissertation

Integrated Master in Bioengineering

Branch of Molecular Biotechnology

Supervisor:
Cristina Barrias (PhD)

Co-Supervisors:
Sílvia Bidarra (PhD)
Ruben Pereira (PhD)
Patrícia Barros Silva (MSc)

Porto, October 2020

Agradecimentos

Em primeiro lugar gostaria de agradecer à Cristina Barrias, não só pela prontidão com que me aceitou neste grupo, mas também por todo o seu otimismo e proatividade que me foi passando ao longo destes árduos meses. De facto, foram muitas a vezes em que sentia que o meu trabalho estava atrasado e à quem das espectativas mas rapidamente me sentia motivado após uma breve reunião consigo. Melhor chefe não poderia ter tido e por isso obrigado, daqui saio com um exemplo.

Em segundo lugar, quero agradecer à Patrícia Barros, por todo o incessante apoio prestado durante praticamente 1 ano. Foram muitas as lutas que travamos ao longo deste tempo, quer com a *printer,* as desinfeções dos *scaffolds,* às imagens do confocal. Ensinaste-me bastante e partilhamos muita coisa e por isso obrigado, daqui saio com uma amiga.

Queria também agradecer à Sílvia Bidarra por estar sempre disponível a ajudar e a debater todo o tipo de problemas que foram surgindo ao longo deste trabalho, sempre com paciência e tranquilidade. Nunca te mostraste hesitaste em apoiar-me em qualquer coisa que surgisse à última da hora e por isso obrigado. Queria também agradecer ao Rúben Pereira, a mais assídua companhia noturna do lab, por todo o seu insight valioso de *printing*.

Não podem faltar agradecimentos aos restantes elementos do nosso lab, como o Marco Araújo (por ter tido a gentileza de produzir e fornecer o famigerado alginato oxidado e modificado com PVGLIG), a Mariana Neves (por toda a pronta disponibilidade em ajudar com o quer que fosse), a Ana Luísa Torres (por todos os seus concelhos e sugestões). De resto queria agradecer à Marta, Natalya e Leonor por toda a companhia, e terem tornado o lab um ambiente sempre divertido.

Por fim, mas não em último queria agradecer à minha família. Sem vocês, isto seria impossível. Obrigado aos meus pais, por serem o meu apoio desde sempre. Obrigado, mana e Gui por me terem dado sanidade mental ao longo destes meses complicados, nas míticas noites na cozinha (Cobra kai!). E claro que não podia deixar de agradecer à Maria Ana por ter sido a minha companheira de guerra ao longo destes anos, falta pouco, mas já estou cheio de orgulho de nós. Um grande obrigado à tua mãe, que está aqui ao meu lado a formatar a minha tese, enquanto acabo isto. Gostava de vos dedicar muito mais tempo, mas falta uma horinha para entregar, penso que compreendem.

The research described in this thesis was financially supported by:

Project ANGIONICHE, refª POCI-01-0145-FEDER-028744 and PTDC/MED-ECT/28744/2017, financed by FEDER funds via COMPETE-POCI (PT2020) and Portuguese funds via Fundaçao para a Ciencia e Tecnologia (FCT).

Resumo

A mama é um tecido altamente heterogéneo e dinâmico, que sofre extensas alterações funcionais e estruturais ao longo da vida, principalmente em condições patológicas. É composto por células epiteliais da glândula mamária, envolvidas por um compartimento estromal altamente heterogéneo, com vários tipos de células, incluindo fibroblastos, e uma complexa rede de matriz extracelular (ECM). Interações célula-célula e célula-matriz são críticas para o desenvolvimento do tecido mamário, homeostasia e progressão de patologias, mas, devido, em grande parte, à falta de modelos *in vitro* adequados, ainda são pouco compreendidas. Nos últimos anos, tem-se verificado uma crescente procura por modelos 3D *in vitro* que preencham a lacuna entre modelos simplistas 2D *in vitro*, e os modelos complexos de animas *in vivo*, que têm vindo a beneficiar do progresso nos campos de biomateriais e engenharia de tecidos.

O objetivo deste trabalho incidiu no desenvolvimento um modelo híbrido 3D *in vitro*, combinando fibroblastos e sua ECM com células epiteliais, adequado para o estudo dos processos, tanto saudáveis e patológicos, do tecido mamário. O desenvolvimento desta plataforma foi baseado num trabalho anterior, onde scaffolds impressos em 3D, foram colonizados por fibroblastos e subsequentemente preenchidos com hidrogel de alginato carregado com células epiteliais. Embora este sistema tenha recriado com sucesso algumas características principais tanto do compartimento estromal como do parênquimal do tecido mamário, encontrava-se associado a algumas limitações em termos de design e propriedades dos scaffolds. Aqui, o objetivo focou-se concretamente na refinação do modelo através da: A) utilização de alginato purificado (em vez de alginato bruto), produção de scaffolds em forma de disco (em vez de um formato quadrangular) e produção de scaffolds liofilizados prontos para utilização; B) utilização de um hidrogel degradável por protéases para a cultura das células epiteliais, de forma a promover a invasão de fibroblastos e facilitar a interação direta célula-célula heterotípica; e C) descelularização de scaffolds, colonizados por fibroblastos.

Neste trabalho, começamos então por demonstrar a adaptação de scaffolds de alginato para um formato circular, de 11 mm de diâmetro, o que permitiu a próxima adaptação dos scaffolds em placas de 48 poços. Notavelmente, após o processo de purificação, o alginato demonstrou reter propriedades reológicas adequadas para a impressão 3D de scaffolds, que por sua vez, apresentaram uma definição e estabilidade mecânica. Numa segunda etapa, procuramos otimizar os parâmetros de deposição de fibroblastos sobre os scaffolds, através da comparação de diferentes designs de scaffolds, densidades de deposição de células e concentrações de péptidos promotores de adesão celular. Notavelmente, a densidade de deposição celular e tempos de cultura foram consideravelmente reduzidos, enquanto a capacidade de os fibroblastos aderirem, esticarem e produzirem ECM endógena, levando a uma coberta aceitável das fibras dos scaffolds, foi assegurada. Adicionalmente, em experiências preliminares, demonstramos que scaffolds de

alginato mantiveram a estrutura macroporosa, após liofilização, e de se readaptarem aos poços das placas de cultura, após rehidratação. Suplementarmente, após uma experiência complementar, o processo de liofilização não deu indícios de afetar a colonização dos scaffolds, indicando a possível futura produção de scaffolds prontos a usar. Numa terceira etapa, alginato oxidado e modificado com PVGLIG foi estudado para cultura de células epiteliais. Foi demonstrado que este hidrogel efetivamente promovia tanto a invasão de fibroblastos e a morfogénese epitelial, sem influenciar a viabilidade celular. Após o estabelecimento da co-cultura 3D, fibroblastos foram, de facto, capazes de invadir regiões centrais dos poros dos scaffolds, aumentando o número de interações heterotípicas diretas célula-célula com os esferóides epiteliais.

De forma a validar o modelo proposto neste trabalho, diversas experiências preliminares foram executadas. Em primeiro lugar, foi testada a discriminação de ambos os tipos celulares, após extração das células dos hidrogéis de alginato, através da marcação celular específica e citometria de fluxo. Um número considerável de fibroblastos foi efetivamente isolado, enquanto que um número altamente reduzido de células epiteliais foi isolado. Uma análise de PCR quantitativo em tempo real (qRT-PCR) demonstrou a expressão de genes correspondentes a actina de músculo liso α, colagénio tipo I e III. Adicionalmente, a solução extracelular, obtida após extração das células, foi passível de ser analisada através de uma análise proteómica, em que diversas proteínas relacionadas com a matriz foram detetadas e isoladas. Apesar destes resultados serem apenas preliminares, estes sugerem que este modelo 3D é poderá servir como uma valiosa plataforma para estudos futuros das interações heterotípicas célula-célula/matriz do tecido mamário, através de uma combinação de variadas abordagens complementares.

Adicionalmente, a rigidez dos constructos foi avaliada, através da microidentação da superfície. Como esperado, foram detetadas diferenças espaciais, com regiões moles e rígidas, que provavelmente correspondiam aos poros preenchidos com hidrogel e fibras impressas, respetivamente. Por fim, numa variação do modelo, scaffold populados com fibroblastos foram descelularizados, onde a remoção de resíduos celulares e manutenção da ECM, foram demonstrados. No futuro, tal variação pode ser utilizada como uma alternativa viável para o estudo isolado das interações entre a matriz derivada dos fibroblastos, e a células epiteliais da glândula mamária.

Em suma, todos os resultados obtidos ao longo desta tese representam melhorias fundamentais, rumo ao desenvolvimento de um modelo in vitro 3D, com versatilidade para o estudo das diferentes interações estroma-epitélio do tecido mamário, tanto em condições saudáveis como em patológicas, com uma clara relevância para medicina regenerativa como para a investigação da biologia tumoral.

Abstract

The breast is a highly heterogeneous and dynamic tissue, undergoing extensive functional and structural changes throughout life, especially under pathological conditions. It is composed by mammary gland epithelial cells, surrounded by a highly heterogenous stromal compartment, with several cell types, including fibroblasts, and a complex ECM network. Cell-cell and cell-matrix interactions are critical for breast tissue development, homeostasis, and disease progression, but are still poorly understood, largely due to the lack of adequate model systems. In the past few years, there has been a growing demand for 3D in vitro models that bridge the gap between too simplistic 2D *in vitro* 2D models and too complex *in vivo* animal models, which have benefited from progress in the fields of biomaterials and tissue engineering.

The goal of this work was to develop a hybrid 3D *in vitro* model of the breast tissue, combining fibroblasts and their ECM with epithelial cells, for the study of its healthy and pathological processes. The development of this platform was based on a previous work, where 3D printed scaffolds colonized with fibroblasts were filled with alginate hydrogel laden with epithelial cells. Although this system successfully recreated some key features of both stromal and parenchymal compartments of breast tissue, it presented some limitations in terms of scaffolds' design and properties. Here, specific aims were to refine the model by: A) using purified alginate (instead of raw alginate), producing disc-shaped scaffolds (instead of square-shaped), and producing ready-to-use lyophilized scaffolds; B) use a protease-degradable hydrogel for the epithelial cultures, to promote fibroblast invasion and facilitate heterotypic cell-cell communication; and C) test the ability to decellularize scaffolds.

Herein, we first demonstrated the successful design and fabrication of circular-shaped alginate scaffolds, with 11 mm-diameter, which tightly adapted to the wells of standard 48 multi-well plates. Notably, after purification, the alginate showed to retain adequate rheological properties as ink for microextrusion 3D printing of the scaffolds that, overall, presented good shape fidelity and structural stability. On a second stage, we optimized the fibroblast seeding process, by testing different scaffold designs, cell seeding densities, and cell-adhesive peptide concentrations. Notably, the cell seeding densities and culture times needed for effective fibroblast colonization were considerably reduced, as compared to the previous work, and cells were still able to spread and produce endogenous ECM, providing acceptable coverage of the scaffold fibers. Moreover, lyophilized alginate scaffolds were shown to maintain their macroporous structure upon rehydration and re-adapt to well-plates. Notable, the lyophilization process also did not seem to hamper cell colonization, showing promising results for future production of ready-to-use-scaffolds. On a third stage, a protease-sensitive hydrogel (oxidized PVGLIG-modified alginate) was tested as 3D matrix for the mono-culture of each cell type. This hydrogel was shown to effectively promote fibroblast spreading and formation of multi-cellular networks, while supporting epithelial

morphogenesis and formation of prototypical mammary acini-like structures, without decreasing cell viability.

To establish the hybrid 3D co-culture system, epithelial cell-laden oxi-PVGLIG- alginate hydrogel was added to the pores of printed scaffolds colonized with fibroblasts. Significantly, along culture, fibroblasts were able to invade and reach central regions of the pores, close to epithelial spheroids, establishing direct heterotypic fibroblast-epithelial cells contacts. To demonstrate the usefulness of the developed 3D hybrid system as a model to study cell-cell/matrix interactions, we isolated both the cells and the extracellular components after co-culture by dissolving the hydrogels and analysed them. Firstly, we attempted to discriminate both cell types by flow cytometry using cell type-specific markers. We were able to isolate a considerable number of fibroblasts, but extremely low numbers of epithelial cells. Quantitative real-time PCR analysis of isolated fibroblasts revealed the expression of α-smooth muscle actin, collagen type I and III genes. Moreover, proteomics analyses of the extracellular solution, obtained following cell extraction, allowed the detection and identification of several ECM-associated proteins. Although these are only preliminary results, they provide a proof-of concept of the relevance of such 3D co-culture system as a platform for the study of heterotypic cell-cell/matrix interactions in 3D, through combination of complementary technical approaches.

In addition, we have assessed the stiffnesses of the system through surface microindentation. As expected, there were spatial differences, with softer and stiffer regions, that probably corresponded to gel-filled pores and printed fibers, respectively. Finally, to analyse a possible variation of the model, scaffolds populated by fibroblasts were decellularized, with successful removal of cell remnants and maintenance of cell-derived ECM. In the future, this setting can be alternatively used for studying the isolated effect of fibroblast-derived ECM on epithelial cells.

Taken together, results from this thesis represent key improvements towards the development of a versatile 3D *in vitro* platform for studying the crosstalk between the stromal and parenchymal compartments of breast tissue, under physiological and pathological settings, with clear relevance both for regenerative medicine and cancer research.

Contents

List of figures

List of Tables

List of Acronyms

2D – two-dimensional

3D – three-dimensional

ADMSCs - reduction mammary fibroblasts

(Calcein) AM – (Calcein) acetoxymethyl

BF – bright field

BM – basement membrane

BME – basement membrane extracts

BSA – bovine serum albumin

CAD – computer-aided design

CAM – computer-assisted manufacturing

Ca^{2+} – calcium ion

$CaCl_2$ – calcium chloride

$CaCO_3$ – calcium carbonate

CAFs – cancer-associated fibroblasts

CLSM – confocal laser scanning microscopy

CO_2 – carbon dioxide

DCIS – ductal carcinoma in situ

dECM – decellularized extracellular matrix

DMEM – Dulbecco's Modified Eagle Medium

DMSO – dimethyl sulfoxide

DNA – deoxyribonucleic acid

DNAse – deoxyribonuclease

ECM – extracellular matrix

EDC – 1-ethyl-3-(3-dimethylaminopropyl)-carbodiimide

EDTA – 2,2',2",2"'-(ethane-1,2-diyldinitrilo) tetraacetic acid

EGF – epidermal growth factor

EHS - Engelbreth-Holm-Swarm

EMT – epithelial-to-mesenchymal transition

Ex/em – excitation/emission

FACS – flow-assisted cell sorting

FBS – fetal bovine serum

FC – flow cytometry

FN – fibronectin

GAGs – glycosaminoglycans

GDL – D-glucono-delta-lactone

H – hour(s)

hASCs – human adipose-derived stem cells

HBSS – Hank's balanced salt solution

hMFs – human mammary fibroblasts

HMVECs - human microvascular endothelial cells

HUVECs - human umbilical vein endothelial cells

lr-ECM - laminin-rich extracellular matrix

MES – 2-(N-morpholino) ethanesulfonic acid

Min – minute(s)

MMPs - matrix-metallopeptidases

Na^+ – sodium ion

NaCl – sodium chloride

NBFs – normal breast fibroblasts

NH_4OH – ammonium hydroxide

NHS – N-hydroxysuccinimide

ON – overnight

PBS – phosphate buffered saline

PDMS - Polydimethylsiloxane

PEG - Polyethylene glycol

Pen-Strep – penicillin-streptomycin

PFA – paraformaldehyde

pHEMA – polyhydroxyethylmethacrylate

PI – propidium iodide

PVA- Polyvinyl alcohol

PVGLIG - proline–valine–glycine–leucine–isoleucine–glycine

Rcf – relative centrifugal force

RMF - Reduction mammary fibroblasts

RGD – arginine-glycine-aspartic acid

RNA – ribonucleic acid

Rpm – rotations per minute

RT – room temperature

S – second(s)

SDS – sodium dodecyl sulfate

TDLU – terminal duct lobular unit

TGF-β – transforming growth factor beta

TME – tumor microenvironment

1. Introduction

Breast cancer is the most frequent malignancy amongst females, being estimated that more than 2 million women are diagnosed with this pathology every year. According to the World Health Organization, it is estimated that more than 600 thousand women died from breast cancer in 2018, highlighting this disease for the highest female mortality rate out of all neoplasms, which places breast cancer as the eighth main cause of female death worldwide [1], [2]. Incremental observations have shown that breast cancer comprises a myriad of subtypes, based on their distinct histopathological and biological features, that demand specific treatment approaches, accordingly to their treatment response [3]. However, due to the highly heterogeneous nature of tumour cells, the pathways that drive the initiation and progression of breast cancer are still poorly understood, and demand further research [4], [5].

In this regard, animal models have proved to be valuable platforms for the study of relevant oncologic events. However, such models present limited success for predicting translation to the clinical setting, due to significant biological differences that these pose towards humans [6]. Furthermore, *in vivo* studies are expensive and challenging to perform, since animal models are highly complex, hindering the inquiry for novel molecular and cellular interactions [7], [8]. In the face of these limitations, two-dimensional (2D) monolayer cultures on plastic have been largely employed to study normal and diseased breast tissue. These simplistic models are advantageous since they offer high control over the experimental variables, which facilitates interpretation of the obtained results [8]. Importantly, 2D cultures permit the simplified study of the different heterotypic interactions that take place in breast tissues, through the direct or indirect co-culture of different cell types, or even through conditioned media transfer. While in direct culture approaches cells are mixed together within the culture environment and thus, apt to establish direct contact, in the other methods cells are only allowed to interact through secreted soluble factors [9], [10]. Nonetheless, despite these simplistic models having demonstrated to be rather useful for over a century, they poorly resemble the structure and function of the mammary tissue and are thus unable to faithfully recapitulate key processes such as the epithelial-stromal crosstalk. This is chiefly caused by the lack of structural complexity, typical of a tissue-like microenvironment, that is central for cell-cell and cell-ECM interactions, which, in turn, define and maintain physiological cell phenotypes [11]–[13]. In order to increase the biological relevance of *in vitro* platforms, researchers have been extensively culturing cells in more advanced systems, namely embedded (3D culture) or “on-top” (2.5D culture) of ECM-mimicking matrices. The combination with ECM-mimicking matrices enables cells not only to self-assemble into complex structures but also, to interact with the matrix itself and sometimes even remodelling it. Cellular aggregation into complex structures may also be promoted using scaffold-free approaches, where

3D *in vitro* settings are established without resorting to supporting matrices [8]. The aforementioned cell culture formats present distinct pros and cons that should be considered accordingly to the specific biological question being addressed. For instance, hydrogel-embedded 3D cultures allow the study of mammary branching and morphogenesis, modelling the *in vivo* tissue organization more efficiently than 2.5D cultures. However, the latter format does not impose any physical barrier to cell activities and may enable easier cellular analysis and less challenging experimental techniques [14]. In turn, scaffold-free 3D cell aggregates, such as spheroids, closely mimic typical tumour features, such as high ECM density, chemical gradients from the periphery to the centre, central hypoxia and even necrosis. Hence, 3D scaffold-free cultures are quite fitting models for *in vitro* drug screening, although the large-scale growth of spheroids remains challenging and evokes the need for the standardization of spheroid generation by high-throughput systems [15]. Nevertheless, standard 2.5D/3D culture platforms often offer scarce control over the culture environment, failing to recreate the high-level of cellular organization found *in vivo*, and eventually leading to variability amongst experiments [8].

Through the past years, the fields of biomaterials and tissue engineering have been rapidly evolving, and thus, the engineering of human-representative 3D breast models is becoming a reality. Indeed, the employment of diverse bioengineering strategies such as 3D (bio)printing technologies and microfluidics, among others, have shown great promise in this regard [16]. 3D (bio)printing technology is increasingly popular, since it enables the patterning of materials and/or cells for the creation of complex 3D structures, with enhanced spatial and temporal control over cell organization. This bottom-up approach enables the assembly of tissue-like structures in a highly controlled manner, while being capable to provide adequate niches for different cell populations, further improving specific cellular activities and functional roles [17]. Interestingly, this technology has also been applied as an approach for enhancing spheroid reproducibility and therefore, contributing to the scale-up of spheroid generation, enabling high content drug screening and disease modelling in the near term [18]. On the other hand, microfluidic devices have also emerged as valuable platforms for the *in vitro* study of breast cancer. These systems may comprise several compartments and channels that range from millimetres to micrometres in size, and allow enhanced control over the cellular, physical and biochemical microenvironment. More specifically, the co-culture of cells within these devices can be performed in a spatially controlled manner, while experimental parameters, such as perfusion rate or signalling gradients, may be tightly regulated in order to closely match *in vivo* setting [17], [19]. This technology is also relevant in controlling formation of tumour spheroids and recapitulating the in vivo vascularized tumours, by permitting perfusion of cell cultures [15]. Overall, these bioengineering approaches show great promise to tackle several of the current challenges associated with the development of clinically relevant breast tissue models, suitable for large-scale mechanistic studies and drug development/screening. Nevertheless, these technologies are still in their infancy, requiring further refining.

In the following sections, the aforementioned subjects and models will be further delved, including a first brief contextualization of the healthy and tumoral features of breast tissue, as well as, the impact of the microenvironment in both settings.

1.1. Mammary epithelial-fibroblastic cells crosstalk in healthy vs. tumoral settings

The breast is a highly heterogeneous and dynamic tissue, composed of glandular structures surrounded by both fibrovascular and adipose tissue, which ensure nutrition, support, and protection [20]. In contrast to other tissues, the mammary structure and functions change throughout the different stages of the female reproductive cycle, due to the effects of several steroid and polypeptide hormones [8]. From birth until puberty, the mammary gland consists of a rather simple ductal network which opens on to the nipple.

Throughout puberty, these structures undergo continuous proliferation and branching, increasing in complexity and size. However, it is only during pregnancy and lactation, that the mammary gland presents fully developed milk-secreting lobules, located at the end of the ducts (**Figure 1A**). Each mammary lobule contains about twenty small glandular structures called acini, that encompass lumens open into the terminal ducts [21], [22].

Altogether these constitute the functional unit of the mammary gland, termed terminal duct lobular unit (TDLU). Histologically, the TDLU is composed of an inner layer of epithelial cells, which lines the lumen, and is connected to the basement membrane, produced by an enfolding outer layer of myoepithelial cells [20] (**Figure 1C**). The mammary epithelium cells are tightly connected to each other by means of apical cell junctions (adherens- and tight-junctions) that prevent solute paracellular trafficking [22]. Moreover, the basement membrane is composed of a variety of proteins, mainly laminin and collagen IV, as well as, proteoglycans and other minor components, such as fibronectin [23].

The interstitial extracellular matrix (ECM) of the stromal compartment is chiefly constituted by curved and randomly organized collagen I fibers, as well as, elastin, fibronectin, tenascin, several glycosaminoglycans (GAGs) [24].

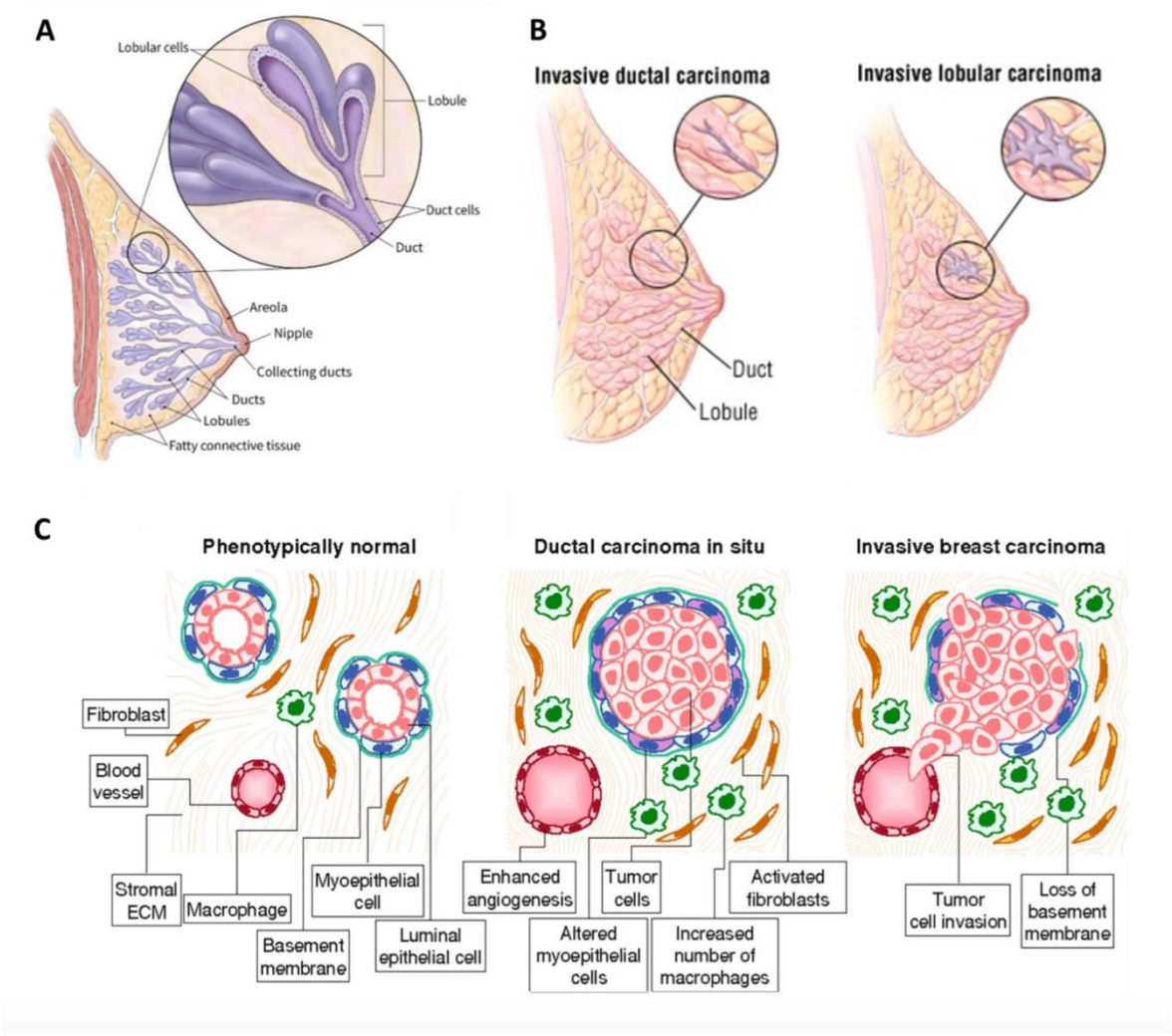

Figure 1. Structural features of breast tissue under both healthy and tumoral settings. Cross sectional view of the healthy breast tissue **A)**, and tumoral breast tissue **B). C)** Stromal and epithelial alterations occurring in breast tissue, ranging from a healthy phenotype to cancer development and progression. Adapted from [25][26][27].

The ECM plays a central role in providing mechanical protection and support to the tissues. For instance, its collagen and elastin backbone provides the tissues tensile strength, while the hydrophilic GAGs provide resistance to compressive forces. Due to their high hydrophilicity, the latter also play a key role in the hydration of the tissues, enabling the exchange of oxygen, nutrients, metabolic by-products, and others, between cells and microvessels. On the other hand, the ECM acts as a physical barrier that supports cell anchorage, migration, and chemotaxis [24]. Beyond support and protection, the ECM also provides key biochemical and mechanical signalling cues, capable of guiding breast epithelial morphogenesis, homeostasis, and disease progression [28], [29]. Cells interact specifically with ECM ligands through transmembrane receptors, which include integrins (collagen, laminin, and fibronectin receptors), dystroglycan (laminin-1 receptor), discoidin domain receptor 1 tyrosine kinase (collagen receptor), and syndecans (co-receptors for heparan sulfate proteoglycans and fibronectin, laminin and collagen) [23]. According to the composition, stiffness, and organization of the ECM, these interactions elicit specific signal

transduction pathways that have an influence on gene expression and cell phenotype. For example, the interaction between epithelial cells and the basement membrane promotes apical-basal cell polarization, with significant impact on glandular function. Moreover, the ECM also acts as a reservoir for several growth factors, cytokines, and chemokines, that are liberated under tight spatial and temporal control. Upon ECM remodulation, mainly through non-enzymatic and/or enzymatic processes (e.g. matrix-metallopeptidase (MMP)-dependent proteolysis) promoted by stromal cells, the bioactive molecules are released, establishing gradient concentrations throughout the tissue. These mechanisms of ECM remodelling are central for other processes, such as cell migration and invasion, since they enable cells to overcome the physical barrier imposed by the matrix network [24], [28].

Regarding the cellular component of the stromal compartment, the breast is mainly composed of fibroblasts, but also of adipocytes, immune cells (such as macrophages and lymphocytes), and endothelial cells, that establish interactions with the mammary gland, critical for its development and homeostasis. Although all mammary cell populations are able to synthesize and secrete ECM components, fibroblasts are essential for maintaining both the ECM and the overall homeostasis of the epithelial compartment [8], [29].

Over the past years, researchers have been unveiling evidence that suggests that tumour progression and therapeutic response are not only dependent on the characteristics of neoplastic cells, but also on their specific interplay with the surrounding environment, termed tumour microenvironment (TME) [30]. Indeed, after suffering genetic mutations, cancer cells undergo uncontrolled proliferation and activate aberrant signalling pathways that, in conjunction with the surrounding non-malignant cells and ECM, prompt the generation of a permissive environment for tumour progression, the TME [31]. Breast cancer may arise from several different tissues, such as fat, vascular, or epithelial. However, the most common type of malignancy is breast carcinoma, which arises from the TDLU, constituting more than 95% of all breast cancer cases (**Figure 1B**). Overall, breast carcinoma can be histologically categorized into two main classes, in situ (DCIS) and invasive carcinoma that, despite presenting distinct pathological features, may present similar symptoms (**Figure 1C**). In situ carcinomas result from non-invasive, but potentially malignant, intraductal proliferation of epithelial cells, which are confined to the ducts and lobules [32], [33]. As a consequence, cells tend to fill the TDLU lumen and form a cellular mass with an avascular, acidic and hypoxic core, which, in turn, prompts further mutations, tumour aggressiveness, and heterogeneity [16]. In contrast, invasive carcinomas are associated with the malignant proliferation of epithelial cells that have penetrated through the duct wall into the stroma [32]. Interestingly, through the analysis of the gene expression profile of both DCIS and invasive carcinoma tissues, researchers demonstrated that the latter exhibits an elevated expression of ECM proteases, in comparison to the former. Such suggests that the disruption of the basement membrane may be a key step for the transition from DCIS towards invasive carcinoma [34]. Moreover, as a consequence of the crosstalk between the epithelium and TME, considerable

changes in gene expression of tumour epithelial cells take place during tumour formation and progression.

In this context, cancer-associated fibroblasts (CAF) are of tremendous importance, since they account for up to 80% of the tumour mass, closely supporting tumour cells survival, proliferation, metastasis, as well as, resistance to anti-tumour therapy [35]. It is proposed that CAF stem from the reversible or irreversible activation of quiescent fibroblasts into myofibroblasts, due to the presence of several growth factors, cytokines, and microRNAs in the TME. As a result, these cells not only undergo extensive proliferation and migration but also acquire a highly contractile and secretory phenotype, triggering wound healing, and homeostatic responses. Further interactions with tumour cells, in conjunction with autocrine signalling, lead myofibroblasts to become hyperactivated, giving origin to highly heterogeneous populations, termed CAF. Alternatively, it is also thought that CAF may stem from other cellular sources, such as endothelial cells, via endothelial-to mesenchymal transition (EMT), mesenchymal cells, pericytes and/or adipocytes [31]. Indeed, this is coherent with studies demonstrating the existence of several different subsets within the CAF population, according to the tumour type, cellular origin, and location [36]. Due to its wide heterogeneity, the interactions between CAF and tumour cells have been regarded as highly complex, since they can both foster cancer promotion and retainment [37]. For instance, through TGF-ß/TGF-ßR or Wnt/ß-catenin signalling, CAF may prompt epithelial tumour cells to acquire a mesenchymal phenotype and motility, through EMT. Consequently, tumour cells lose epithelial hallmarks (e.g. cell polarization, cellular adhesions), and acquire mesenchymal features (e.g. N-cadherin, vimentin), including increased migration and invasion potential, as well as, chemoresistance [38], [39]. Thus, a better understanding of such complex events is of extreme relevance, as breast cancer mortality is chiefly associated with advanced, metastatic tumours [30]. Additionally, the epithelial-fibroblastic interactions may also occur through paracrine mechanisms, which not only promotes metabolic crosstalk, but also other processes related to cancer development, such as angiogenesis, inflammation and cancer immunity. Regarding the latter phenomenon, CAF may show both immunosuppressive and immunopromoting effects, though the secretion of diverse cytokines and chemokines that interact with immune cells [37]. Moreover, CAF are also implicated in the promotion of angiogenesis and tumour progression, facilitating tumour perfusion and invasion. Interestingly, CAF tend to scatter at the interface between blood vessels and tumour cells, increasing the interstitial fluid pressure of the tissue, which functions as a physical barrier to numerous therapies [31]. All in all, it is well recognized that CAF constitute key players within the intricate epithelial-stromal crosstalk, modulating tumour proliferation, perfusion, and invasion, as well as immune response and therapy resistance. On top of that, CAF are responsible for depositing and remodelling the ECM components present within the TME, which constitute fundamental processes for the development of a tumour-supporting environment [37].

The ECM present within the breast TME not only supports cancer cell transformation but also aids the creation of a microenvironment permissive for cancer progression [40]. This is due to the

fact that CAF exhibit an aberrantly increased deposition of ECM components such as collagen I, tenascin, and fibronectin, which are responsible for desmoplastic reactions throughout the TME, protecting the tumour from immune responses and chemotherapeutics [8], [31]. Oppositely to healthy breast tissue, the tumour collagen I fibrous network is composed of thick and linear fibers, organized in a parallel arrangement, which assist cancer cell invasion and migration [8]. In addition, the breast tumour tissue exhibits increased stiffness as a result of cross-linking mechanisms, catalysed by lysyl oxidase or transglutaminase, which are extensively secreted by both epithelial and stromal cells. The inherent increased stiffness associated with tumoral ECM not only leads to further promotion of tumour cell migration and invasion but also, hinders the infiltration of immune cells and drugs [8], [16], [40]. In contrast, hyperactivated fibroblasts also present altered proteinase secretion (e.g. MMPs, cathepsins), which highly remodel the surrounding ECM. Consequently, the ECM components that serve as physical barriers are degraded, allowing for the migration of tumour cells, as well as, other processes required for cancer development, as angiogenesis. Importantly, the enzymatic activity of certain secreted endopeptidases, such as MMP-3, induces the cleavage of transmembrane proteins, involved in the maintenance of cell adhesion complexes (E-cadherin), promoting EMT [31], [40].

Overall, all the aforementioned events and aberrant alterations highlight the importance of CAFs in supporting breast tumour development and progression, either through paracrine and juxtracrine signalling or through deposition and remodelling of ECM components. However, the underlying mechanisms of the epithelial-fibroblastic crosstalk remain poorly understood and call for an improved understanding of the complex interactions that take place within the TME. As such, the development of relevant breast *in vitro* models, capable of recapitulating the *in vivo* setting, while enabling the simple dissection of the different molecular and cellular interactions, are highly demanded.

1.2. In vitro models to study mammary epithelial-fibroblastic cells crosstalk

In vitro breast tissue models are not only essential for the study of the different biological mechanisms of both healthy and diseased tissues, but also constitute valuable tools for the fields of drug discovery, diagnostics, and regenerative medicine. As previously stated, these models enable a high control over the biochemical, mechanical and cellular experimental content, as well as, a simplified visualization of the biological processes, which would be otherwise challenging to achieve *in vivo*. Furthermore, in contrast to *in vivo* approaches, these models benefit from less time-consuming techniques, relative ease of use, the possibility of exclusive use of human cells, and a reduction of associated ethical concerns and costs [9], [19]. Throughout this section, available *in vitro* platforms will be discussed to a greater extent, beginning with 2D models,

followed by further delving on the transition to 3D models, and finally by discussing emerging bioengineering trends, which show great promise to increase the complexity of the current *in vitro* models.

2.1.1. 2D models

Conventional *in vitro* studies have largely employed carcinoma immortalized or primary cells as single monolayer cultures, in order to elucidate the role of different mechanisms on malignant progression [35], [41]. Despite the fact that these simple platforms are adequate for the straightforward assessment of cell response to different stimuli, they significantly lack important microenvironmental features, at both cellular and matrix levels [8]. The emergence of co-culture techniques, combining distinct cell types within the culture environment, enabled researchers to study the effects of heterotypic interactions taking place during cancer progression. Indeed, these co-culture systems largely contributed to the unveiling of several endocrine, autocrine, juxtracrine, and paracrine interactions between parenchymal and stromal cells, considered pivotal for multiple malignant processes, as metastasis, proliferation, and angiogenesis [41]. Direct and indirect co-culture systems, including the use of conditioned media, constitute the main strategies developed to study the role of fibroblasts on cancer cell behaviour and will be further explored in the following sections.

Direct contact 2D models

Direct co-culture entails culturing distinct cell types together within the same culture compartment, allowing direct cell-cell contacts to be established. Thus, such platforms not only allow for paracrine interactions to be established, but also of juxtracrine interactions that naturally occur between epithelial and fibroblastic cells [9]. Indeed, direct cell–cell contact has shown to be instrumental in tumour growth and progression through the effects of several adhesion molecules, such as N-cadherin and EMMPRIN [41]. For instance, such was demonstrated by Troester and colleagues, who established both direct and indirect co-culture techniques of different cancer cell lines and fibroblasts, in order to assess the impact of their interactions on gene expression. This work revealed that gene expression significantly differed between the two culture systems, highlighting the biological relevance of cell-cell contact in the environment. Interestingly, the authors were also able to observe that each tumour subtype interacted in a specific way with fibroblasts, pointing out the heterogeneous nature of the epithelial-fibroblastic cells crosstalk [42]. Similarly, another study underlined the importance of direct cell-cell interaction effects on the promotion of CAF transformation in fibroblasts, suggesting that paracrine signalling between

epithelial cells and fibroblasts may also require juxtracrine interactions for this transition to occur [43].

Despite being highly relevant, establishing direct co-culture models to study the epithelial-fibroblastic crosstalk mechanisms is often technically challenging. For lysate-based cell type specific analysis (e.g. gene expression analysis), the different cell populations must be sorted prior to lysis, via fluorescence-activated cell sorting (FACS), for example. This may be difficult to implement, as it requires sufficient amounts of cells and stringent choice of cell-specific markers. For this reason, many studies often rely primarily on image-based techniques or nonspecific lysate-based analysis.

Indirect contact 2D models

Although they only allow to assess paracrine cellular interactions, involving bi-directional crosstalk via soluble factors, indirect co-culture models are easier to use, as the different cell types remain physically separated [9], [41]. For compartmentalization, transwell inserts or Boyden Chambers have been largely employed, since they allow culturing one cell type on the well bottom, whereas the other cell population is cultured on an insert with a porous membrane, suspended within the well. In addition to being well fitted for studying the isolated effect of paracrine interactions, this system is also suitable for scrutinizing the effects of chemical gradients created across the membrane, as well as, mechanisms of cell migration and invasion [19].

For example, cellular migration assays can be performed by seeding epithelial cells on the membrane and fibroblasts on the well bottom, and subsequently quantifying epithelial cell migration through the membrane pores, to assess the chemotactic role of the fibroblastic secretome and/or the epithelial invasion potential [19]. This assay has been employed to evaluate and compare the invasion potential of different cancer cell lines, both in the presence and absence of fibroblasts on the well bottom [42]. In another study, cancer cells have been cultured in the presence of fibroblast-conditioned media derived from different fibroblast subsets that were extracted from distinct zones of the tumour tissue [44]. Indeed, the use of conditioned media is quite alluring, due to the ease of assigning a soluble factor to its producing cell type, and of testing its role on a specific biological response.

Scratch-based assays can be performed as another method for studying the effects of paracrine interactions on epithelial cell migration. More specifically, this assay is carried out by inflicting a wound on an epithelial monolayer seeded on the well bottom, and subsequently observing cells migrating towards the originated void, while they interact with fibroblasts seeded on the membrane [19]. Hence, this approach not only enables the *in vitro* mimicking of wound healing responses but also the analysis of the impact of fibroblasts on the process. Similarly, this assay has also been carried out by several groups but resorting to fibroblast-conditioned media [42] or to a direct co-culture approach [44]. However, as already stated, indirect co-culture approaches do

not take into account direct and reciprocal epithelial-fibroblastic interactions, which hampers the faithful representation of the in vivo events [9].

Overall, *in vitro* 2D models have considerably aided the understanding of the complex heterotypic interactions that take place both in healthy and tumoral breast tissues, while demanding simple, standardized, and reproducible approaches. Still, as previously mentioned, these models widely lack physiological relevance, namely in terms of structural complexity and low-degree of stromal interactions, fundamental for recreating the mammary structure and functions [13]. For example, mammary fibroblasts grown on a culture dish as a 2D monolayer, tend to gain forced polarity, which consequently alters their interactions with breast epithelial cells, and may ultimately lead to erroneous assessment of cell behaviour [17]. Therefore, throughout the years, researchers have been striving to shift the *in vitro* paradigm towards the development of 3D models that more closely recapitulate both healthy and tumoral breast microenvironments.

2.1.2. 3D models

As both the development and homeostasis of the mammary tissue largely depend on sustainable crosstalk with the surrounding 3D microenvironment, namely the ECM, the faithful recreation of the epithelial functionality and structure is not attainable in 2D cultures. In fact, even upon the addition of other important cell types, like fibroblasts, 2D models remain largely deficient in relevant biological cues and devoid of a tissue-like 3D architecture and support. Thus, culturing epithelial breast cells in a 2D setting presents important limitations that hamper the effective maintenance of a functional differentiated phenotype [35].

Strikingly, in 1977, Emerman and Pitelka demonstrated that epithelial differentiation, featuring milk protein expression, could be maintained through the culture of mice-derived mammary epithelial cells on floating collagen membranes, in the presence of lactogenic hormones. Indeed, this 2.5D culture setting not only enabled the endogenous production and secretion of milk proteins, but also the formation of some acinar-like structures with endogenous BM, in contrast to other platforms such as glass, plastic or attached collagen substrates [45]–[47]. Subsequent studies have demonstrated that the expression of tissue-specific genes was intimately related to the secretion of BM components by cells, which is allowed to occur in floating collagen gels culture [48], [49]. In the following years, other studies revealed that confluent murine mammary epithelial cells were also able to rearrange into tissue-like structures when 'sandwiched' between two collagen layers [50]. In this setting, cells are cultured in a 3D environment, where they can interact in all directions with both neighbouring cells and ECM, as well as migrate through the 3D collagen matrix [19]. However, it has been suggested that due to the absence of BM components, as laminin-1, cells cultured on collagen often exhibit a reverse or lack of polarity. In this regard, the embedment of cells in reconstituted basement membranes such as Matrigel™, a solubilized laminin-rich ECM extracted from mouse sarcoma, has proven to be quite effective in supporting the formation of acinar-like structures with central lumen and correct polarization [51]–[53].

As incremental data unveiled the role of 3D in vitro models in supporting tissue-specific functions and morphology, researchers rapidly took advantage of these platforms to study different mechanisms underlying breast cancer processes. Indeed, 3D cultures have been shown capable of supporting different cancer hallmarks, such as cellular heterogeneity, morphology, growth, and migration, which are poorly represented in 2D models [19], [54]. For instance, when cells are grown as monolayers, and forced to adapt a flat shape, the morphological distinction between normal and cancer epithelial cells is highly hindered. In contrast, when cultured in Matrigel™ matrices, cancer cells form highly proliferative and disorganized structures, with altered polarization and no BM, which can be easily distinguished from structures derived from normal epithelial cells [53]. In fact, this culture method further enables the morphological discrimination of multiple cancer cell lines, which would otherwise form indistinguishable monolayers in 2D cultures [55]. Importantly, such tumoral structures may even comprise a high-level degree of cellular heterogeneity, consistent with the solid tumours found in the physiological context [56]. As previously discussed, *in vivo* cancer cells undergo extensive proliferation which, subsequently, leads to the formation of a thick cellular mass. As a result, the transport of metabolites, oxygen, nutrients, and others to the core of the structure is severely limited, prompting further mutational events, which, in turn, lead to an increase of the cellular heterogeneity [16]. Similarly, 3D cancer models are capable of mimicking these mass transport limitations, as opposed to monolayer cultures, where cells are equally exposed to nutrients, oxygen, chemicals, and physical factors. This is highly advantageous, as 3D in vitro platforms are proving to be much more relevant preclinical models for predicting drug efficacy and toxicity. As a matter of fact, 2D models often overestimate the efficacy of drugs, since in lifelike 3D settings they have to surpass several barriers like the ECM or complex cellular structures before reaching target cells. Thus, 3D models allow to predicting *in vivo* drug response much more accurately, allowing to better establish therapeutic total amounts and delivery profiles [56].

In addition, 3D platforms are also valuable tools for performing cell migration assays. In contrast to the 2D setting, these models are not limited to one single plane and more faithfully mimic the physical barriers found *in vivo*. Therefore, cells cultured in 3D exhibit distinct migration mechanisms that could provide far more relevant insights in the field of tumour biology [19]. Such advantages were shown in several studies, as the ones performed by Ewald and colleagues, that employed 3D collagen type I hydrogels to evaluate the invasiveness of different cancer cells present within primary breast tumours [57]. In addition, other groups also demonstrated that through the use of 3D in vitro models, it was possible to assess the influence of several ECM properties (as alignment and stiffness) in tumour breast cell migration and invasion processes [58], [59].

Finally, 3D cultures have also proved to be valuable tools for the study of the mechanisms underlying epithelial-fibroblastic cells crosstalk, that take place in both during normal and neoplastic development. Beebe and colleagues demonstrated that when human fibroblasts are

cultured in a 3D setting, they secrete an increased amount of signalling molecules and proteases, that further instigate the invasive behaviour in cancer cells. Such differential behaviour is in part associated with different polarization, as fibroblasts cultured in 2D only establish contact sites on one side, which then dictate focal adhesion clustering and cytoskeletal rea-arrangements. Hence, fibroblasts are propelled to adopt a forced and unnatural polarity, which has shown to affect intracellular signalling, and therefore, cell-cell signalling [50], [60].

To sum up, the transition from 2D to 3D models considerably enhanced the structural relevance of *in vitro* models, facilitating the study of the breast tissue in both healthy and tumoral settings. Throughout the years, researchers developed a myriad of scaffold-based and scaffold-free techniques, that enable the establishment of structures that resemble solid breast tumours and healthy/diseased breast tissue [17]. In the following sections, these approaches will be discussed to a greater extent, with concomitant description of different studies that reported the establishment of 3D co-cultures comprising both epithelial and fibroblastic breast cells.

Scaffold-free models

Amongst the 3D approaches developed with the purpose of studying tumour biology, scaffold-free breast models draw great attention due to the capability of efficiently mimicking the solid tumour cytoarchitecture, micromilieu, and pathophysiological responses. While scaffold-based approaches may be preferable for recapitulating breast architecture and function, as well as, developmental and malignant processes, scaffold-free approaches are typically employed for generating breast spheroid cultures that closely resemble solid tumour masses [15]. In these 3D systems, cells are prompted to self-assemble into a spheroidal organization, as a result of culture conditions that favour cell-cell contact over cell-substrate interactions [17]. Once spheroids have reached diameters over ca. 200 μm, chemical gradients are established, promoting the formation of a hypoxic core, that could lead to central necrotic events, as the diameter reaches lengths over 500 μm [15]. Thus, the cellular/ECM arrangement established within 3D spheroids enables the accurate modelling of both the inner non-proliferative and outer proliferative regions of solid tumours [17]. Therefore, the generated structures are highly similar to tumour masses found *in vivo*, closely recapitulating their characteristic structure, stiffness, gradients, cellular heterogeneity, and therapeutic responses [16]. In addition, these 3D cellular models are widely employed due to their relatively simple and reproducible generation, which have been improved through the continuous refinement of high-throughput handling and analysis techniques [15], [17]. Such models are quite fitting for large-scale drug testing, as spheroids can be studied independently inside multi-well plates, enabling the concomitant assessment of multiple drugs [17]. Importantly, epithelial/tumour breast spheroids can co-incorporate fibroblasts for the simulation of the TME, through a myriad of techniques; these include mixed spheroids, tumour spheroids co-cultured with fibroblast spheroids, tumour spheroids cultured on fibroblast

monolayers, tumour spheroids placed within fibroblast suspensions and vice-versa [15]. In these models, tumour-fibroblast interactions are established, and cells naturally secrete ECM components (as laminin, collagen, and fibronectin), mimicking the TME without resorting to exogenously added ECM components, frequently derived from other species [61]. However, it is important to have into account that not all tumour cell lines are capable of generating spheroid cultures due to the lack of E-cadherin expression of some specific lines, as MDA-MB-231 or SKBR3, for example [17]. Nonetheless, to circumvent such issues, the introduction of additives such as basement membrane extracts (BME), as cultrex® BME, into cell suspensions, or the co-culture with ECM-secreting stromal cells can prompt such cell lines to form tight and stable spheroids [62].

A plethora of experimental methods have been reported to establish spheroids in culture, such as agitation methods, hanging drop techniques, culture over non-adherent surfaces (e.g. liquid overlay technique), aqueous two-phase systems, and magnetic levitation [16], [63]. In agitation methods, cells are continuously agitated within a liquid-filled bioreactor chamber, hindering adherence to the container walls and bottom whereas, cellular aggregation is promoted [17]. Several bioreactors have been developed for this purpose, namely spinner flasks, gyratory rotators, and rotary cell culture systems [56]. Although this approach allows the easy generation of a large number of spheroids, the establishment of controlled co-culture conditions is challenging, hindering adaptation to subsequent high throughput platforms. In aqueous two-phase systems, cells are entrapped within an aqueous drop immersed in another less aqueous phase. This method is highly advantageous since it is easily adapted to robotic dispensing tools for spheroid formation in standard microwell plates, being suitable for high-throughput analysis [64]. By way of illustration, Tavana's group developed a liquid robotic handler to dispense dextran drops containing both fibroblasts and breast cancer cells into a polyethylene glycol phase contained within 384-microwell plates. The group was able to evaluate the sensitivity of heterospheroids to specific chemotherapeutic drugs and observed that, in fact, fibroblasts conferred therapeutic resistance to tumour cells [65]. As for hanging drop culture techniques, cell suspension drops are placed on culture plates and arranged in an upside-down orientation, that promotes gravity-mediated cell aggregation. This arrangement can be achieved by either flipping the drop-containing substrate or by resorting to novel extensions of this approach that employ special plates comprising an array of through-holes for high throughput spheroid generation [64]. For instance, Atkinson and colleagues, co-cultured breast cancer cells, and normal human dermal fibroblasts in Gravity PLUS™ 96 well plates, which allowed spheroid maturation after some days of culture. Interestingly, the authors observed that the inclusion of fibroblasts not only allowed spheroid formation but also, promoted it when cultured with MDA-MB-231 cells, which were growing diffusively in monocultures. Thereafter, the spheroids were transferred to Gravity TRAP™ assay plates, where several chemotherapeutic drugs were assessed for their potential of sensitizing mammary cancer cell lines to radiation, through the high throughput analysis of the corresponding spheroid area [66]. With regard to liquid overlay methods, spheroids are generated through culturing cells on

round-bottom surfaces that display non-adherent properties, due to prior coating techniques with hydrophilic polymers, such as agarose [16]. Knuechel and colleagues generated homotypic spheroids of diverse cancer cell lines, as well as, of normal skin/breast cancer-derived fibroblasts by culturing each cell type on an agarose-coated 96 well plate. Subsequently, the different breast cancer lines were co-cultured with both fibroblast populations by placing each pair of spheroids on different wells. Through this method the authors were able to circumvent the high variability associated with mixing single-cell suspensions, avoiding the formation of intratumoral fibroblast clusters that differ in number, shape, size, and location between spheroids. Moreover, this co-culture system allowed for the analysis of each cancer cell line invasiveness through both the assessment of their aggregation and potential to invade adjacent fibroblast spheroids. Indeed, through the analysis of these attributes, the authors were able to discern the most aggressive phenotype (SK-BR-3) from the least aggressive (MCF-7). Additionally, the group reported that although tumour spheroids were able to produce some ECM components, the production significantly increased upon co-culture with fibroblasts [67]. In turn, another group reported the establishment of breast tumour and fibroblast mixed spheroids within 96 well plates coated with poly-2-hydroxyethyl methacrylate (pHEMA). The group was able to observe that these co-culture conditions promoted tumour cell survival, as well as, differential cytokine secretion, showing that antibody-mediated targeting of these interactions could lead to a reduction of tumour cell survival [68]. On the other hand, commercial ultra-low attachment plates can be employed for the generation of heterotypic spheroid cultures, following a brief centrifugation process [62]. As for magnetic levitation methods, cells are bonded to magnetic nanoparticles capable of bringing cells together under the influence of an external magnetic field, leading to the generation of large-sized spheroids, in a time-effective manner [17]. Jagannathan demonstrated that heterotypic tumour-fibroblast spheroids could be generated resorting to this technique while achieving a high control over the tumour densities and composition. In less than 24 h, this group was able to produce spheroids in the range of mm^2, with a high concentration of fibroblasts in the periphery that produced an enfolding high-density fibrotic capsule, analogous to the *in vivo* setting. Such was correlated with drug penetration studies which revealed that drug penetration through the spheroids was lower when upon higher fibroblast densities [61].

Besides the aforementioned techniques, 3D bioprinting and microtechnologies, as micropatterning and microfluidics, are also being exploited for the standardization and enhancement of large-scale spheroid production, for subsequent adaptation to high-throughput screening experiments [15]. For example, Priwitaningrum developed a 3D co-culture spheroidal array, by co-seeding fibroblasts and breast cancer cells on PDMS-microstamped petri dishes, produced through a hot embossing process and Pluronic coating. In this setting, cells were briefly centrifuged following seeding, forming heterotypic spheroids within 48 h. Similar to the previously described works, this study demonstrated that fibroblasts present within heterospheroids significantly hindered nanoparticle penetration throughout the structures, highlighting the

therapeutic preponderance of fibroblasts [69]. These technologies, specifically 3D bioprinting, will, however, be explored to a greater extent throughout the following sections.

Scaffold-based models

Heterotypic scaffold-based breast models, where cells can be either entrapped or cultured on top of 3D substrates that closely mimic breast tissue properties, constitute an alternative strategy to recreate both the *in vivo*-like tumoral and healthy tissue features. In contrast to the previously described scaffold-free approaches, scaffold-based models enable a more faithful representation of both the TME composition and functions, since the latter promotes a proper ECM assembly in the extracellular space, essential for supporting adequate epithelial morphogenesis, in both settings. Indeed, scaffold-free models poorly recapitulate some malignant features, such as strong desmoplastic reactions, as a result of the poor interactions established with the ECM, which heavily influences tumour progression and chemoresistance [70]. Notably, when comparing normal fibroblasts and CAFs cultured in 3D matrices, it is possible to discern significant differences regarding the composition and arrangement of the secreted ECM proteins, cell growth, metabolic activity, and cell/ECM mechanical properties. In contrast, when cultured as spheroids, such properties are rather similar for both cell types, despite each presenting distinct phenotype, which may not be ideal for accurately representing the mammary tissue *in vitro* [71]. Additionally, cells present in spheroid models establish rather strong cell-cell interactions, resulting in a tight spheroid morphology that greatly hampers the diffusion of antitumoral drugs into its inner layers. Epithelial spheroids, in particular, are extremely rich in intercellular junctions, which tightly links cells to one another, and thus hinders the penetration of exogenous molecules. In contrast, when administered to scaffold-based models, such molecules present higher diffusion rates, since cells in this setting are found to possess a more loosely packed morphology, closer to the *in vivo* scenario, being thus, a more useful model to study the efficacy of drugs and molecular targets [70].

Presently, 3D models are established either by culturing cells “on-top” porous 3D scaffolds or by establishing hydrogel-embedded cultures. Nonetheless, it is important to take into account that the former may not represent a fully 3D culture, being instead considered a 2.5D culture setting, as the initial cell-matrix interactions will take place at the scaffold surface, similar to the events observed in 2D [72]. 3D artificial structures can derive from several bulk materials. However, polymers are the most widely used material due to their tunability at both chemical and structural levels, and compatibility with diverse fabrication methods [73]. In addition, hydrophilic polymers are able to establish 3D hydrogel networks, through means of interactions between different polymer chains, capable of swell in the presence of water [74]. These characteristic high-water content, permeability, and porosity of hydrogels are of paramount importance for cell culturing, by allowing the diffusion of oxygen, nutrients, metabolic by-products, and soluble factors,

throughout the water-filled regions surrounded by the 3D network, as well as, intercellular communication, supporting cell survival and function [75]. Furthermore, the substrates employed to model ECM can be modulated to match the desired stiffness, specific to that of native tissues [76]. Polymers are mainly categorized into natural polymers or synthetic polymers.

Synthetic polymers as polyethylene glycol (PEG) and polyvinyl alcohol (PVA), are materials that draw great interest due to their well-defined composition and easily tuneable mechanical, physical, and chemical properties. These synthetic hydrogels are intrinsically bioinert, since they lack cellular recognition domains and thus require the inclusion of bioactive moieties that are naturally present in native tissues. Nonetheless, the employment of bioinert materials may be quite beneficial since it allows for an enhanced control over cell behaviour, due to the selective coupling of specific bioactive molecules. To this end, synthetic materials are often chemically modified with peptide motifs that promote cell adhesion and colonization (e.g. RGD), and carefully designed degradable linkages or MMP-sensitive peptides to render the polymer susceptible to degradation. However, despite the development of synthetic polymers being experiencing an accelerated growth through the years, some materials still struggle with the lack of biocompatibility of their monomers and degradation by-products, hindering their application towards the preclinical and clinical setting [77], [78].

Natural polymers encompass several materials that can be obtained from a plethora of biological sources, and can be further classified into two distinct categories, namely protein-based and polysaccharide-based, with each presenting specific pros and cons. Protein-based hydrogels, such as collagen, gelatin, and fibrin, amongst others are widely used for 3D cell culture since they exhibit intrinsic biocompatible and biodegradable properties, where both the original material and degradation by-products are non-toxic [79]. Furthermore, protein-based natural hydrogels may display other inherent bioinstructive capabilities, naturally promoting cell adhesion and proliferation throughout the material without the need of prior peptide grafting into the polymer chains [78]. Moreover, as observed *in vivo*, cells are also able to naturally degrade these hydrogels, whilst secreting endogenous ECM, propelling the establishment of an accurate stromal compartment. Natural hydrogels may also derive from native tissues, such as basement membrane extracts or decellularized tissues that can contain several mixed proteins, GAGs, and soluble factors [80]. ECM-derived hydrogels have been extensively used for establishing 3D breast models throughout the years, being basement membrane-like gels the most commonly employed materials, which, as previously stated, consist in laminin-rich ECM (lrECM) gels extracted from Engelbreth–Holm–Swarm (EHS) mouse sarcoma. The most implemented lrECM gels are Matrigel™ and Cultrex®, both also rich in several other ECM components as collagen IV, sulfate proteoglycans, and diverse growth factors [81]. Therefore, despite this highly heterogeneous composition promoting a close recapitulation of the native ECM, its effects on cells are poorly controlled, and gradually fade away along culture time, since several molecules are lost [78]. Alternatively, the use of decellularized ECM (dECM) has been growing popular throughout the

years. To this end, cells must be efficiently removed from the tissue through the application of detergents and enzymes (e.g. DNAse), while ensuring that both its native ultrastructure and tissue-specific biochemical/biomechanical signals are well preserved. Importantly, the obtained dECM can be minced and further processed with collagenase and/or pepsin enzymes, for instance, giving origin to water-soluble, low-molecular weight, tissue-specific hydrogels. Nevertheless, such approach is still in its infancy, considering, not only that both decellularization and processing protocols require further refinement, but also, the inevitable viable organ donor shortage [78], [80]. Overall, despite protein- and ECM-derived hydrogels multiple advantages, their application may be hampered by characteristic weak mechanical properties, low control over remodelling, and batch-to-batch variability [77]. Additionally, the analysis of the cell secreted ECM components can become challenging, since discerning cell-derived ECM proteins from the proteins originally present in the hydrogel represents a difficult task.

In contrast, polysaccharide-based hydrogels are quite suitable for the analysis of endogenous ECM components, since they are devoid of proteins naturally present in the native tissues. Polysaccharides, such as chitosan, alginate, hyaluronic acid, and others, can be extracted from multiple biological sources, such as animals, plants, and algae. The properties of this class of polymers greatly depend on the substitution patterns on each monomer, which, in turn, form either branched or linear polymers through the establishment of glycosidic bonds. Polysaccharide hydrogels benefit from additional advantages, when compared to protein-based materials, such as lower immunogenicity and superior capability of swell in water. Still, some types of polysaccharides, such as alginate, do not contain cell-interactive domains and thus are not able to naturally promote cell adhesion and degradation. Nonetheless, polysaccharide polymers have plenty functional groups, as carboxyl groups, that facilitate chemical modifications with several bioactive moieties, such as peptide sequences, and enable tailoring these polymers accordingly to the desired application [78].

To form 3D hydrogel networks, polymers can undergo several crosslinking mechanisms that can be categorized into physical, chemical and enzymatic crosslinking [82]. Physical crosslinking is an attractive approach, since polymers can be crosslinked under mild conditions (neutral pH, physiological temperature, aqueous media) by means of non-covalent interactions (electrostatic, hydrophobic, hydrophilic interactions) between polymer chains [83] [84]. Most of these interactions are temperature-dependent or ion-dependent, which leads gels to a phenomenon entitled thermal gelation and ionic gelation, respectively [85]. In turn, some of the chemical crosslinking mechanisms promote the formation of 3D networks by means of condensation reactions, crosslinking by Schiff base formation [86] or photo-crosslinking [87]. Conversely, enzymatic crosslinking is based on the use of enzymes for promoting the reaction. Mammalian transglutaminase, for instance, is a calcium-dependent enzyme commonly employed for gel crosslinking, due to its ability to establish covalent bonds between the γ-carbonyl group of a glutamine residue and the ε-amino group of a lysine [88], [89]. These different mechanisms can

be employed as a way to enhance the hydrogel's structural and mechanical properties, as well as, to tune its degradation kinetics. However, each method has its drawbacks. Chemical crosslinking, usually makes use of toxic agents, as glutaraldehyde, for example, that may be hazardous for cells, although more cytocompatible crosslinkers, as genipin, can also be employed [90]. In turn, photocrosslinking demands the addition of photogenerators, that may be cytotoxic, and further exposure to a UV light source, which may compromise cell viability [91]. Ionic crosslinking can be inefficient when applied to relatively large constructs, and is characterized by less stable bonds [92]. Importantly, too high crosslinking degrees should be avoided, since that may subsequently interfere with the key and dynamic processes of endogenous ECM deposition/degradation [91]. Moreover, high degrees of crosslinking can also prejudice the water uptake and swelling of the constructs, essential to promote the diffusion of gases, nutrients, and metabolic by-products, as earlier stated [90], [93].

The brisk progression of materials' science over the last decades enabled researchers to develop increasingly intricate models that are highly valuable for the *in vitro* study of the mammary tissue. However, while other materials have been proposed, the vast majority of the epithelial-fibroblastic heterotypic breast models found in literature still include Matrigel as a substrate. Furthermore, due to the challenge of effectively isolating different cell populations for subsequent analysis, as well as, of assigning a soluble factor to its producing cell type, most of the described heterotypic cell models comprise simple cocultures of mammary epithelial cells with a single stromal cell type [81]. Some studies on the establishment of 3D co-cultures, comprising mammary epithelial cells and fibroblasts, with or without additional stromal cell types, may be found summarized in **Table 1**.

Table 1. Description of some heterotypic co-culture models for in vitro studies of fibroblast-epithelial and cell-ECM interactions.

3D Substrate	Cells	Setup	Purpose	Findings	Ref
Matrigel	MCF7 or MCF7S1 cancer cells and human mammary fibroblasts (HMF3s) or BJ cell lines	Cell aggregates cocultured between two Matrigel layers	Study the soluble factors produced by fibroblasts that promote invasion of tumour cells	Upon 3D co-culture, MCF7S1 cells demonstrated enhanced invasion properties, correlated with an enhanced expression of S100A4 protein and MMP-2, as well as, of a range of different cytokines, by fibroblasts.	[94]
	h-TERT-immortalized Reduction Mammary Fibroblasts (RMF) and Human Mammary Epithelial Cell line	Co-culture of fibroblasts and epithelial cells on top of solidified hydrogel	Development of a 3D heterotypic model for studying tumour-stroma crosstalk, while ensuring minimum handling for isolating cells for subsequent analysis	Cells establish spheroids with fibroblasts clustering in the interior, while epithelial cells cluster on the exterior, and form multi-cellular projections into the matrix; Manipulation of the fibroblasts may lead to altered epithelial cell invasiveness, easily quantified by changes in numbers and length of epithelial projections	[95]
Collagen type I	HMT-3522 or HMT-3522 T4-2 (mammary epithelial cells) and RMF or HMF (mammary fibroblasts)	Cells were embedded in collagen type I gels of different concentrations, leading to distinct stiffness degrees	Study the role of mammary stromal fibroblasts in regulating differentiation and proliferation of mammary epithelial cells	Fibroblasts are able to reverse the perturbations of epithelial morphogenesis caused by increased matrix stiffness, and induce acinar morphogenesis even in gels of high rigidity; In floating hydrogels, fibroblasts promote gel contraction capable of reversing the phenotype of malignant epithelial cells	[96]
Collagen type I or Collagen type I crosslinked with PEG-diNHS	MCF10A, MDA-MB-231 (mammary epithelial cells) and HFb (human fibroblasts, CCD-1065Sk)	Co-culture of GFR-Matrigel-coated epithelial spheroids and fibroblasts embedded in hydrogel	Study the effect of fibroblast signalling and/or of changes in matrix stiffness on tumour cell migration	Stiffened matrix leads to an activated phenotype for fibroblasts and to an increased invasive behaviour of MDA-MB-231 cells but not of MCF10A; Presence of fibroblasts in stiff substrates leads to a decrease of the epithelial invasive behaviour, while undergoing increased contractile activity, and decreased activation-associated protein expression	[97]
Collagen type I and/or Matrigel	MCF10A & RMF	Co-culture of fibroblasts and epithelial cells embedded in hydrogels seeded into 35 mm well inserts	Study the effect of ECM and fibroblast interactions on epithelial morphogenesis	When grown in Matrigel-collagen gels, epithelial cells established mainly lobular structures but also some ducts, in contrast to collagen-only gels, where mostly ducts developed; Fibroblasts cultured in Matrigel-collagen gels formed star-like cell clusters, in contrast to the homogenous distribution observed in collagen-only gels; The presence of fibroblasts propelled ductal network formation in Matrigel-collagen gels	[12]

Table 1. (Cont.)

3D Substrate	Cells	Setup	Purpose	Findings	Ref
Matrigel and collagen I	Primary mouse mammary epithelial cells and fibroblasts	Co-culture of epithelial organoids and fibrospheres embedded in hydrogel	Study the qualitative and quantitative effects of mammary fibroblasts on mammary epithelial branching morphogenesis	Observation of the directionality and radius of epithelial–stromal interactions	[98]
Porous Silk Fibroin Scaffold	NIH3T3 mouse fibroblasts, EMT6 mouse breast cancer cell lines	Cell suspensions seeded on top of porous silk fibroin scaffolds	Study the impact of epithelial-fibroblastic interactions on gene expression, and CAF generation; Cytotoxic drug testing	Downregulation of ß-catenin and increased expression of vimentin were observed in cancer epithelial cells upon coculture (EMT-related changes), together with a trend of increased CAF markers (α-SMA and CD44) in fibroblasts	[99]
Matrigel/collagen mixture contained in porous silk protein scaffolds	MCF10A, hMFs and hASCs (human adipose-derived cells)	Cells embedded in Matrigel-collagen gels seeded on top of preconditioned silk porous scaffolds	Establish a 3D triculture breast model suitable for the long-term study the mechanisms underlying both embryonic development and neoplastic transformation	The presence of stromal cells inhibited epithelial proliferation and induced the formation of polarized alveolar and ductal structures, with enhanced expression of casein α- and -ß mRNA	[100]
Methacrylated gelatin	CAFs and MCF-7 or MDA-MB-231	CAF cell suspension was seeded on top of the substrate and cultured for 3 days before seeding epithelial cell suspension on top of the substrate	Study the effect of CAF on breast cancer metastasis	CAFs propel EMT of epithelial cells, promoting an increase in N-cadherin expression, as well as, a decrease in E-cadherin expression	[101]
Alginate	MCF-7 and HDFs	Tumour cell aggregates were embedded in alginate hydrogel together with HDFs.	Develop model to study tumour-stroma crosstalk and drug resistance	Observation of epithelial cells phenotypic alterations typical of in vivo tumours (migration from capsules and proliferation) under the influence of fibroblasts, which produced increased levels of collagen; such changes were not seen in MCF-7 monocultures	[102]
Star-shaped poly (ethylene glycol)/maleimide-functionalised heparin hydrogel	HMVECs or HUVEC, CAFs or NBFs isolated from mammary tissue and MCF10A	Cell suspensions tri-cultures embedded in the hydrogel	Study the mechanisms of CAFs on microvascular-like network formation and epithelial spheroid morphology	CAF promoted the formation of dense endothelial networks, with a greater number of vessels, and branching points, as well as, a longer morphology, in comparison to cultures with NBF; the influence of CAFs on mammary epithelial cells could also be observed through changes in the morphology of the mammospheres	[103]

1.3. Alginate hydrogels

One of the most largely employed natural, non-animal derived hydrogel is alginate. Alginate is an anionic polysaccharide copolymer derived from brown algae, comprised by linear blocks of (1,4)-linked b-D-mannuronic acid (M) and a-L-guluronic acid (G) monomers, linked together in varying sequences and fractions. These blocks can be composed of either consecutive G monomers (-GGGGGG-), M monomers (-MMMMMM-), or of alternating M and G monomers (-GMGMGM-), in which all may vary in length and number, depending from their biological source (**Figure 2A**) [104]. Commonly, the G content for algal alginates ranges between 30% and 70% [72]. Alginate hydrogels have been drawing great interest for many biomedical applications, due to their biocompatibility, low toxicity, relatively low cost, and mild gelation by ionic crosslinking through the addition of divalent cations, such as Ca^{2+} [104]. Since alginate is extracted from natural sources, it is often associated with several impurities such as endotoxins, heavy metals, proteins, and others, which could lead to lower reproducibility rates amongst experiments, but also to possible activation of immune cells. Therefore, it is often desired that alginate is purified by several complementary techniques, so that high purity levels can be achieved, promoting alginate bioinertness [105].

Alginate presents a polyanionic character at neutral pH, due to acidic pKa values of its monomers, each comprising a carboxyl group. Alginate's polyanionic character in conjunction with conformational features of alginate polymer chains, leads to intramolecular electrostatic repulsions, forcing alginate chains to adopt random coil conformations, and to achieve high viscosity levels, even at low polymer concentrations. Alginate chain conformation strongly depends on the solution's ionic strength, and alginate aqueous solutions display non-Newtonian characteristics, with their viscosity decreasing with increasing strain rate (shear thinning behaviour[72], [106] [107]. Besides ionic strength, the viscosity of an alginate pre-gel solution may also depend on the temperature, polymer concentration and molecular weight [107].Rheological properties are quite relevant for 3D culture and 3D printing, since high viscosity may decrease cell viability during mixing and extrusion processes due to high shear stress, and it directly affects "printability" [108].

Alginate polymer chains can undergo ionic crosslinking events that lead to hydrogel formation. Such crosslinking events are directly related to the relative content of G monomers present in the alginate chains, as the structure of the G blocks allows for a high degree of coordination of these cations. Although alternating blocks may also contribute, to a lesser extent, to this process, G blocks of adjacent polymer chains are particularly amenable to ionic crosslinking via electrostatic interactions with multivalent cations. As a result, G blocks form interchain junctions, termed egg-box structures, leading to the gelation phenomenon (**Figure 2B**). Therefore, the stiffness of the generated hydrogel is highly dependent on the polymer molecular weight, concentration, monomer composition and distribution, as well as, of the stoichiometry between the glucuronic carboxylic groups and divalent cations [72], [107]. Several ionic crosslinkers, as calcium chloride ($CaCl_2$), have been extensively used to promote external (or diffusion) gelation, in which ions are

allowed to diffuse from an external source into the alginate solution. Although this approach demands relatively simple techniques, it also leads to extremely rapid and uncontrolled gelation, due to the high solubility of the crosslinking ions. In this regard, internal gelation methods, where divalent cations are released in a more controlled manner from an inert and insoluble source suspended within the alginate solution, may be preferable. For instance, calcium carbonate ($CaCO_3$) can be added to alginate solutions for releasing calcium ions in a pH-dependent manner, being insoluble at neutral pH. The co-incorporation of a slowly hydrolysing acid, such as glucono-δ-lactone (GDL) trigger a decrease of pH, and thus the release of Ca^{2+} ions, that become homogeneously dispersed throughout the alginate solution and free to establishing electrostatic interactions with alginate [72]. Therefore, internal gelation methods may lead to the formation of more homogeneously crosslinked alginate matrices, when compared to external gelation. Furthermore, this approach allows for the *in situ* gelation of alginate, which is suitable for their use as injectable biomaterials, capable of adapting to complex shapes, according to the desired application [109], [110]. Nevertheless, it is important to take into account that ionically crosslinked alginate hydrogels tend to lose both their mechanical and structural properties throughout culture/implantation time, due to the progressive release of crosslinking ions into the external milieu. If required, alginate hydrogels may be reticulated by chemical crosslinking mechanisms that allow for a more precise control over the mechanical and swelling properties of the hydrogels, and enhanced stability [111].

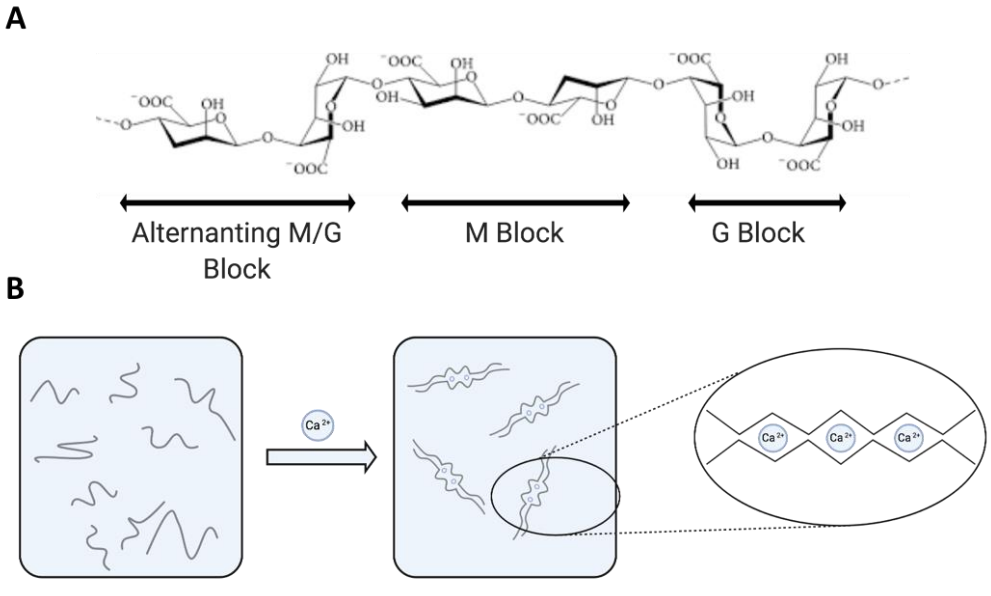

Figure 2. Schematic representation of the behaviour of alginate polymer chains. A) Alginate chains are characterized by the presence of alternating MG blocks, M blocks and G blocks (left to right). **B)** Alginate's external gelation process, from a viscous pre-gel solution to a crosslinked hydrogel with chains forming an "egg-box" structure.

As earlier stated, alginate displays a “bioinert” behaviour, not being capable of supporting cell mammalian attachment, due to the lack of specific receptors for these polymers. Furthermore, as alginate hydrogels display a highly hydrophilic nature, they are not able to adsorb bioactive serum proteins. To overcome this, it is necessary to functionalize alginate with ECM-derived peptide motifs, as the integrin-binding arginine—aspartic-acid—glycine (RGD) sequence, capable of supporting cell attachment, survival, and proliferation [112], [113]. To this end, researchers have been resorting to multiple chemical strategies, such as t carbodiimide-based reactions, in order to covalently graft this and other peptides of interest into the polymer backbone. In short, via a water-soluble EDC(1-ethyl-(dimethylaminopropyl) carbodiimide), amide bonds are established between peptide amine groups and alginate carboxyl groups. Multiple studies showed the positive effect of RGD modification of alginate hydrogels, not only on cell adhesion, but also on cell viability, proliferation and differentiation [110], [111], [114], [115].

Similarly, alginate is also inherently non-degradable in mammals, since mammalian cells lack the enzymes (alginase) capable of cleaving its polymer chains [104]. Strategies for fine tuning the degradation of alginate hydrogels include their modification with hydrolytically-degradable covalent bonds or with MMP-cleavable linkages [72]. Our group has reported the modification of alginates with a protease-labile double-end grafted crosslinking peptide that can be cleaved by matrix MMPs. The enzymatically cleavable substrate, a oligopeptide incorporating the MMP-sensitive hexapeptide proline–valine–glycine–leucine–isoleucine–glycine (PVGLIG), was double-end grafted into the polymer chains by carbodiimide chemistry [116], [117]. As a result, mesenchymal stem cells cultured within PVGLIG/RGD alginate matrices, were able to spread and establish multicellular networks, in contrast to RGD alginate matrices, in which cells remained essentially round and randomly dispersed. Such hydrogel formulation supports allow entrapped cells to overcome the physical barrier provided by the polymeric network, since cells become capable of enzymatically degrading the MMP-sensitive peptides that partially crosslink the alginate chains, either by contact-dependent proteolysis or by protease secretion. In the same study, cells showed upregulated secretion of MMP-2 in PVGLIG/RGD-alginate hydrogels, as compared to RGD-alginate hydrogels, suggesting that the presence of MMP-sensitive peptides modulates their proteolytic phenotype [117]. The oxidation of alginate has also been applied for increasing alginate hydrogels degradability, being the most common oxidation reagent sodium periodate ($NaIO_4$). This reaction results in the opening of the polysaccharide monomer rings between adjacent hydroxyl groups, that become susceptible to hydrolytic degradation, and originates two highly reactive aldehyde groups that can be harnessed for further functionalization. Importantly, there is a concomitant significant decrease in viscosity, and ionic gelation may be hindered when the polymer oxidation extension is above 10%, even though carboxylate groups remain conserved during the process [106]. Oxidized alginate has been applied to cell culture, and, for instance, these hydrogels have been shown capable of supporting hMSCs derived from bone marrow or adipose tissue viability and proliferation [115], [118].

Alginate presents several other important features as 3D matrices for cell culture, including transparent optical properties, suitable for easy microscopic evaluation, or the possibility of gently reverting its ionic crosslinks, through the dissolution with chelating agents, such as EDTA. This approach enables a fast release of cells entrapped in alginate hydrogels, under mild conditions, for further downstream processing such as flow cytometry, among many other techniques [72], [117].

1.4. 3D (bio)printing

Throughout the years, a plethora of biomaterial processing technologies have been developed with the aim of engineering clinically-relevant tissues, although most of them have demonstrated large limitations related with biocompatibility, control precision and controllability. In this regard, 3D (bio)printing technology is a revolutionary tissue engineering approach that has been rapidly emerging [119]. 3D (bio)printing is used to fabricate defined 3D geometric patterns through an automate and reproducible deposition of an ink with or without living cells, in a layer-by-layer fashion, with precise spatial control of the placement of the functional components [120], [121]. Computer-based 3D models of the constructs must be generated via graphic user interfaces, or created from clinical images, with techniques such as computed tomography, CAD-CAM techniques, MRI, and others. This technology can follow 3 different approaches such as i) biomimicry, where the histological organization of native tissues is reproduced, ii) autonomous self-assembly, in which cells are the major driver of histogenesis, and iii) the use of mini-tissues building blocks, where building blocks, such as spheroids, are assembled into a larger construct by means of a rational design and self-assembly mechanisms [121]–[123]. The most common printing approaches are based on continuous filament printing (microextrusion-based printing) and drop-on-demand printing, which includes inkjet-based and laser-based printing as the most employed strategies (**Figure 3**) [121], [124].

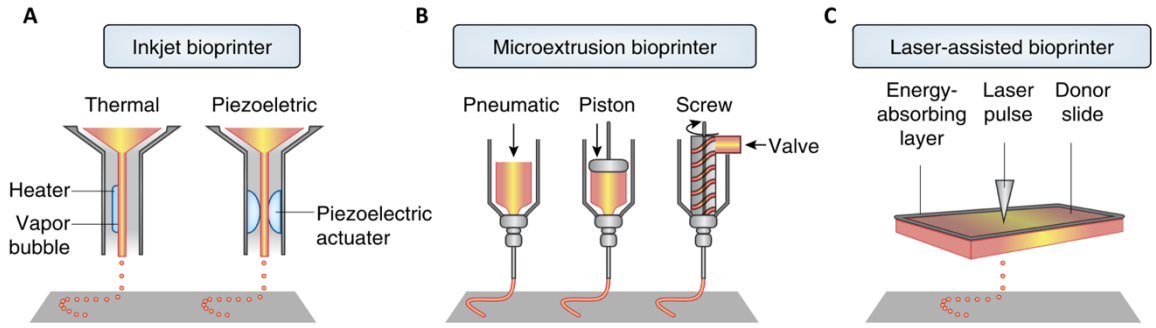

Figure 3. Main current 3D (bio)printing approaches. A) Inkjet printers generate droplets by means of thermal or piezoelectric forces, **B)** extrude continuous filaments by means of pneumatic or mechanical forces, and **C)** laser-assisted printers generate droplets by means of exposure to focused lasers. Adapted from [121].

Inkjet printers eject isolated droplets of bioink, by means of thermal or acoustic forces generated by actuator systems, (thermal and piezoelectric inkjet printers, respectively), forcing the bioink to be collected onto a substrate (**Figure 3A**). Depending on the type of actuation system used, there are different advantages/disadvantages associated with this technique. In general, despite being a low-cost, high resolution, fast printing technology, compatible with many types of materials and that preserves cell viability, it is challenging to achieve biologically relevant cell densities. Another downside of inkjet bioprinting consists in the need of using bioinks in a liquid form, with viscosities ranging from 3.5 to 12 mPa/s. For this reason, rapid post-printing polymerization procedures are required, which may alter the physical and chemical properties of the supportive matrices and affect cell viability [121]–[123].

Microextrusion printers extrude continuous filaments, of a wide range of materials, using pneumatic- or mechanical-based dispensing systems (**Figure 3B**). Although this technique may affect cell viability due, to the high shear stresses imposed on cells, it has the ability to deposit cells in high densities that, in conjunction to a good vertical printing ability, leads to the generation of constructs with relevant tissue dimensions, albeit with less resolution when compared to other printing methodologies. Importantly, the shear stresses can be decreased by resorting to lower extrusion pressures, as well as, by employing nozzles with lower gauge values (i.e. higher internal diameter). Moreover, this approach has shown to be quite effective for printing multicellular cell spheroids, which subsequently, fuse with each other giving origin to the desired 3D structure [121]–[123].

Laser-assisted printers typically consist of a pulsed laser beam, a focusing system, a 3 layered ribbon (composed by a support transparent to the laser radiation wavelength, usually made of glass, a thin absorbing layer, normally consisting of gold or titanium, and a transfer layer that contains cells and/or hydrogel, prepared in liquid solution) and a substrate that faces the ribbon (Figure 3**C**). Briefly, by exposing the absorbing layer to focused laser pulses, high-pressure bubbles are generated, which, subsequently, propel the formation of bioink droplet that are then collected and crosslinked on the substrate. This technique provides very high resolutions, allowing for single-cell depositions and is nozzle-free, thus evading problems such as nozzle clogging. Additionally, it can print a wide range of materials, with reasonable cell densities, while avoiding shear stress, which in turn results in high cell viabilities. However, this is a high-cost technique, where little is known about the effect of laser exposure to cells, there is a risk of deposition of metallic residues, and setting-up the system is challenging, especially when multiple materials and cells have to be co-deposited [121]–[123], [125].

The enhanced spatial control provided by 3D (bio)printing technologies, in conjunction with the inclusion of tissue-specific biochemical and biophysical features, allows researchers to generate more clinically-relevant breast models, highly valuable for cancer research [126]. Duan and colleagues fabricated 3D bioprinted breast models, containing primary cancer cells (21PT) and adipose-derived mesenchymal stem/stromal cells (ADMSCs), for studying cell response under the

treatment with doxorubicin (DOX). Shortly, researchers employed a methacrylated hyaluronic acid/gelatin composite hydrogel for encapsulating cells, and subsequently printed discs composed of 21PT laden bioinks, surrounded by ADMSC-laden bioinks (**Figure 4A**). Through this model, the group was able to study the influence of the thickness of the ADMSC compartment on DOX penetration and on the response breast cells to this drug [127]. In a similar study, breast cancer cells (MDA-MB-231), and fibroblasts (IMR-90), were embedded within an alginate/gelatin hydrogel, and printed following a specific rational design (**Figure 4B**). The resulting bioprinted constructs consisted of a central hub of MDA-MB-231 cells vicinal to cell-free hydrogel regions, which in turn were flanked by regions of an IMR-90-laden hydrogel. In this heterotypic breast model, breast cells were shown aggregate into spheroids, whilst fibroblasts migrate towards these cells [128].

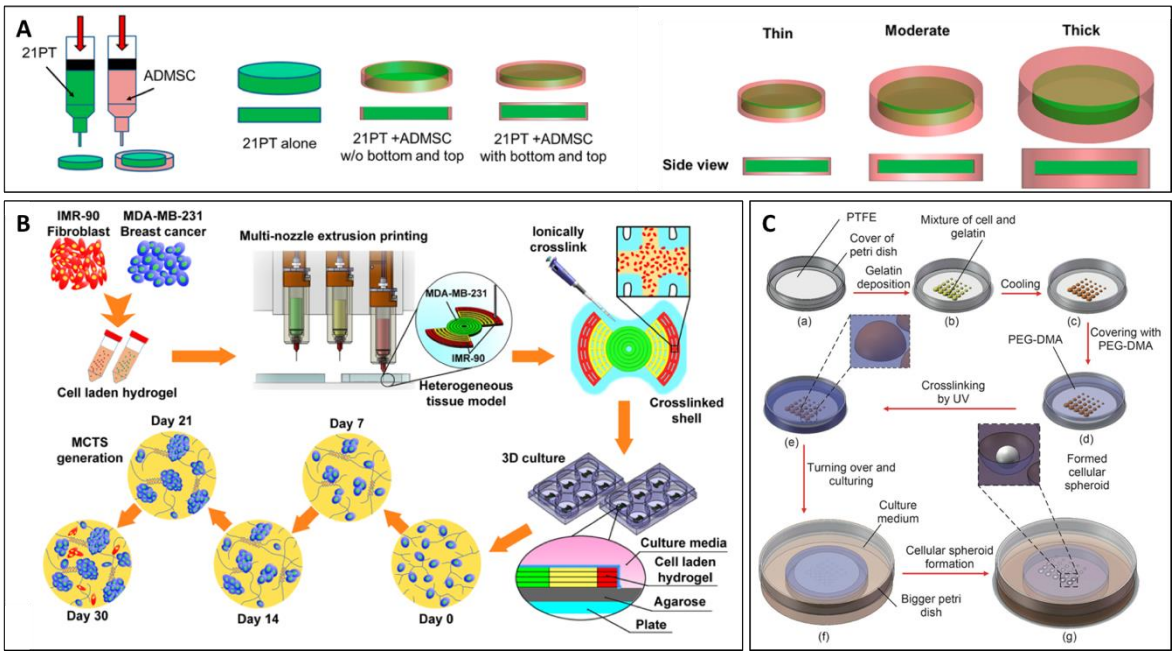

Figure 4. Schematic representation of some (bio)printing approaches for developing 3D breast tissue models. A) 3D bioprinted cancer model with 21PT-laden methacrylated hyaluronic acid/gelatin in the middle and ADMSC-laden hyaluronic acid/gelatin around. Through variations of the printing process distinct thicknesses of the ADSC were obtained. **B)** 3D bioprinting of a breast cancer model with IMR-90-laden (red), MDA-MB-231-laden (green), and cell-free (yellow) bioinks, following a complex design. **C)** Schematics of concave-well fabrication and in situ cell seeding for cellular spheroid formation. MCF-7-laden gelatin is printed in drop array disposition **(b)** and allowed to thermally crosslink **(c).** Subsequently, the printed array is covered by PEG-DMA UV-crosslinked polymer **(d, e).** Cell-laden gelatin array is then turned over and incubated at 37ºC, to allow gelatin to liquefy, and ultimately lead to the formation of multicellular spheroids. Adapted from [18], [127], [128].

As earlier stated, this technology has also been applied as an approach for enhancing spheroid reproducibility, thus leading to the scale-up of spheroid formation. For instance, Ling et al. demonstrated a facile bioprinting-based method for spheroid formation, using MCF-7 encapsulated within sacrificial gelatin arrays **(Figure 4C)**. In this study, homotypic breast cancer spheroids were generated in situ on PEG-diacrylate concave structures, eliminating the need for a manual cell seeding step, which may cause cell loss and non-uniform cell distribution. Thus, this approach enables spheroid generation in a controlled and high throughput manner, enabling high-content

drug screening and disease modelling [18]. Alternatively, another group was able to generate scaffold-free multicellular breast tissues, containing patient-derived cancer cells, fibroblasts, endothelial cells, and adipocytes, through bioprinting these cells within an alginate/gelatin-based hydrogel. Following 48h past printing, this hydrogel was removed, after treatment with alginate lyase and culture at 37ºC, establishing a breast model that recapitulates several neoplastic features, and that allows the study of different heterotypic interactions, as well as, their impact on cancer progression [129].

1.5. Motivation

A previous work from our lab [130] reported the development of a hybrid 3D *in vitro* model of breast tissue, combining fibroblasts and their ECM with epithelial cells. To build the model, porous scaffolds were produced by extrusion printing of square-shaped 3D scaffolds made of peptide-modified alginate, and then populated with human mammary fibroblasts. Seeded fibroblasts were able to adhere, spread and produce endogenous ECM, providing adequate coverage of the scaffold surface, without obstructing the pores. On a second stage, a peptide-modified alginate pre-gel laden with mammary gland epithelial cells was used to fill the scaffold's pores, forming a hydrogel in situ by ionic crosslinking. Throughout time, epithelial cells formed prototypical mammary acini-like structures, in close proximity with fibroblasts and their ECM.

Although this hybrid 3D system successfully recreated some key features of both stromal and parenchymal compartments of breast tissue, namely by promoting heterotypic cell-cell and cell-matrix crosstalk, it presented some limitations in terms of scaffolds' properties. In particular, scaffolds: **i) were produced with non-purified alginate, with less defined composition; ii) were square-shaped, and so did not fit adequately into the wells of standard tissue culture plates,** and **iii) had to be produced shortly before being used**. Additionally, the **hydrogel for epithelial culture was not permissive to fibroblasts proteolytic invasion, hindering direct stromal-epithelial cell-to-cell contact**. One possible variation of this 3D model would be to **decellularize the stromal compartment**, before adding the epithelial-laden hydrogel. This would allow isolating the effect of the ECM on epithelial cells from cell-cell interactions with fibroblasts.

To address those limitations and challenges, key goals of this thesis were to (Graphical Abstract):

A) Refine the design of the 3D printed scaffolds, by:

i. Using purified alginate instead of raw alginate
ii. Design disc-shaped samples fitting the wells of standard culture plates
iii. Produce lyophilized scaffolds, ready-to-use and with better cell retention

B) Improve the properties of the hydrogel for epithelial cultures, by using a protease-degradable hydrogel, to facilitate fibroblast invasion into the epithelial compartment and improve direct heterotypic cell-cell communication.

C) Test the ability to decellularize the printed 3D scaffolds with fibroblasts, with preservation of cell-derived ECM, for futures studies on epithelial cells-ECM interactions.

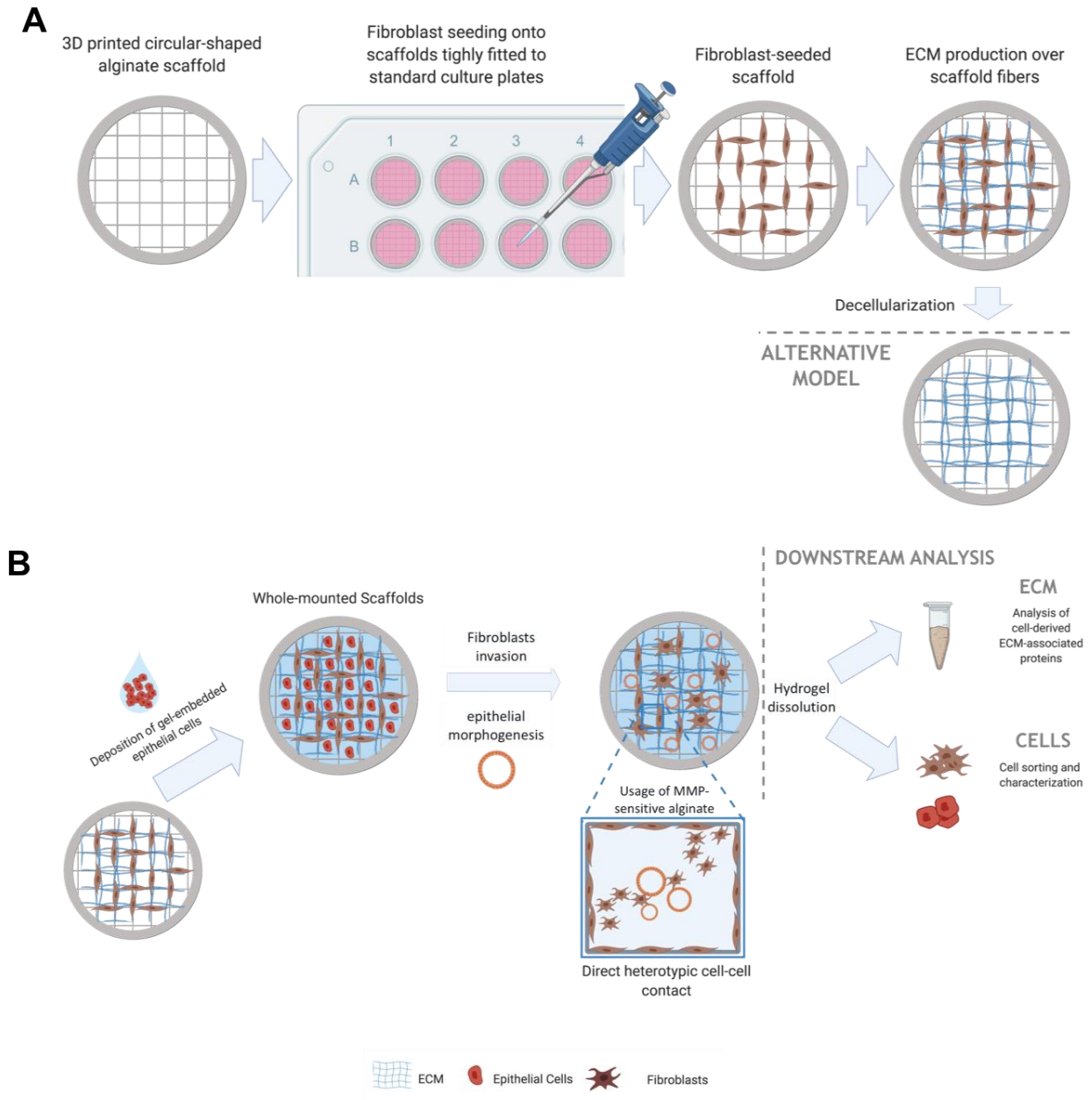

Graphical Abstract. Proposed multi-component 3D heterotypic model. **A)** 3D-printed circular alginate-scaffolds, tightly fitted to well plates, are seeded with mammary fibroblasts, which proliferate and produce ECM on top of the scaffold, creating a stromal compartment. Two strategies can be followed: direct addition of the gel precursor solution to the scaffold colonized with fibroblasts, or addition of the gel precursor solution to the scaffold, after decellularization. Epithelial cells will be in contact with fibroblasts-derived ECM, but not with fibroblasts. **B)** The pores of the scaffold are filled with a gel-precursor solution laden with epithelial cells, forming a hydrogel where epithelial cells will undergo morphogenesis. After co-culture cells may be extracted from the hydrogel and separated for isolated downstream analysis, while the obtained ECM solution also may be analysed.

2. Materials and Methods

2.1. Alginate

Pharmaceutical grade sodium alginate (LF 20/40, FMC Biopolymers) was used to produce the 3D printed scaffolds, while ultrapure sodium alginate (PRONOVA UP LVG, Novamatrix, FMC Biopolymers) was used for cell embedding. The two types of alginate presented similar guluronic acid contents (ca. 70%) and molecular weights (ca. 150 kDa). Prior to the printing process, pharmaceutical grade alginate was purified as previously described [117]. Briefly, a 1 wt.% alginate solution was prepared by dissolving alginate within distilled water, overnight (ON). Thereafter, 0.5g of activated charcoal were added per g of alginate, and the solution was stirred for 1 h. Next, the solution was vacuum-filtered with a 0.22 µm filter. The filtered solution was frozen at -20°C ON for subsequent lyophilization. After lyophilization, the purified alginate was stored at -20°C until used. Covalent grafting of the oligopeptidic RGD sequence [(Glycine)4-Arginine-Glycine-Aspartic-Acid-Serine-Proline; abbreviated G4-RGDSP; Peptide International, USA] to both alginate types was performed by aqueous carbodiimide chemistry as previously described [110], [117]. Briefly, MES (Sigma-Aldrich, St. Louis, MO) buffer solution was produced and its pH was adjusted to 6.5, using NaOH. Under stirring conditions, 1 g of alginate solution was added to 100 mL of MES buffer solution (1% w/v), and the solution was left stirring ON, protected from the light. Then, N-hydroxy-sulfosuccinimide (Sulfo-NHS, Pierce, 27.4 mg per g of alginate) and 1-ethyl-(dimethylaminopropyl)-carbodiimide (EDC, Sigma) were sequentially added at a molar ratio of 1:2, followed by 60 mg of RGD peptide (Genscript) per g of alginate. Following 20 h of stirring, the reaction was quenched by adding 18 mg of hydroxyl amine per 1 g of alginate. Finally, modified alginate was purified by dialysis, which was performed along the next 3 days, with decreasing NaCl concentrations. After dialysis was completed, the RGD-modified solution was, once again, purified with activated charcoal, vacuum-filtered with a 0.22 µm filter, and then frozen at -20°C ON, lyophilized and stored at -20°C until use. The amount of grafted peptide per gram of alginate was quantified using the BCA Protein Assay (Pierce) as previously described [117].

2.2. Alginate Extrusion-Based 3D Printing of RGD-Alginate Hydrogel Scaffolds

Purified pharmaceutical grade alginate (LF20-40) was mixed with a solution of sodium chloride (0.9 wt.% NaCl, VWR, Radnor, PA) at 4 wt.%, and left stirring ON at room temperature (RT, ≈ 20°C). For different experiments, different types of alginate were used (non-purified and purified) with different amounts of RGD (0, 400 µM or 600 µM). For printing, a sodium alginate gel-precursor solution was extruded into a 12.5 mM Calcium chloride (CaCl2, VWR, Radnor, PA), in 0.9% NaCl, crosslinking bath contained in a Petri dish (v = 50 mL), using a syringe pump (Programmable Aladdin

Syringe Pump (AL-1000), NewEra PumpSystems Inc., Farmingdale, NY; equipped with a 10 mL (12 mL) luer-lock SOFT-JECT syringe with 0.210 mm nozzle diameter, at an extrusion flow of 2 mL/h, and printing speed of 170 mm/min (**Figure 5**).

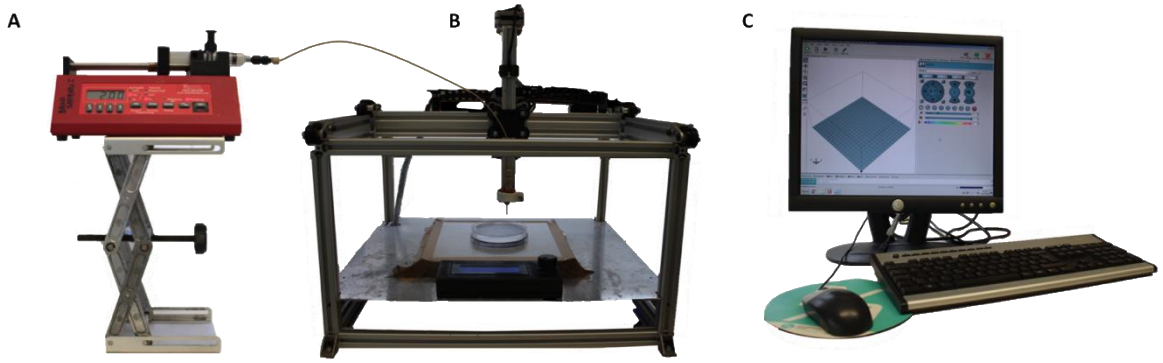

Figure 5. Schematics of the extrusion-based 3D printing system. A) Alginate formulation is extruded at a fixed rate through a syringe pump. It flows along the extrusor-to-printer circuit until it reaches **B**), where it is extruded through the nozzle into a crosslinker's solution placed on the deposition platform. **C)** Design of the structure is controlled by a dedicated software.

The printing code generated using NCPlot (NCPlot Software LLC, Muskegon, MI) was uploaded into Repetier Host software (Hot-World GmbH & Co. KG, Germany). The needle (internal diameter, Ø = 210 µm) was aligned and stabilized inside the CaCl2 solution and printing was initiated. After printing, the 3D-printed alginate scaffold was retrieved from the crosslinking bath. A second crosslinking step was necessary for all scaffolds, to improve mechanical stability and robustness before washes and seeding. For this, the scaffolds were soaked in a 20 mM CaCl2 solution for 5-10 min. Afterwards, scaffolds were thoroughly washed in distilled water to remove excess calcium and sterilized in decreasing concentrations of ethanol (96 and 80% v/v for 15min, and 70% v/v for 30min). Scaffolds were then washed with HBSS and transferred to a sterile low adherence 48-well plate, and washed twice with unsupplemented media, inside a laminar flow hood, to remove any traces of ethanol, and finally stored in supplemented fibroblast media, for 24h.

2.3. Scaffold Lyophilization and Rehydration

For some experiments, scaffolds were lyophilized after being subjected to two distinct treatments, following the printing process. On one hand, some scaffolds were sterilized as described above, washed twice in filtered (0.22 µm) distilled water, in order to remove any remaining salts, and then frozen at -20ºC for 2h. On the other hand, some scaffolds were merely washed twice with distilled water, after the printing process, and then frozen at 20ºC for 2h. After freezing, scaffolds were lyophilized ON. For rehydration, non-sterile lyophilized scaffolds were sterilized as described above, washed twice with unsupplemented media, and incubated ON with

supplemented media. Alternatively, sterile lyophilized scaffolds were directly rehydrated with cell suspension.

2.4. Scaffold Analysis

Analysis of printed scaffolds was performed with a stereomicroscope (SZX10, Olympus Life Science Solution). For detailed scaffold analysis, image processing software ImageJ® (National Institute of Health) was used [131].

2.5. Cell Sources and Maintenance

Human mammary fibroblasts from primary cultures (hMF, ScienCell Research Laboratories, Carlsbad, CA) were routinely cultured in fibroblast medium, supplemented with 2% of fetal bovine serum (FBS), 1% fibroblast growth supplement, and 1% penicillin/streptomycin (Pen/strep; Innoprot, Spain). Cells were maintained in culture and re-fed every two days with this media. Cells used for seeding scaffolds were from passages 5 to 11.

Human mammary gland epithelial cells (MCF10A, ATCC - American Type Culture Collection) were routinely cultured in epithelial cells media: Mammary Epithelial Cell Growth Medium supplemented with, 20 ng/mL epidermal growth factor (EGF), 0.01 mg/mL insulin, 500 ng/mL hydrocortisone, 4 μL/mL pituitary bovine enzyme (PromoCell), and 100 ng/mL cholera toxin (Sigma-Aldrich) 1% Pen-Strep. All growth factors were purchased from Sigma-Aldrich. MCF10A cells were maintained in culture from passage 5 until passage 16, and re-fed with supplemented media every two to three days.

2.6. Culture of hMF On-Top of 3D Printed Scaffolds

To establish the fibroblast culture on top of the printed scaffolds, cells were trypsinized from T75 culture flasks and counted. Afterwards, cells were centrifuged at 300 rcf for 5 min, and cell pellets resuspended in a specific volume, dependent on the cell seeding density. Cellularized scaffolds were then incubated at 37ºC, and additional media was added after 2 h. Media was changed every 1 or 2 days.

2.7. Metabolic Activity Assay

Metabolic activity quantification was assessed through the resazurin assay, in accordance with the manufacturer's protocol. Briefly, 3D constructs were incubated in 20% v/v resazurin (Sigma-Aldrich) solution in their respective media for 2h at 37ºC. Thereafter, 200 µL/well were transferred into a 96-well black plate with clear bottom and fluorescence was measured (Ex=530 nm, Em= 590 nm) in a Synergy MxTM (BioTek) reader. Results are expressed as relative fluorescence units (RFU).

2.8. Decellularization

Cellularized scaffolds were first rinsed with a hypotonic solution of deionized ultrapure water (18 MU, Milli-Q UltraPure Water System, Millipore, Burlington, MA) for 5min. After it was incubated with a detergent solution made of 0,5% Triton X-100 (Sigma-Aldrich, St. Louis, MO) with 1/740 ammonium hydroxide (NH_4OH, VWR, Radnor, PA) for 18min. After, scaffolds were thoroughly washed with HBSS, they were then kept in 25 U/mL DNAse I solution for 25min (ThermoFisher Scientific, Waltham, MA) and again rinsed with HBSS. Scaffolds were stored in HBSS until fixation or further processing/analysis. All steps of the decellularization protocols were performed in the orbital shaker, at 37°C and 80-100 rpm. All decellularization solutions were prepared in Hank's Balanced Salt Solution (HBSS, Gibco® Life Technologies, Carlsbad, CA).

2.9. Monoculture of hydrogel-embedded hMF and MCF10A cells

Hydrogel discs with hMF and MCF10A monocultures were prepared. Briefly, MCF10A cells were trypsinized, centrifuged (300 rcf, 5 min), counted and resuspended at an adequate density in media. Cells were then mixed with sterile-filtered (0.22 µm) RGD-/oxi-PVGLIG- modified ultrapure alginate (PRONOVA UP LVG, Novamatrix, FMC Biopolymers, Oslo, Norway) gel precursor solution at a final density of 2×10^6 and 5×10^6 cells/mL, for hMF and MCF10A, respectively. The PVGLIG-modified alginate used for this work (with an oxidation degree of 17%), was kindly modified and provided by a fellow researcher from our group. The cell-laden gel-precursor solution was then dispensed (20-30 µL drops) between Teflon plates with 500 µm-thick spacers. To promote in situ hydrogel formation, an internal gelation strategy was followed using calcium as ionic crosslinker, as previously described [98]. In brief, a sterile suspension of CaCO3 (FlukaTM Honeywell Research Chemicals, Munich, Germany) in 0.9 wt.% NaCl was mixed with the alginate solution at a Ca2+/-COO^- molar ratio of 0.288, and the gelling process was triggered through the addition of filtered (0.22 µm) fresh GDL in 0.9 wt.% NaCl at a CaCO3/GDL molar ratio of 0.125 [114]. The process was started with an RGD- and PVGLIG- modified alginate solution at 1.7 wt.%, reaching the final concentration of 1 wt.% alginate with 40 µM of RGD and 200 µM of PVGLIG after adding all the previously described components to the cell suspension. As controls, oxidized and non-oxidized RGD-only-modified hydrogel discs with hMF and MCF10A monocultures were also prepared. The Teflon plates were kept in a Petri dish, at 37°C in a 5% v/v CO_2 incubator. 20 to 30 minutes after triggering the gelling process (which started when adding the GDL component [104]), the discs were retrieved from Teflon plates with a spatula, placed in 24 multi-well plates, and covered by the respective media for each cell type. Media was refreshed after 30 minutes.

2.10. Live/dead Assay

To assess cell viability within the alginate monocultures, discs with cultured hMFs were subjected to the Live/Dead assay. Stock solutions of Propidium Iodide (PI, 1 mg/mL in ddH2O, Invitrogen, Carlsbad, CA) and Calcein AM (1 mg/mL in DMSO, Invitrogen, Carlsbad, CA) were prepared beforehand. Each disc was washed with HBSS and incubated in 500 µL HBSS, containing 2.5 µg/mL of Propidium Iodide and 2.0 µg/mL of Calcein AM stock solutions, at 37 °C for 20 minutes. Live cells were shown in green fluorescence by Calcein AM (ex/em ≈ 495 nm/≈ 515 nm), and dead cells stained red by aqua-fluorescent reactive dye PI (ex/em ≈ 540 nm/≈ 615 nm). Analysis was carried out by confocal laser scanning microscopy (CLSM, Leica TCS SP5, Wetzlar, Germany) immediately after incubation time. Live and dead cells were counted using Fiji.

2.11. Rheological measurements of hydrogel-embedded hMF and MCF10A monocultures

The rheological behaviour of the hydrogel discs was investigated using a Kinexus Pro Rheometer (Malvern, Pennsylvania, USA) at 37°C in a water-vapor saturated environment ensured by the rheometer chamber. Hydrogel discs were analysed at day 1 under standard culture conditions. After 24h of culture, samples were incubated with medium containing HEPES (N-(2-Hydroxyethyl) piperazine-N'-(2-ethanesulfonic acid) to buffer the media in air. Sample discs were cut using a 4 mm diameter biopsy punch and placed onto the bottom geometry plate (Ø = 8 mm). All samples were assayed using a plate-and-plate geometry (4 mm diameter, sandblasted surfaces) and were compressed to 20% of their original thickness to avoid slippage. Stress sweeps (0.1 Hz) were first performed to determine the linear viscoelastic region (LVR). Frequency sweeps (0.01–1 Hz) were then performed within the LVR. The values of the shear moduli (G' and G") and phase angle, were obtained at a frequency of 0.05 Hz. Samples were analysed in triplicate.

2.12. Culture of hydrogel-embedded MCF10A cells within 3D-printed alginate scaffolds

Hydrogel-embedded MCF10A epithelial cells were added to the 3D-printed alginate scaffolds with fibroblasts. For this, MCF10A cells were trypsinized, centrifuged (300 rcf, 5 min), counted and resuspended at an adequate density in media. Cells were then mixed with sterile-filtered (0.22 µm) RGD-/PVGLIG- modified ultrapure oxidized alginate (PRONOVA UP LVG, Novamatrix, FMC Biopolymers, Oslo, Norway) gel precursor solution at a final density of 5×10^6 cells/mL. To promote in situ hydrogel formation inside the scaffolds, an internal gelation strategy as described above. The process was started with an RGD- and PVGLIG- modified alginate solution at 1.7 wt.%, reaching the final concentration of 1 wt.% alginate with 40 µM of RGD and 200 µM of PVGLIG after adding all the previously described components to the cell suspension. As control, non-oxidized RGD-only-

modified MCF10A-laden precursor-solutions were also prepared. The gel-precursor solutions (80 µL) were then quickly applied on top of each fibroblast-seeded alginate scaffold. The whole-mounted scaffolds were then maintained in 48-well plates, at 37°C in a 5% v/v CO2 incubator. 20 to 30 minutes after triggering the gelling process (which started when adding the GDL component [104]), a mixed media (fibroblast medium/ Mammary Epithelial Cell Growth Medium, 70/30 ratio) was added to the scaffolds. Media was refreshed after 30 minutes.

2.13. Immunofluorescence analysis by confocal microscopy

Scaffolds were fixed at the endpoint of each experiment, and later used for CLSM. For fixation, scaffolds were first washed with HBSS and then fixed with 4% v/v paraformaldehyde (PFA, Sigma-Aldrich, St. Louis, MO) in HBSS, for 30 min at RT. After this, scaffolds were washed twice with HBSS and stored at 4°C until used. For CLSM analysis, different combinations of antibodies were used to perform immunofluorescent stainings on whole-mounted samples. Scaffolds were first incubated in 3 wt.% of bovine serum albumin (BSA, Merck KGaA, Darmstadt, Germany) in HBSS, for 45 min at RT, to minimize non-specific adsorption of antibodies. Prior to the latter step, whole mounted samples were incubated in 0.2% w/v Triton X-100 (in HBSS) for cell permeabilization (applicable to intracellular markers). After BSA blocking, immunostaining was carried out using the adequate antibodies for each specific analysis: to analyze cell morphology (actin cytoskeleton) samples were stained with flash phalloidin 488 (BioLegend, 1:100); to analyze ECM components, samples were incubated with the following primary antibodies (ON at 4ºC): anti-rabbit Fibronectin (Sigma-Aldrich, 1:150). To analyze acinar-like structure formation, samples were stained with the epithelial-cells markers anti-rabbit E- cadherin (Cell Signaling Technology, 1:200). To detect hMF, anti-mouse Vimentin (Santa Cruz, 1:50) was used. Then, scaffolds were washed 3 times with 1.5 wt.% BSA in HBSS (5 min each), and subsequently incubated, for 1 h, protected from the light, with DAPI, as well as, with the following secondary antibodies: Goat anti-rabbit 594 and/or Chicken anti-mouse 647 (Molecular Probes, Invitrogen, 1: 1,000, 1h at RT). Next, samples were washed 3 times with HBSS (5 min each) and stored until use. Before use, scaffolds were mounted with VECTASHIELD® Antifade mounting media (Vector Laboratories, Inc., Burlingame, CA) and analyzed by CLSM on the same day.

2.14. Analysis and quantification of spheroids formation

For quantification of spheroids number and size, MCF10A-embedded hydrogels were fixed, permeabilized and blocked, at different time points (day 7 and 14), as described above. F-actin filaments were stained with Alexa Fluor 488 phalloidin and nuclei were counterstained with DAPI. Discs with stained cells within alginate matrices were imaged by CLSM, and multicellular spheroids were measured using Fiji. Two independent gels were analyzed for each condition and time point.

2.15. Flow cytometry and proteomics

To distinguish hMF and MCF10A populations, flow cytometry (FC) analysis was performed. Since flow cytometry requires cells in suspension, these had to be retrieved from scaffolds. To do this, scaffolds were washed once with HBSS and incubated with 10mg/mL alginate lyase (Sigma-Aldrich, St. Louis, MO) in PBS at 37ºC, for 10min. Subsequently, 100mM sodium citrate (VWR, Radnor, PA) in PBS was added to scaffolds for 20 min at RT. Thereafter, scaffolds were treated with a 0.25% trypsin/50mM EDTA solution for 5 min. The obtained solution was then centrifuged at 1000 rpm for 5 min and the supernatant was collected, frozen at -20ºC, and lyophilized for subsequent proteomic analysis. Cells were blocked with 5 wt.% BSA in PBS (45min) and stained with conjugated anti-CD90 antibody (laser 647, dilution 1:100, BioLegend, San Diego, CA) and anti-E-cadherin antibody (PerCP-Cy™5.5, BD-Biosciences, dilution 4:100) for 1h. Then cells were washed with FACS buffer (2% FBS/PBS), and filtered with a 70μm-filter. Cells were analyzed by flow cytometry using BD FACSAria™ II (BD-BioSciences, San Jose, CA), with FACSDiva software (BD-Biosciences, San Jose, CA). All cells were kept on ice during processing and before FACS. The FC results were analyzed using FlowJo v10.0 1-month trial (FlowJo, Ashland, OR). Optimal experiment settings to facilitate gating and reduce background noise were established by using unstained 3D hMF and MCF10A monocultures and co-cultures, as negative controls; in the other hand, stained hMF and MCF10A 3D monocultures were used as positive controls for each marker expression. Sorted cells were then centrifuged (1000rpm), and cell pellets stored at -80ºC.

After lyophilization of the supernatant, the lyophilizate was dissolved in SDS buffer (5% SDS, 10% glycerol, 60mM tris-HCL; pH=6.8; Sigma-Aldrich), and heated at 95ºC, for 5min. Thereafter, the solution was centrifuged (16,000 g; t=10min), and the supernatant (SDS-soluble proteins) were collected. The pellet (non-soluble SDS proteins) was dissolved in urea buffer (8M urea, 4% SDS, 60mM Tris-HCL, 12.5mM EDTA; Sigma-Aldrich) and left for 30min. Subsequently, the solution was centrifuged (16,000; t=10min), and supernatant added to the SDS-soluble supernatant. Samples were frozen at -80ºC, until subsequent proteomic analysis. Samples were analyzed by the proteomics department technical unit. Proteins were solubilized with 100 mM Tris pH 8.5, 1% sodium deoxycholate, 10 mM tris(2-carboxyethyl) phosphine (TCEP) and 40 mM chloroacetamide for 10 minutes at 95ºC at 1000 rpm (Thermomixer, Eppendorf). Each sample was processed for proteomics analysis following the solid-phase-enhanced sample-preparation (SP3) protocol as described in PMID30464214. Enzymatic digestion was performed with Trypsin/LysC (2 micrograms) overnight at 37ºC at 1000 rpm.

Protein identification and quantitation was performed by nanoLC-MS/MS. This equipment is composed by an Ultimate 3000 liquid chromatography system coupled to a Q-Exactive Hybrid Quadrupole-Orbitrap mass spectrometer (Thermo Scientific, Bremen, Germany). Samples were loaded onto a trapping cartridge (Acclaim PepMap C18 100Å, 5 mm x 300 μm i.d., 160454, Thermo Scientific) in a mobile phase of 2% ACN, 0.1% FA at 10 μL/min. After 3 min loading, the trap column was switched in-line to a 50 cm by 75μm inner diameter EASY-Spray column (ES803, PepMap RSLC,

C18, 2 µm, Thermo Scientific, Bremen, Germany) at 250 nL/min. Separation was generated by mixing A: 0.1% FA, and B: 80% ACN, with the following gradient: 5 min (2.5% B to 10% B), 120 min (10% B to 30% B), 20 min (30% B to 50% B), 5 min (50% B to 99% B) and 10 min (hold 99% B). Subsequently, the column was equilibrated with 2.5% B for 17 min. Data acquisition was controlled by Xcalibur 4.0 and Tune 2.11 software (Thermo Scientific, Bremen, Germany).

The mass spectrometer was operated in data-dependent (dd) positive acquisition mode alternating between a full scan (m/z 380-1580) and subsequent HCD MS/MS of the 10 most intense peaks from full scan (normalized collision energy of 27%). ESI spray voltage was 1.9 kV. Global settings: use lock masses best (m/z 445.12003), lock mass injection Full MS, chrom. peak width (FWHM) 15s. Full scan settings: 70k resolution (m/z 200), AGC target 3e6, maximum injection time 120 ms. dd settings: minimum AGC target 8e3, intensity threshold 7.3e4, charge exclusion: unassigned, 1, 8, >8, peptide match preferred, exclude isotopes on, dynamic exclusion 45s. MS2 settings: microscans 1, resolution 35k (m/z 200), AGC target 2e5, maximum injection time 110 ms, isolation window 2.0 m/z, isolation offset 0.0 m/z, spectrum data type profile.

The raw data was processed using Proteome Discoverer 2.5.0.400 software (Thermo Scientific) and searched against the UniProt database for the Bos taurus and Homo sapiens proteomes and the NIST human spectral library. A common protein contaminant list was also considered. The MSPepSearch and Sequest HT search engines were used to identify tryptic peptides. The ion mass tolerance was 10 ppm for precursor ions (both software) and 20 ppm / 0.02 Da for-fragment ions (MSPepSearch and Sequest HT, respectively). Maximum allowed missing cleavage sites was set 2. Cysteine carbamidomethylation was defined as constant modification. Methionine oxidation and protein N-terminus acetylation, Met-loss and Met-loss+acetyl were defined as variable modifications. Peptide confidence was set to high. The processing node Percolator was enabled with the following settings: maximum delta Cn 0.05; decoy database search target FDR 1%, validation based on q-value. Protein label free quantitation was performed with the Minora feature detector node at the processing step. Precursor ions quantification was performing at the processing step with the following parameters: Peptides to use unique plus razor, precursor abundance based on intensity, and normalization based on total peptide amount.

2.16. RNA expression quantification

RNA was extracted using the Quick-RNA MiniPrep (Zymo Research), as recommended by the manufacturer. Subsequently, 250 ng of total RNA were reversed transcribed to single stranded cDNA using PrimeScript RT Reagent Kit (Perfect Real Time).

One-step Quantitative Real-Time PCR (qRT-PCR) was prepared in Multiplate™ 96-Well PCR Plates (MLL9601, Bio-Rad) using the SYBR™ Green PCR Master Mix. Primers for GAPDH, α-smooth actin muscle, collagen type I and III were used (OriGene; **Table 2**). The qRT-PCR was run on an CFX 96™ Real-Time PRC System C100 Touch™ Thermal Cycler (Bio-Rad) and cycling conditions were: (i) 95 °C (2 min), (ii) 40 cycles – 95 °C (15 s), 60 °C (1 min). All samples were run in the qPCR

plates as triplicates for each gene. The data were processed in CFX Maestro Software and mRNA expression levels were computed by the relative quantification method based on the exponential transformation of ΔCt values ($2^{-\Delta Ct}$). Col I, Col III, and αSMA expression was normalized against the endogenous control GAPDH. The presented data are expressed as the mean of the three technical replicates.

Table 2. PCR primers for GAPDH, αSMA, Col I and III.

PCR primers	Primers sequence 5' to 3'
GAPDH	Forward: GTC TCC TCT GAC TTC AAC AGC G Reverse: ACC ACC CTG TTG CTG TAG CCA A
αSMA	Forward: CTA TGC CTC TGG ACG CAC AAC T Reverse: CAG ATC CAG ACG CAT GAT GGC A
Col I	Forward: GAT TCC CTG GAC CTA AAG GTG C Reverse: AGC CTC TCC ATC TTT GCC AGC A
Col III	Forward: TGG TCT GCA AGG AAT GCC TGG A Reverse: TCT TTC CCT GGG ACA CCA TCA G

2.17. Microidentation of the whole-mounted scaffolds

The effective Young's Modulus (E_{eff}) of the scaffold was determined by microindentation (PIUMA, Optics11, The Netherlands) after 1 day of culture. The sample was retained within an agarose mold and fixed to a glass substrate with glue. Probe calibration, i.e., determination of the geometrical factor, was performed in culture medium supplemented with HEPES buffer (DMEM HEPES) and against the rigid glass substrate. Measurements were performed with the sample and probe immersed in DMEM HEPES at room temperature using a spherical probe with a radius of 24 µm and cantilever spring constant of 0.49 N/m.

The probe was brought into contact with the sample performing an automated "find surface" procedure. A loading-holding-unloading cycle was performed using the indentation depth control mode ("I-mode") at a maximum indentation depth of 2 µm. The measurements were performed in a matrix scan mode for a matrix of 4 x 9 points with a 75 µm stepsize. Obtained data was fit to Hertz contact model (10 % Pmax) using Piuma Dataviewer software (Dataviewer V2.1.10, Optics11).

3. Results and Discussion

3.1. Printing of the 3D alginate scaffolds

The first step towards the establishment of a 3D *in vitro* model, suitable for recapitulating some of the key aspects of both healthy and diseased breast tissue, lied on the generation of 3D macroporous scaffolds to build the stromal compartment. To this end, a microextrusion printing approach was selected as the scaffold fabrication technique, through the employment of a custom-built 3D printer. Despite presenting reduced resolution when compared to other printing technologies, such approach allowed for the facile, rapid and effective generation of 3D constructs with relevant dimensions, while contouring high costs. Furthermore, the open-source *Repetier Host software*, which can be readily obtained by other research laboratories was used as the user-printer interface. Alginate was chosen as the scaffold's constituent biomaterial, since it offers a wide breadth of advantages over other possible candidate hydrogels. Relevant features include its: ***bio-inertness***, that in conjunction with the presence of chemically-modifiable functional groups allow to perform specific modifications for enhanced control over cell behaviour; ***transparent optical properties***, highly advantageous for straightforward microscopic evaluation of samples along culture; ***reversible ionic crosslinking***, via treatment with chelating agents and/or alginate degrading enzymes, allowing to dissolve the hydrogel, and thus enable the fast and mild retrieval of cells for further downstream analysis.

The adopted printing strategy relied on the extrusion of an alginate pre-gel solution directly within a $CaCl_2$ crosslinking bath, prompting rapid external ionic gelation, and thus leading to the formation of well-defined filaments. Due to the alginate's higher density, these filaments tend to settle in the substrate, and subsequently give rise to defined 3D structures, in a layer-by-layer fashion. According to previous work from our lab, **i)** the syringe pump was set to an extrusion rate of 2 mL/h; **ii)** the printing speed was set at 170 mm/min; and **iii)** the alginate pre-gel and $CaCl_2$ solutions were used at concentrations of 4 wt.% and 12.5 mM, respectively [130].

3.1.1. Refinement of the 3D design

One of the initial goals of this work was to optimize the previous 12 X 12 mm crosshatch square-shaped scaffold design to a new circular-shaped crosshatch. We postulated that such adaptation would provide the ability to adequately fit the printed scaffolds into standard tissue culture plates. This should increase the efficiency of subsequent cell seeding/gel filling procedures, by maximizing cell-scaffold contacts and avoid gel slippage from the construct. In this regard, scaffolds were designed to fit the 11 mm diameter of 48 multi-wells, since it would offer a good compromise between the reduced resolution associated to the extrusion printing approach and the

scaffold downsizing, in comparison to 24 and 96 multi-well plates (15.6 and 6.4 mm, respectively). Several circular-shaped designs were generated through the NCPlot software (**Figure 6**) which differed in the number of layers (L=4 or 6), and outer circles (C) integrating the construct, albeit the scaffold's pore dimensions remained the same as previously established, across all designs. Moreover, the diameter of the scaffolds was set to 10 mm, taking into account the possible swelling of the hydrogel, upon immersion in culture medium.

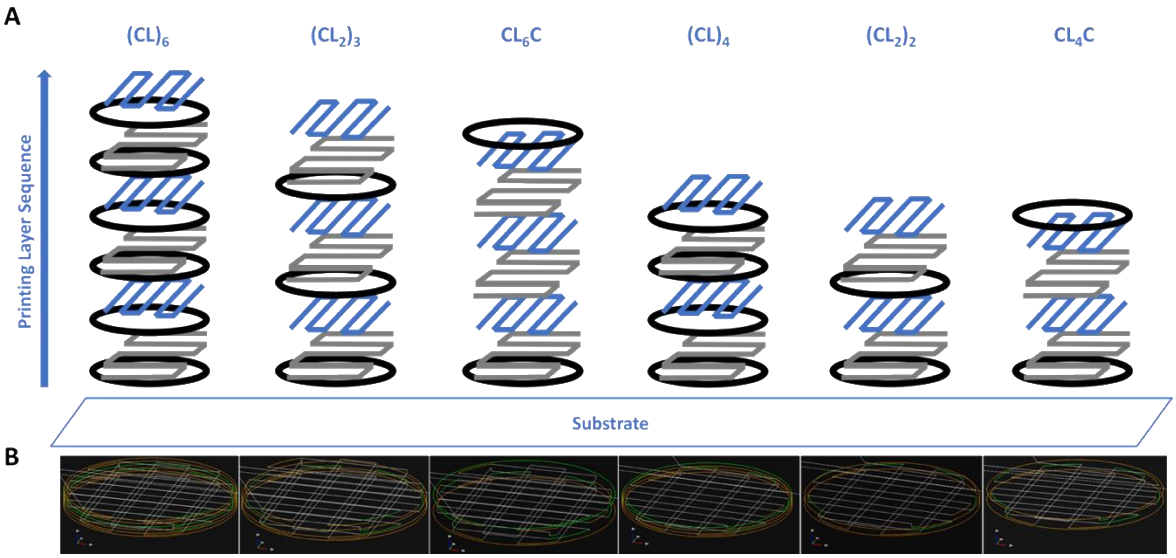

Figure 6. Printing design layout. The different proposed designs are depicted as layered sections (A), as well as, their respective virtual design, generated through the NCPlot software **(B)**. The design nomenclature is dependent on the number of repetition patterns of each design, comprised by outer circles **(C)** and inner lines (L). That said, $(CL)_6$ and $(CL)_4$ correspond to six and four repetition units of one outer circle and one inner line, respectively; $(CL_2)_3$ and $(CL_2)_2$ correspond to three and two repetitions units of one outer circle and two inner lines, respectively; CL_6C and CL_4C correspond to two outer circles containing six and four inner lines in between, respectively.

Following the generation of the different G-codes corresponding to each specific design, all scaffolds were then printed, and subsequently assessed according to several parameters such as: **i) reproducibility**, essential to ensure similar physical and mechanical properties between different scaffolds sharing the same design; **ii) shape-fidelity**, where both the pores and the circular shape are well preserved; **iii) mechanical stability**, which allows the scaffolds to maintain their structural integrity throughout time, while facilitating physical manipulation. The resultant printed scaffold designs are depicted in **Figure 7**. Importantly, before the pictures were taken, scaffolds were subjected to a sterilization protocol and washed, as aforedescribed, and then incubated with media ON, to ensure that the constructs structure would be properly assessed, by taking swelling into account. For these preliminary trials, only non-purified alginate hydrogel was used. Out of all proposed designs, the ones that exhibited less pronounced reproducibility amongst printing attempts were CL_6C and CL_4C, due to the wide gap present between the initial and final outer circles of the constructs. Indeed, such gap has also demonstrated to significantly impact the shape fidelity of the obtained structures, since there is a reduced support for subsequent layers,

during the printing process. Furthermore, the presence of a higher number of outer circles conferred the scaffolds enhanced structural stability, and thus facilitated their manipulation for subsequent experiments. For these reasons, these two designs were, from this point, discarded.

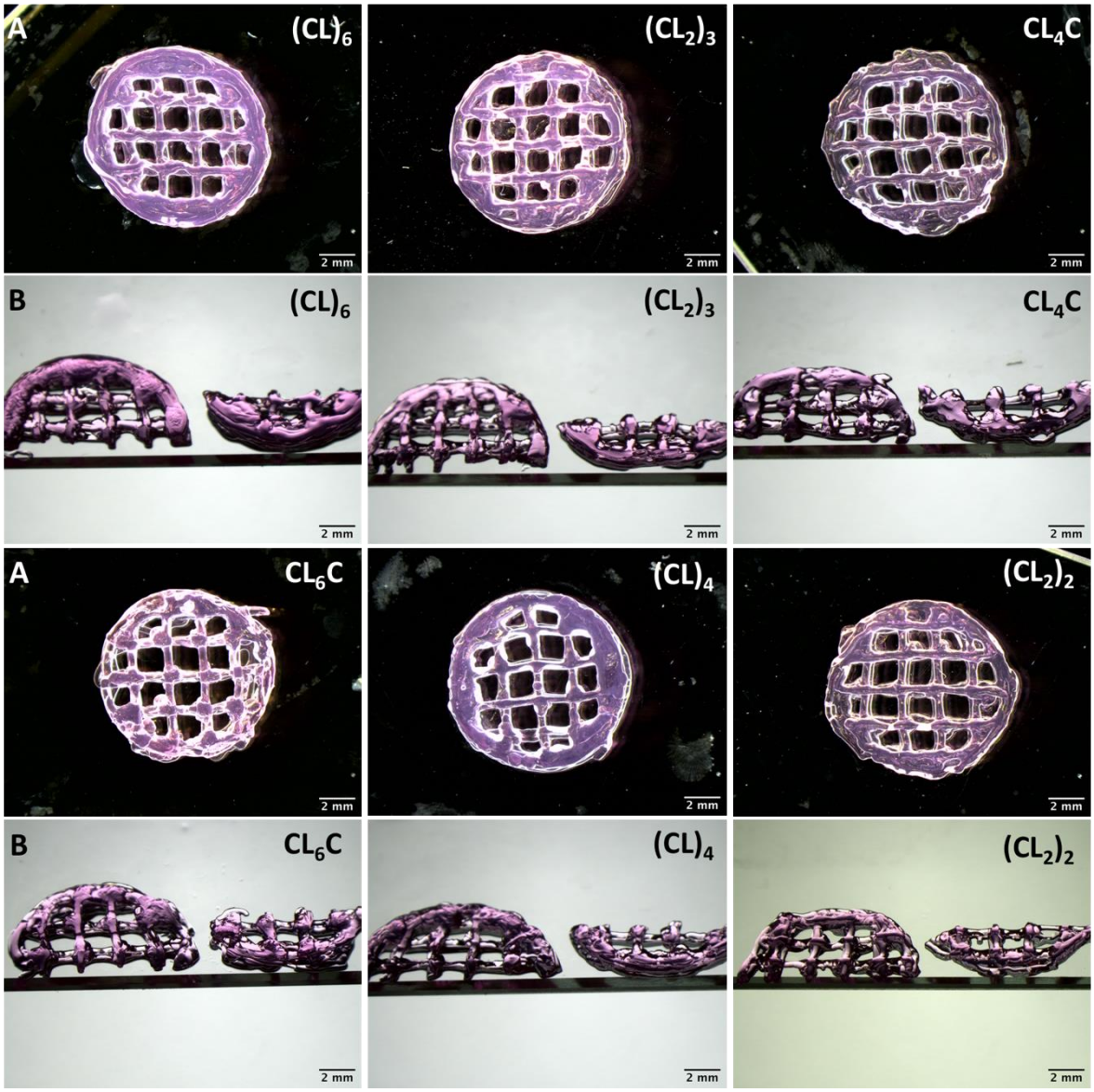

Figure 7. Characterization of non-purified alginate 3D scaffolds. Illustrative image showing the resulting shape of the alginate scaffolds produced, accordingly to their corresponding designs. Herein, scaffolds are depicted in **A)** top view and **B)** cross-section view. Scale bar: 2 mm.

In addition, the $(CL)_6$ design was also abandoned, due to its excessive peripheral thickness, resulting from the layering of six outer circles. When comparing with the other designs, the higher outer thickness observed in $(CL)_6$ resulted in a loss of pore resolution in the periphery, as well as, a significant height difference between the peripherical and central areas of the scaffolds. The remaining designs ($(CL)_4$, $(CL_2)_3$, $(CL_2)_2$), exhibited both satisfactory reproducibility and shape fidelity, and were therefore selected for the subsequent fibroblast seeding experiments, so that the impact of the scaffold design on the seeding efficiency could be evaluated.

3.1.2. Printing of the 3D scaffolds with purified alginate

Once the most promising circular designs were selected, we focused on producing 3D alginate scaffolds using purified alginate, instead of the previously used raw (pharmaceutical grade) alginate. It is well-recognized that alginate developed for most industrial purposes does not offer neither well defined physicochemical compositions nor high purity levels, which are key for medical applications. Several impurities such as polyphenols, endotoxins, and proteins are often present within raw alginate, which may largely impact cell behaviour and strongly compromise reproducibility amongst experiments [105]. Hence, the obtained purified alginate was used to print 3D scaffolds ($(CL)_4$, $(CL_2)_3$, $(CL_2)_2$), using the same printing settings that were optimized for the raw alginate (**Figure 8**).

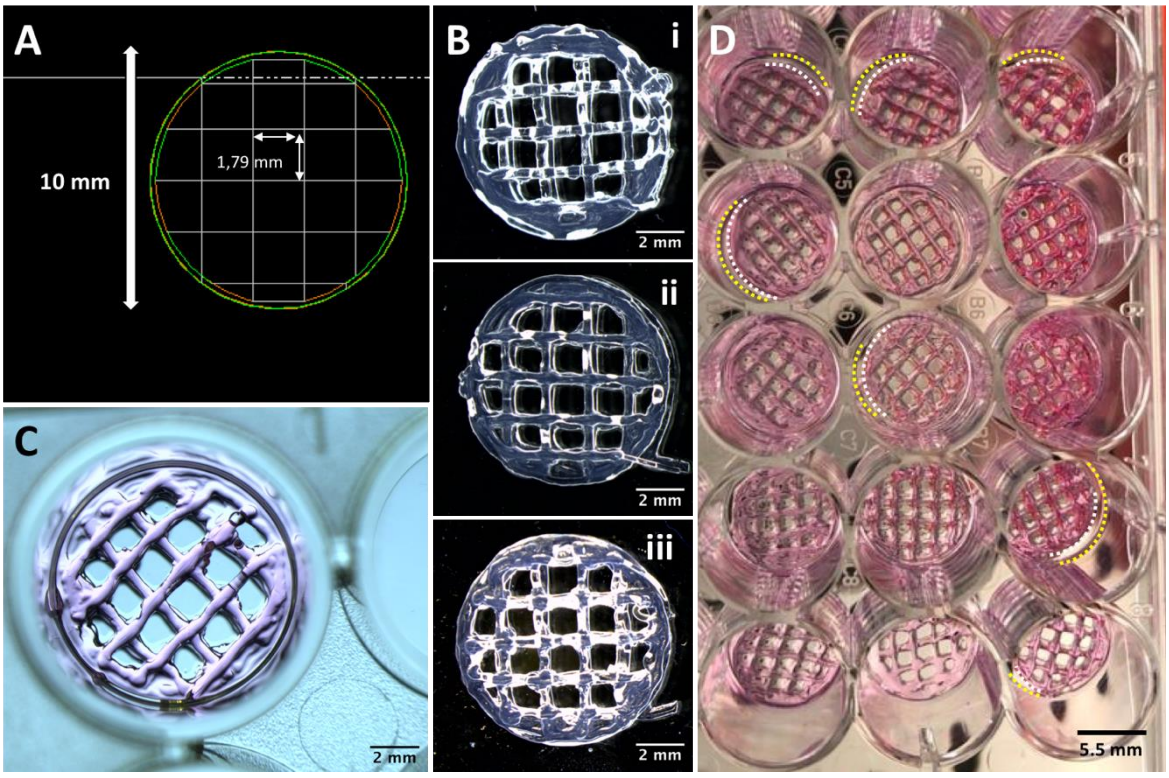

Figure 8. Characterization of purified alginate 3D scaffolds. A) CAD-design of the 3D scaffold in a top view, presenting both the theoretical diameter and pore size. **B)** Alginate scaffolds printed accordingly to the i) $(CL)_4$, ii) $(CL_2)_2$, and iii) $(CL_2)_3$ designs. In preliminary assessments, scaffolds were shown to be able to tightly adapt to 48 multi-well plates **C),** although in subsequent experiments intra-variability was observed for all designs (dashed-yellow and -white lines delimit the wells and scaffolds, respectively) **D)**. Scale bars: 2 mm.

Upon preliminary printing trials, purified alginate was shown to possess adequate rheological properties for the 3D printing of scaffolds under the settings previously established. Additionally, neither the shape fidelity nor the mechanical stability of the printed structures appeared to become compromised (**Figure 8B**), as result of the material transition, and thus the printing settings were no further optimized. Importantly, when introduced inside 48 multi-well plates,

purified alginate scaffolds initially seemed to adequately fit the well bottom area (**Figure 8C**). Nonetheless, in following experiments, when scaffolds were printed in higher numbers for all designs, some intra-sample variability was observed in this regard (**Figure 8D**). For this reason, new scaffold designs were developed, in which the only alteration made consisted in a slight increase of the scaffolds' diameter from 10 mm to 11 mm (**Figure 9**).

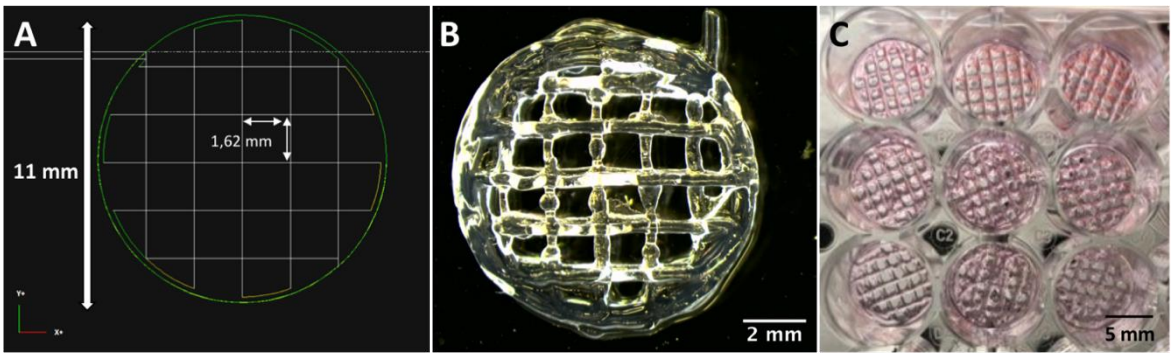

Figure 9. Refinement of purified alginate 3D scaffolds. A) CAD-design of the 3D scaffold in a top view, presenting both the theoretical diameter and pore size. **B)** Top view of a printed alginate scaffold. **C)** The refined scaffolds were shown to tightly adapt to 48 multi-well plates, without significant intra-variability. Scale bars: 2 mm.

As a result of this change, the pores would have to be increased in size from 1.79x1.79 mm to 1.99x1.99 mm, if maintaining the same the number of pores. However, such wide pore dimensions could negatively impact cell retention within the pores, in subsequent cell seeding experiments, and thus prevent uniform cell seeding throughout the scaffolds. Therefore, a higher number of pores was used in the crosshatch, leading to a decrease in pore size to 1.62x1.62 mm (**Figure 9A**). This did not show to have an effect on the resolution of the printed structures (**Figure 9B**). Notably, the printed scaffolds were able to tightly adapt to the 48 multi-well plates, without any significant intra-sample variability across the different designs (**Figure 9C**).

3.2. Lyophilization of the 3D alginate scaffolds

One great limitation of the approach chosen for this work, was the requirement of having to produce the alginate scaffolds shortly before being used. Such problem highly hinders the long-term storage of the alginate scaffolds, which, in turn, would ensure the prompt availability of samples whenever needed. In this context, the possibility of freeze-drying the alginate scaffolds would be extremely advantageous, since it would allow storage in dried state, making storage and transport easier. Freeze-drying, or lyophilization, is a technique where water is removed from frozen materials under reduced pressure, by sublimation of the frozen water fraction [133]. Accordingly, we aimed to produce ready-to-use lyophilized scaffolds and evaluated their ability to preserve the overall structure upon the processes of lyophilization and rehydration. As such, two

distinct protocols were established and followed: **i) lyophilization prior to sterilization protocol**, where scaffolds were merely washed with distilled water, to remove any traces of remaining salts, lyophilized, and then rehydrated and sterilized for subsequent cell seeding; **ii) sterilization prior to lyophilization**, where the scaffolds were sterilized upon printing, washed, lyophilized, and then rehydrated directly with cell suspension (**Figure 10**). The latter protocol was developed in order to assess the possible positive impact of rehydration on cell seeding efficiency. Using both protocols, scaffolds lyophilization did not impair their overall structure, preserving both their circular-shape and macroporous structure. Notably, upon rehydration, scaffolds regained their original dimensions, and thus perfectly readapted to the 48 multi-well plates. A closer observation of the microscopic effects of these processes on the alginate filaments will be provided in future sections, as well as, the impact of direct scaffold rehydration with cell suspension on cell seeding efficiency.

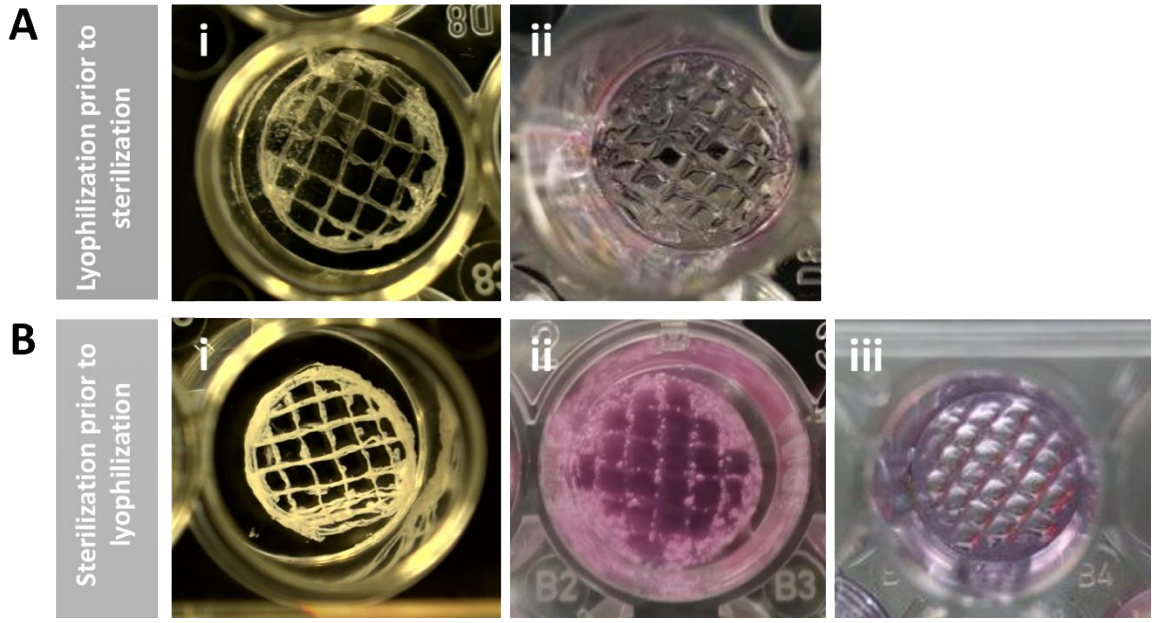

Figure 10. Lyophilization of the 3D alginate scaffolds. Two distinct lyophilization protocols were followed: **A)** scaffold lyophilization prior to sterilization protocol, where scaffolds are subjected to i) lyophilization and ii) rehydration before sterilization; **B)** scaffold sterilization prior to lyophilization protocol, where scaffolds were first i) sterilized and lyophilized, ii) then rehydrated directly with cell suspension (t=0h), and iii) finally incubated to allow complete hydration of the structure (t=24h).

3.3. Establishment of the stromal compartment

Following the establishment of circular-shaped scaffolds with purified alginate, our aim was to optimize the seeding process of human mammary fibroblasts (hMF) onto printed constructs. The main goal was to establish a homogenous stromal compartment, characterized by uniform attachment of fibroblasts throughout the scaffold, and later deposition of endogenously-produced ECM components along the scaffold's fibers. To this end, we have modified alginate polymer chains with an integrin-binding arginine—aspartic-acid—glycine (RGD) sequence by carbodiimide chemistry. This modification is mandatory, since alginate is intrinsically bioinert to mammalian cells, as previously stated, and thus requires the grafting of integrin-binding ECM-derived peptide motifs, capable of supporting cell attachment, survival, and proliferation. Importantly, we have observed that RGD coupling to the polymer chains did not have a significant impact on the rheological properties of alginate solutions, hence, the previously optimized printing parameters remained unchanged. In order to ensure a successful seeding procedure, it is important to maximize the contact of cells with the RGD-modified scaffolds, while avoiding cell leakage from the scaffold to the well bottom. As stated earlier, this rationale underlined the refinement of the scaffold design, since tightly adjusting the construct to standard tissue culture plates would, in theory, maximize cell-scaffold interactions and thus seeding efficiencies.

Presently, the different cell seeding strategies described in the literature can be classified into two main categories: static and active. The most commonly used method to seed a scaffold is static seeding, which consists in pipetting a cell suspension directly onto the scaffold surface, allowing cells to infiltrate and colonize the structure. After the deposition of the cell suspension onto the construct, the scaffold is then incubated for several minutes or hours to allow for cell attachment to occur. Despite this approach being simple, fast, and inflicting little hydrodynamic damage to the cells, it is often associated with inhomogeneous distribution and poor seeding efficiency (10-25%) [134]. Nonetheless, such limitations can be overcome when resorting to active seeding techniques, which require an external force, as centrifugation, rotation, vacuum, magnetic/electric fields, amongst others. While active seeding may improve cell seeding efficiency, uniformity, and cell penetration into the structures, as compared to static seeding, it also involves more complex and time-consuming techniques, which may be challenging to implement in clinical settings. Moreover, exposing cells to external stresses, may impair cell viability [134]–[136].

According to previous work from our lab, a static cell seeding approach was chosen herein, for simplicity. In this section, we sought to optimize both the cell seeding density and volume and determine which of the previously established designs was able to provide higher seeding efficiencies. Hence, cell seeding experiments were performed, in which $1.5x10^5$ and $3.0x10^5$ cells were resuspended in a 100 μL seeding-volume, and pipetted onto the $(CL)_4$, $(CL_2)_3$, and $(CL_2)_2$ scaffold designs, all with RGD concentration of 400 μM, based on previous optimizations. In order

to assess if mammary fibroblasts were able to adhere and proliferate on printed constructs, we used the resazurin assay to assess metabolic activity, which is intimately related to the number of viable cells present (**Figure 11**). Scaffolds were also fixed and stained for CLSM analysis, to validate that cells were, in fact, colonizing the scaffolds and also assess if there was ECM production and deposition over the scaffold's fibers (**Figure 12**).

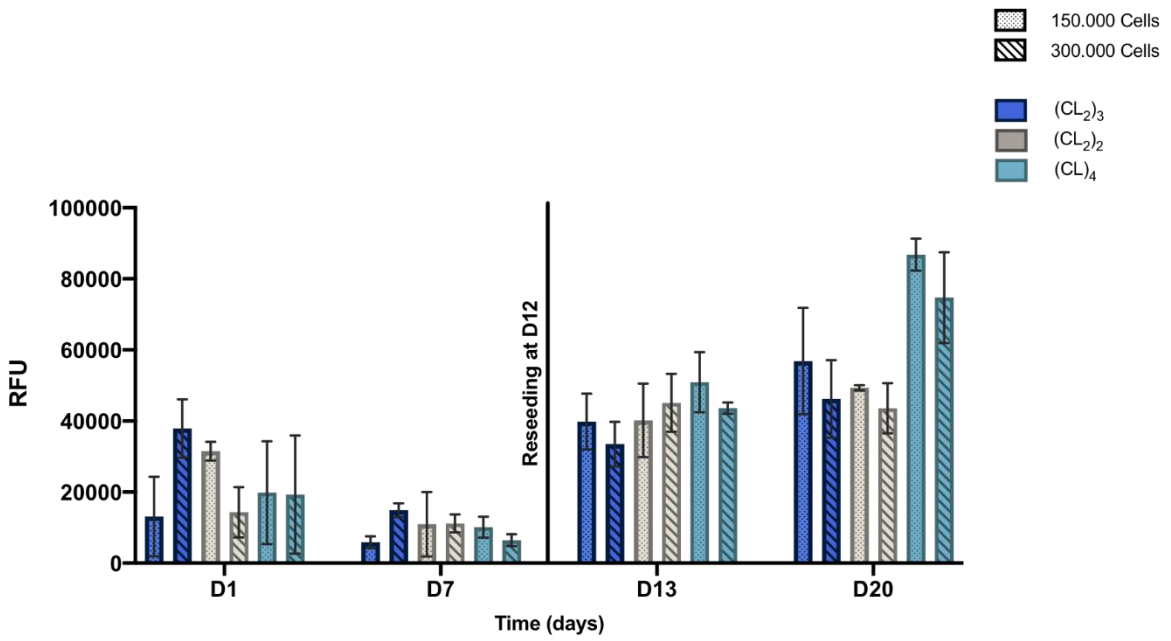

Figure 11. Effect of cell seeding density and scaffold design on the metabolic activity of hMFs along time, measured with the resazurin assay. hMF metabolic activity was assessed upon seeding $1.5x10^5$ and $3.x10^5$ cells onto alginate scaffolds presenting distinct designs ($(CL)_4$, $(CL_2)_3$, and $(CL_2)_2$), during 20 days of culture. An additional seeding procedure of $1.0x10^5$ cells was performed at day 12. This represents an illustrative experiment from a total of n=2, where no considerable differences were observed across the different designs, and a reseeding step was shown to be beneficial.

Along culture of the cell-seeded scaffolds, a general decrease metabolic activity was observed from day 1 to day 7, for all designs and the two cell concentrations tested. Some cell loss may be potentially associated to the mechanical manipulation of the scaffolds upon well transfer, which was performed prior to each measurement, in order to ensure that non-adhered cells were excluded. This may have also affected D1 measurements and possibly explain the apparently random effect of doubling the cell density. At day 7, all scaffolds presented similar metabolic activity, regardless of the nature of the design or the initial cell seeding density. To further promote scaffold colonization, a reseeding step was performed at day 12, with $1.0x10^5$ fibroblasts resuspended in a volume of 100 μL for all scaffolds. This led to a considerable increase of metabolic activity levels in all scaffolds at day 13, which remained constant, or even increased, until day 20. The much higher seeding efficiency observed upon reseeding may be due to presence of endogenous ECM components over the scaffold's fibers, produced by the initially seeded cells, as depicted in **Figure 12**, which certainly increased the number of adhesion sites present in the scaffolds. Additionally, the extended culture periods also allowed cells to proliferate and

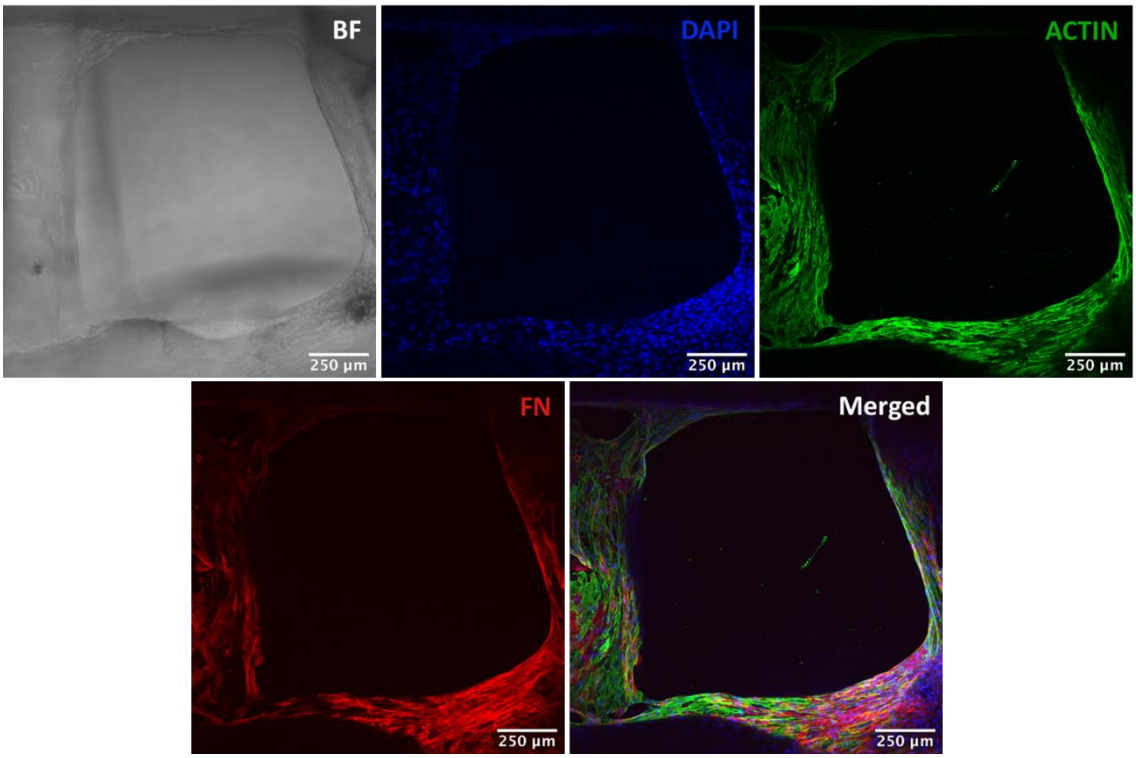

Figure 12. hMF distribution/activity around pores of printed scaffolds. Representative CLSM images with cell nuclei stained in blue, F-actin skeleton in green, fibronectin (FN) fibers in red. Pore details are shown in BF images. Scale bars: 250 µm (10x magnification). Images represent illustrative regions of the whole scaffolds.

effectively colonize the scaffolds. Indeed, this seeding approach led to the successful deposition of stromal-like tissue throughout the scaffold, where cells were not only able to spread, but also, of depositing and assembling a fibronectin-rich ECM network. By comparing the results obtained using $1.5x10^5$ and $3.0x10^5$ cells for the initial seeding, we saw no considerable impact of doubling the cell density on seeding efficiency, and thus decided to use the lower cell density for subsequent experiments. Moreover, as corroborated in additional experiments (data not shown), no considerable differences were observed between the different designs used. For this reason, we have selected the $(CL)_4$ from this point on, since it presented the highest reproducibility printing rates out of all designs, due to the increased stability of filaments throughout the printing process. It also facilitates manual handling due to the higher number of outer circles present in the structure. However, it remains important to carry out future additional seeding experiments with more replicates to confirm these results and their statistical significance.

Next, we compared the effect of the RGD concentration on the seeding efficiency. We hypothesized that if upon reseeding, cells were able to more effectively colonize the scaffolds, presumably due to an increase of cell-attachment sites, increasing the RGD concentration of scaffolds could lead to a similar outcome. Additionally, after seeding, some cells tended to self-aggregate into fiber-like structures on top of the constructs, limiting the number of cells effectively adhering to the scaffolds. This could be possibly circumvented with superior RGD

concentrations that would favour cell-scaffold interactions over cell-cell interactions [115]. Importantly, the seeding volume was also increased from 100 to 150 μL to better cover the scaffold. The aim was to minimize the formation of such cellular structures, since cells deposited on top of the scaffolds could be subjected to surface tension stimuli that might propel cellular aggregation. To maintain the previously selected cell seeding density, the number of cells per scaffold was increased to $2.25x10^5$ cells. Seeding experiments were performed on scaffolds presenting RGD concentrations of 400 and 600 μM. A preliminary seeding experiment (n=1) was also performed on a sterile lyophilized scaffold, with an RGD concentration of 600μM, to assess the effectiveness of cell attachment during scaffold rehydration. As depicted in **Figure 13**, the general trend observed from day 1 to day 7 was a decrease in metabolic activity, as seen in previous experiments, for all conditions. Nonetheless, scaffolds with 600 μM of RGD, including the lyophilized, demonstrated to be able to maintain higher metabolic activity along culture, although differences were not statistically different. Such findings were further supported by CLSM analysis (**Figure 14**), which demonstrated that scaffolds with 600 μM RGD presented higher amounts of spread cells (actin straining in green) and coverage by ECM components (FN actin in red), as compared to 400 μM RGD. Therefore, although these experiments should be repeated to confirm statistical significance, we selected an RGD concentration of 600 μM for subsequent experiments.

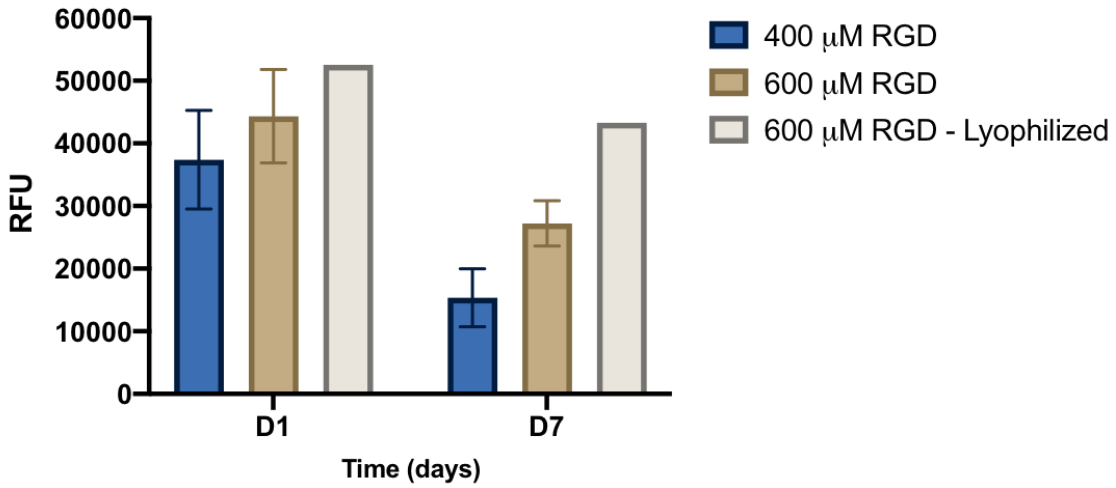

Figure 13. Effect of the RGD concentration on hMF metabolic activity along time. hMF metabolic activity was assessed upon seeding $2.25x10^5$ cells onto alginate scaffolds with RGD concentrations of 400 and 600 μM RGD, during 7 days of culture. This represents an illustrative experiment from a total of n=2, where differences were observed between the different RGD concentrations. A lyophilized scaffold, comprising an RGD concentration of 600 μM also included in the measurements.

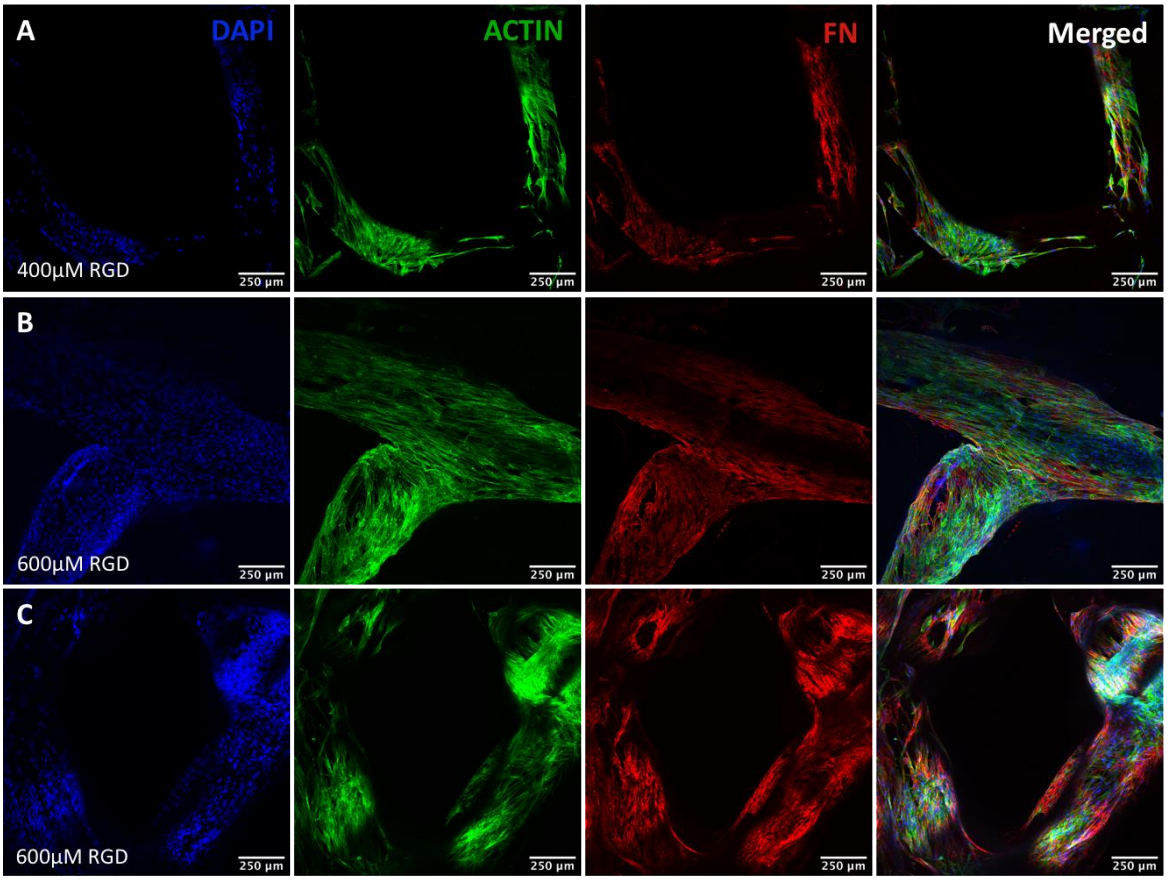

Figure 14. Effect of the RGD concentration and lyophilization process on hMF distribution/activity around pores of printed scaffolds after 7 days of culture. CLSM representative images of cells seeded onto **A)** 400 µM and **B), C)** 600 µM RGD-modified alginate scaffolds, after 7 days of culture. **C)** was lyophilized prior to the seeding procedure. Cell nuclei stained in blue, F-actin skeleton in green, FN fibers in red. Scale bar: 250 µm (10x magnification). Images represent illustrative regions of the whole scaffolds.

The highest metabolic activity observed for lyophilised scaffolds at days 1 and 7 (**Figure 13**) may result from the *in situ* swelling process (direct rehydration with cell suspension) that should maximize cell-scaffold contact, as cells are pulled towards the scaffold fibers. Notably, the lyophilized scaffold progressively recovered the original architecture, showing structural features similar to that of non-lyophilized scaffolds (**Figure 15**). However, the impact of the freeze-drying technique on the structural maintenance of printed constructs should be further assessed. For example, freezing conditions, as the freezing time, rate, and temperature, may differently affect the morphology and size of ice crystals and thus the microscopic structure of the scaffolds [137], [138]. Other parameters that also should be taken into account are the impact of the vacuum pressure and the length of the freeze-drying process.

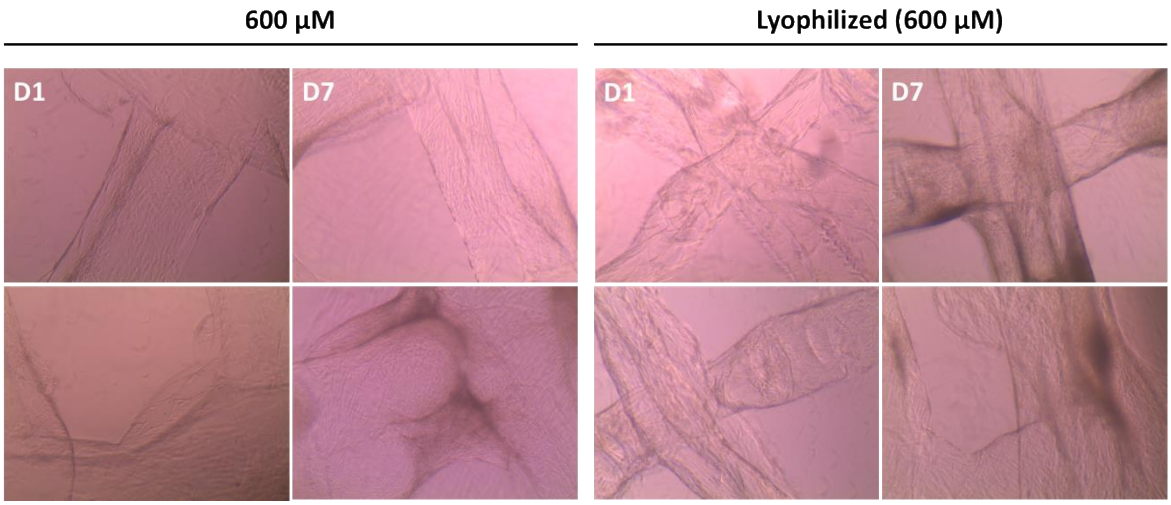

Figure 15. Effect of scaffold lyophilization on cell seeding and fibers structure. Inverted microscope images of the hMF-seeded scaffolds, comparing the effect of the lyophilization process on the seeding performance and microscopic structural maintenance, in scaffolds presenting an RGD concentration of 600 µM. Images were taken at day 1 and day 7 of culture.

As stated before, the ECM is fundamental for providing biochemical and mechanical signalling cues, which are, in turn, essential for supporting breast epithelial morphogenesis, homeostasis, and even disease progression. Therefore, it is important to assure the presence of different ECM components on scaffold's fibers that will largely influence epithelial cell behaviour, after the establishment of the co-culture. Through CLSM analysis, and in addition to fibronectin, the presence collagen type I and IV was also demonstrated (**Figure 16**). Indeed, fibroblasts were shown to effectively produce and secrete along the scaffolds' fibers, with a relative well-distributed arrangement. Collagen type I, a main component of interstitial matrices, is essential for supporting epithelial cell branching during the mammary gland development. In turn, collagen type IV, a key constituent of the basement membrane, is central for the maintenance of epithelial tissue polarity. In addition, both proteins are involved in malignant processes, related to tumour progression and metastasis [139], [140]. Through additional close examinations, it was shown that these ECM components are found assembled into organized fibrillar networks, over the scaffold's fibers (Figure S1).

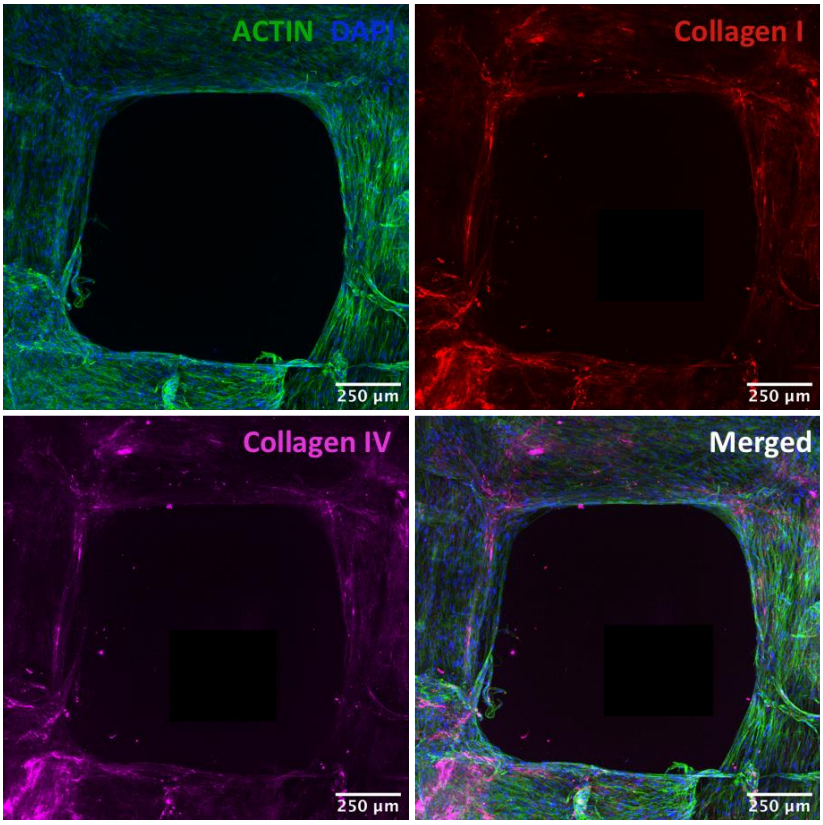

Figure 16. Characterization of other hMF-derived ECM components deposited over 3D scaffolds. Representative CLSM images of alginate 3D scaffolds (600 µM RGD) seeded with $2.25x10^5$ hMFs, after 10 days of culture. hMFs on top of printed scaffolds were able to spread (F-actin, green), and produce collagen type I (red) and collagen type IV (magenta), with a good overall distribution over the scaffold pores. Scale bar: 250 µm (10x magnification).

3.4. Establishment of the parenchymal compartment

After the establishment of a breast stromal compartment, we tried to develop a parenchymal compartment, capable of recapitulating key features of the epithelial mammary gland tissue. Our lab previously established an alginate-based 3D *in vitro* model with mouse mammary epithelial cells that successfully support epithelial morphogenesis and development of acinar-like structures after 14 days of culture, comparable to the ones found *in vivo* [114]. Later on, MCF10A-laden RGD-alginate pre-gels were introduced into the pores of 3D printed alginate scaffolds, where they were allowed to gel *in situ,* to establish a hybrid 3D co-culture model [130]. However, such setting, does not promote significant hMF invasion into the pore-filling alginate gel, as cell migration relies solely on the reduced ability of cells to mechanically overcome the physical barrier imposed by the gel network. As a result, most of the cultured hMF remained attached to the scaffolds' fibers, minimizing heterotypic direct cell-cell interactions.

In this work, we tried to circumvent such limitation through the use of a protease-sensitive alginate, which should provide a more permissive environment for fibroblastic migration and

invasion through the hydrogel via proteolytical mechanisms. To this end, we used PVGLIG-modified alginate hydrogel, obtained through double-end grafting of the peptide sequence to alginate chains, by reductive amination coupling chemistry. As explained earlier, this hexapeptide sequence is sensitive to the proteolytic action of several MMPs, including MMP-2, MMP-9 and MMP-14 [116], [117], [141]. Before peptide grafting, alginate chains are partially oxidized with sodium periodate ($NaIO_4$), which led to the opening of polysaccharide monomer rings for subsequent reductive amination coupling. Notably, unreacted oxidized groups may further contribute to hydrogel degradation, via hydrolytic chain scission, making the network more flexible and viscous-like, which may also facilitate cellular motility [106]. Prior to establishing fibroblast-epithelial co-cultures, monocultures of both cell types were generated in PVGLIG-modified hydrogels to evaluate cell response. Hydrogel composition (1 wt.% alginate, 17% oxidation degree, 200 μM and 40 μM of PVGLIG and RGD, respectively) was selected accordingly to previous optimizations by others.

3.4.1. Monoculture of PVGLIG/RGD alginate hydrogel-embedded hMF and MCF10A cells

Firstly, hMF and MCF10A cells were individually cultured within PVGLIG/RGD-modified alginate hydrogel to assess both viability and morphology along culture. The main goal was to ascertain the ability of the protease-sensitive alginate to promote fibroblasts activity and mobility, while also supporting epithelial morphogenesis. In preliminary experiments we assessed and compared hMF viability throughout the first 7 days of culture within **i)** oxidized PVGLIG-modified alginate (PVGLIG), **ii)** oxidized alginate (OX), and **iii)** blank alginate, that did not undergo through oxidization nor PVGLIG-coupling reactions (**Figure 17**).

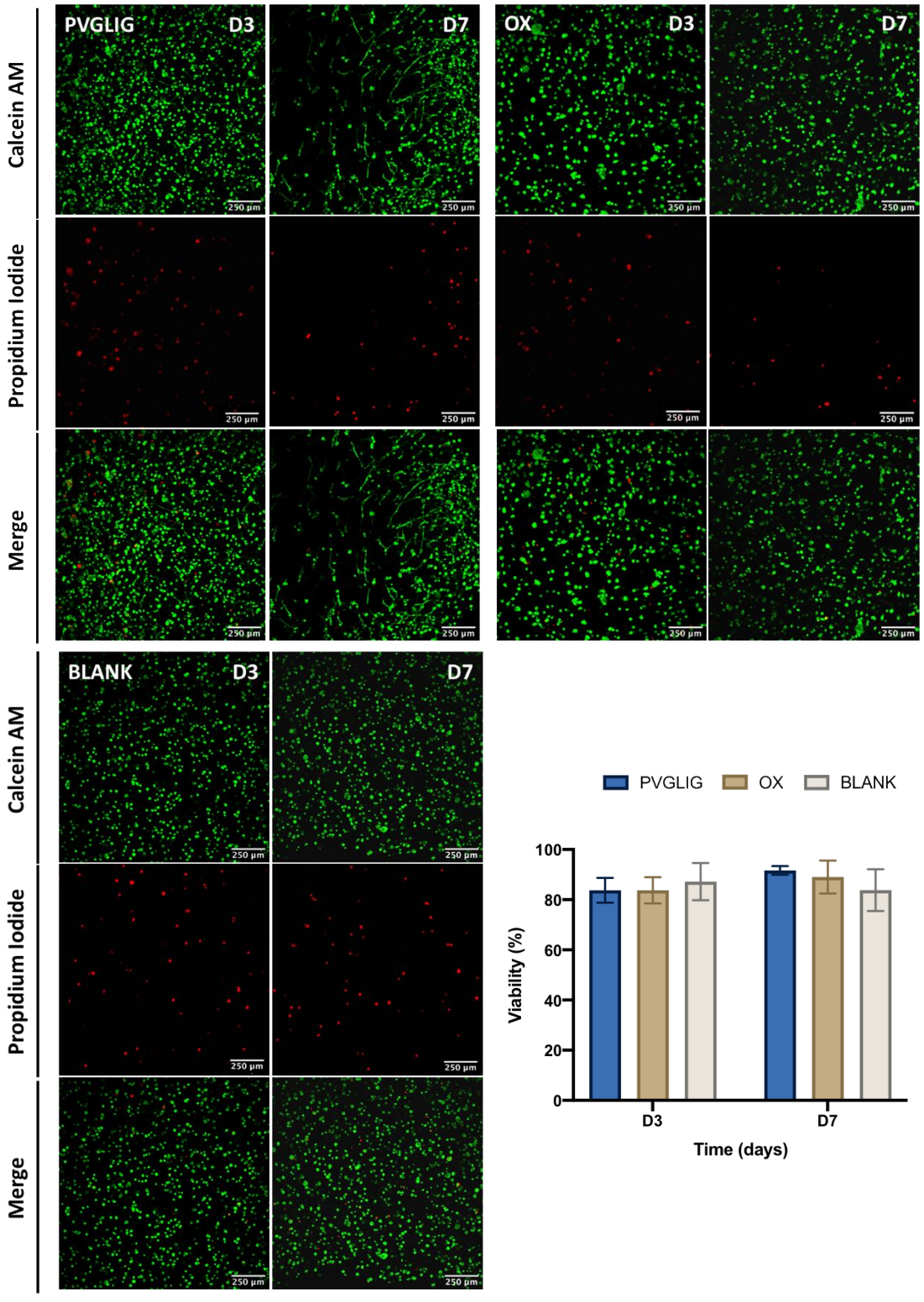

Figure 17. Live/Dead assay of fibroblast (hMF) embedded in oxidized PVGLIG-modified alginate (PVGLIG), oxidized alginate (OX) and RGD-modified only alginate (BLANK). A) Qualitative images of hMF viability throughout 7 days of culture, and **B)** quantitative representation of the corresponding cellular viability. Scale bars: 250 µm (10x magnification).

CLSM images of hMF live/dead staining (**Figure 17**) showed no significant cellular death upon 1-week culture within oxidized alginate hydrogels, with or without PVGLIG modification (PVGLIG and OX, respectively). Hence, the degree of alginate oxidation used herein did not seem to negatively impact fibroblast survival along culture. Indeed, these findings are in accordance with studies found in the literature, where fibroblast cytotoxicity was reported to occur at oxidation degrees of 25% or above [142]. Such cytotoxicity events can be due to the increase of the amount of reactive free aldehyde groups that are generated during the alginate oxidation process [142]. By looking at live cells (green) it was possible to detect hMF spreading within the PVGLIG-modified alginate, whereas in the other hydrogels cells seem to remain round, highlighting the preponderant role of the grafted PVGLIG sequences in supporting fibroblast spreading. This was corroborated with actin staining, as depicted in **Figure 18**. Inside MMP-sensitive PVGLIG/RGD-alginate, fibroblasts were able to spread and establish cell–cell interactions forming multicellular networks. In contrast, in MMP-insensitive control RGD-alginate hydrogels cells remained essentially round. Interestingly, throughout hMF culture within oxidized PVGLIG-alginate, fibroblasts clearly promoted the shrinkage of the hydrogel discs. This probably resulted from the looser matrix that was generated after enzymatic cleavage of PVGLIG-based crosslinks, and eventual chain scission of oxidized alginate, which gave hMF the ability to contract and remodel the surrounding 3D network (**Figure S2**) [115].

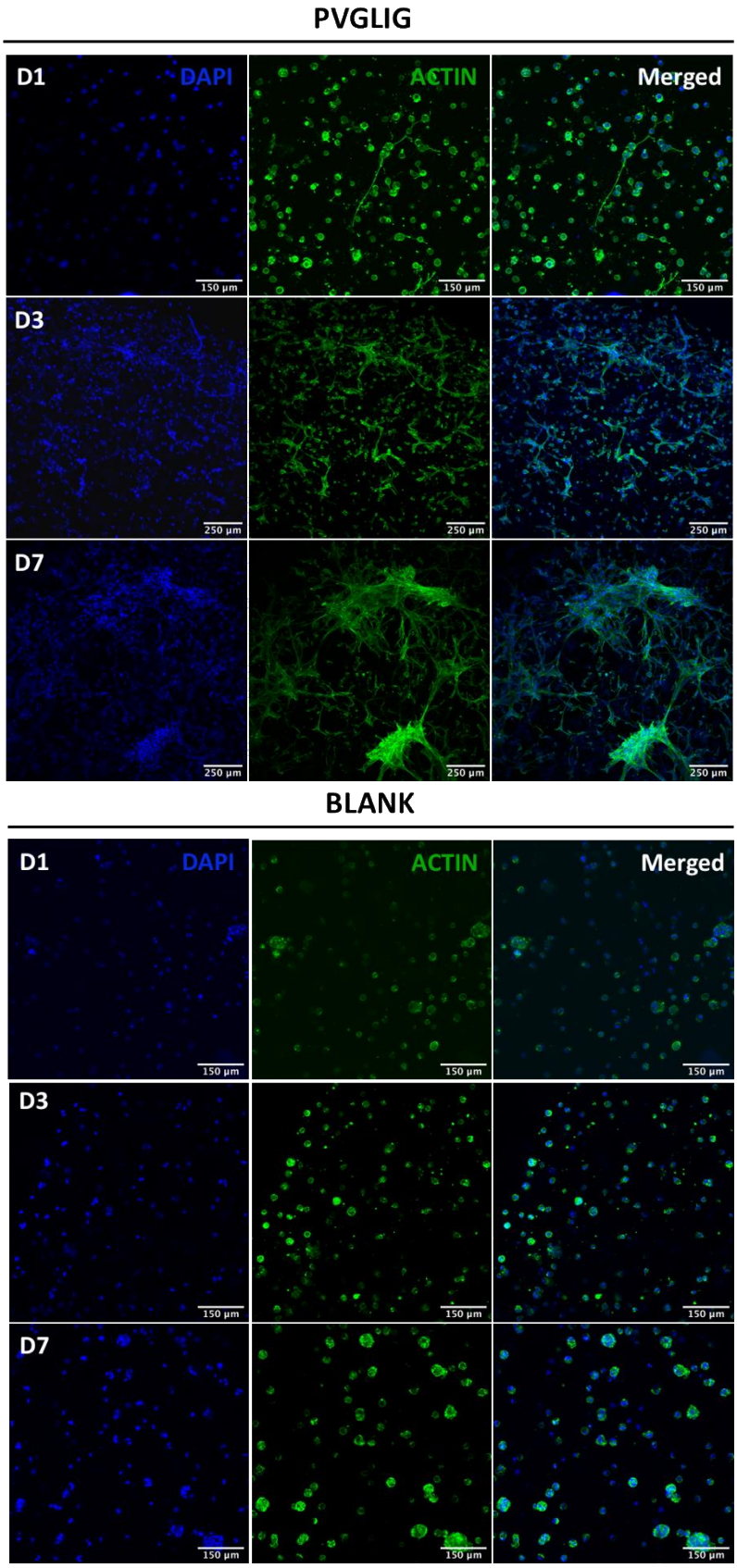

Figure 18. Representative CLSM images of hMF cells within PVGLIG and BLANK alginate hydrogels throughout a 1-week culture. Fibroblasts were able to establish early cellular in day 1, which eventually developed towards an increasingly intricated fibroblast network throughout culture (left). In contrast, hMF grown in BLANK hydrogels remained round throughout all culture timepoints (right). Scale bars: 150 µm and 250 µm (20x and 10x magnification, respectively).

Importantly, through additional stainings with anti- fibronectin and vimentin antibodies, it was possible to confirm the production of these proteins by hMF within this hydrogel (**Figure 19**). Vimentin is a widely studied mesenchymal marker and represents a major constituent of the intermediate filament family of proteins for several cell types, such as fibroblasts, being its presence often used to discern fibroblasts from other cell types. Fibronectin staining suggests that fibroblasts within this hydrogel retained their capability of producing ECM components, essential for the remodelling of the extracellular space. However, it was mainly localized to the intracellular and pericellular regions, which may suggest that the hydrogel network may have hindered the assembly of a well-defined extracellular fibrillar FN meshwork. In future studies, more attention should be focused on understanding the extent to which hMF are able to establish ECM-derived networks throughout these hydrogels, as well as, the related kinetics of PVGLIG degradation, mediated by these cells, through enzymatic degradation assays.

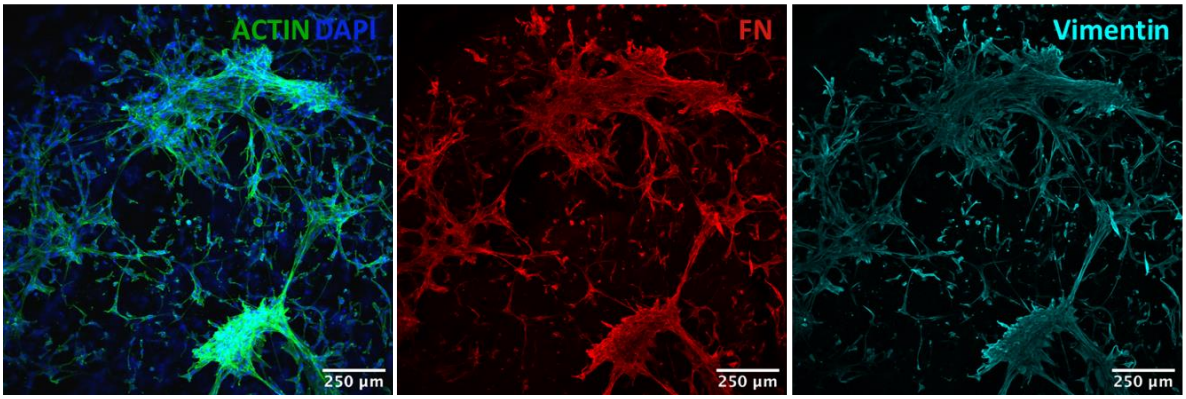

Figure 19. Representative CLSM images of hMF cultured for 7 days within PVGLIG alginate. hMF were able to maintain the expression of vimentin, a mesenchymal marker, and fibronectin, while establishing intricate fibroblast network after 1 week of culture within oxidized PVGLIG-modified alginate. Scale bar: 250 µm (x10 magnification).

Next, we assessed the capability of the oxidized PVGLIG-modified alginate to support MCF10A proliferation and assembly into multicellular spheroids. For this reason, MCF10A monocultures were established within PVGLIG and blank alginates, and maintained in culture for 14 days. At days 1, 7, and 14 MCF10A-laden alginate discs were stained for CLSM analysis.

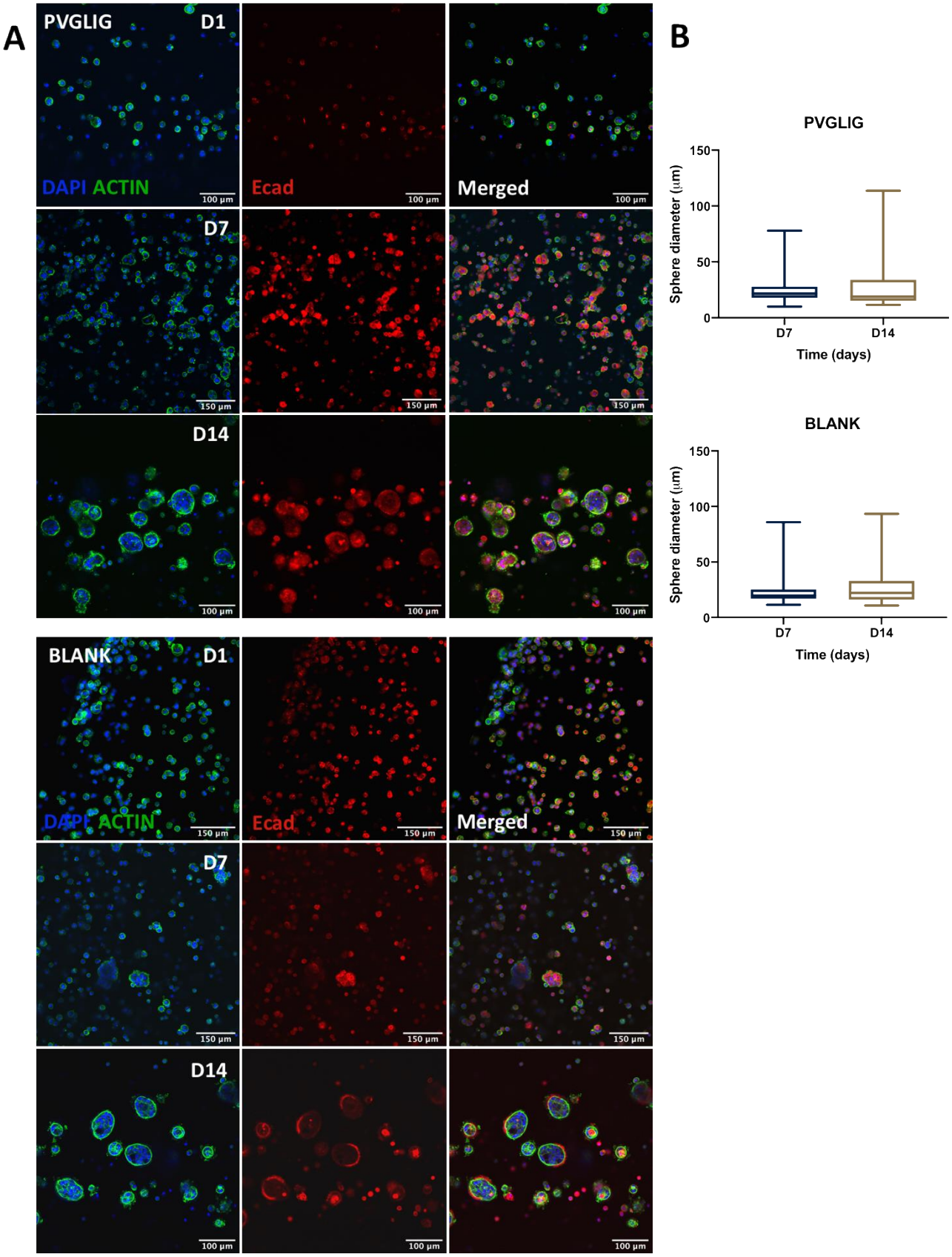

Figure 20. MCF10A cells cultured within PVGLIG and BLANK alginate hydrogels throughout a 2-week culture. Epithelial cells were able to form multicellular spheroids throughout culture, as depicted in the CLSM images **(A)**, that by day 14 reached an average diameter of 26 and 27 µm for PVGLIG and BLANK alginate, respectively.

Figure 20 shows that, in both conditions, MCF10A were able to proliferate and form multicellular spheroids, which reached an average size of 26 and 27 μm by day 14, in PVGLIG and blank alginate hydrogels, respectively. These results are consistent with previous work from our group, where mouse epithelial cells were shown to assemble into spheroids that reached an average size of around 30 μm, after 2 weeks of culture [114]. Furthermore, no significant differences regarding the average spheroid size were observed from day 7 to day 14, although the highest spheroid dimensions were observed at day 14 for both conditions.

Mammary epithelial cells undergo epithelial morphogenesis in a highly mechanosensitive way. Both cell morphology, growth rate, and invasiveness are highly dependent on the compliance and stiffness of the surrounding cellular microenvironments. For this reason, upon 3D *in vitro* culture, epithelial cells should be embedded in a compliant matrix, with a stiffness similar to that of mammary tissue (≈150 Pa), in order to recapitulate physiological formation of acinar-like structures [143]. Thus, it is of uttermost importance to design hydrogels displaying adequate stiffness. Through rheological analysis of MCF10A and hMF hydrogel-embedded monocultures performed at day 1, it was shown that the stiffness of the oxidized PVGLIG-modified alginate (G'≈ 130 and 120 Pa, respectively) was comparable to that of healthy mammary tissue (**Figure 21**). It was also possible to observe that the elastic component (G') was superior to the viscous component (G"), with a corresponding phase angle around 5°, as expected in predominantly solid-like viscoelastic matrices.

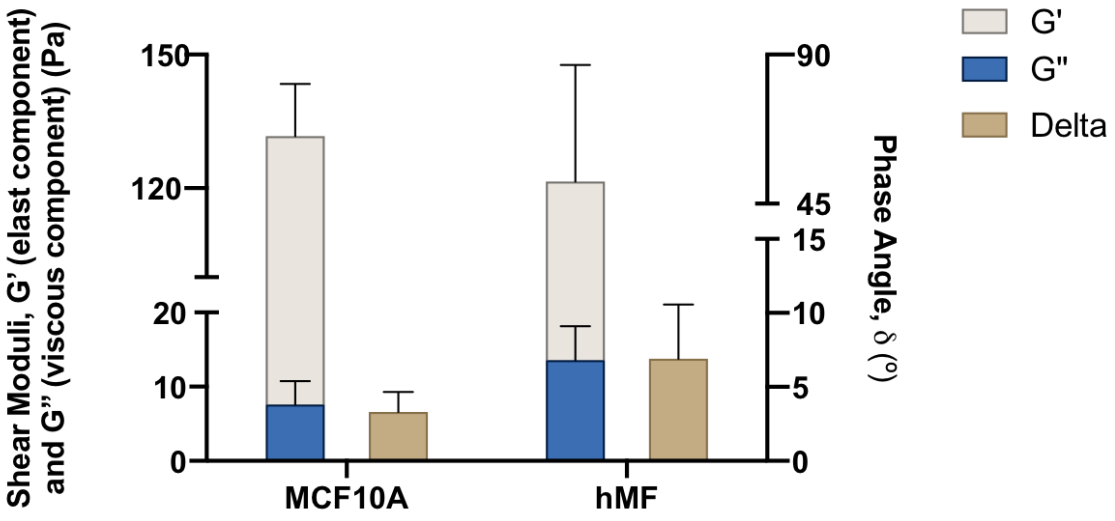

Figure 21 Rheometer analysis of MCF10A and hMF cells embedded within PVGLIG alginate at day 1 of culture. Viscoelastic properties (elastic, G' and viscous, G" components of the shear moduli, and phase angle, δ) of 1 wt.% oxidized PVGLIG-alginate with MCF10A and hMF.

3.4.2. Establishment of the parenchymal compartment

Following the study of the individual behavior of each of cell type upon culture within protease-sensitive hydrogels, we proceeded to the establishment of the co-culture 3D model, proposed in this work. For this, epithelial cells were mixed with oxidized PVGLIG-modified alginate hydrogel precursor solution and subsequently added to the pores of the 3D printed alginate scaffolds, 7-10 days after hMF seeding, leading to the establishment of a hybrid 3D co-culture model. In this setting, hydrogel-entrapped epithelial cells were grown for an additional period of 7-14 days. Notably, the scaffold circular shape was highly advantageous for gel incorporation, since it allowed for the cell-laden pre-gel to be fully retained within the scaffolds' pores, without flowing before the sol-gel transition. After gelling, 11mm-diameter discs were obtained, as depicted in **Figure 22Ai**, which displayed a good overall structural stability for, at least, 14 days of culture (**Figure S3**). Following 14 days of culture, scaffolds were analyzed by CLSM (**Figure 22**).

Figure 22A shows that fibroblasts attached to the scaffolds' fibers were able to progressively invade and migrate throughout the oxidized PVGLIG-alginate along the first 2 weeks of co-culture. Indeed, by day 14 it was possible to observe hMF in the center regions of the scaffolds' pores, where fibroblastic networks were established. At the same time, MCF10A cells were found distributed throughout the scaffold, namely within the pores, where they proliferated and assembled into spheroids and acini-like structures resembling to the ones previously documented [114]. Notably, in this model fibroblasts were apparently able to migrate towards the growing spheroids, hence enabling the successful establishment of direct heterotypic cell-cell contacts throughout the construct, as envisaged (**Figure 22B**;**Figure S 4**).

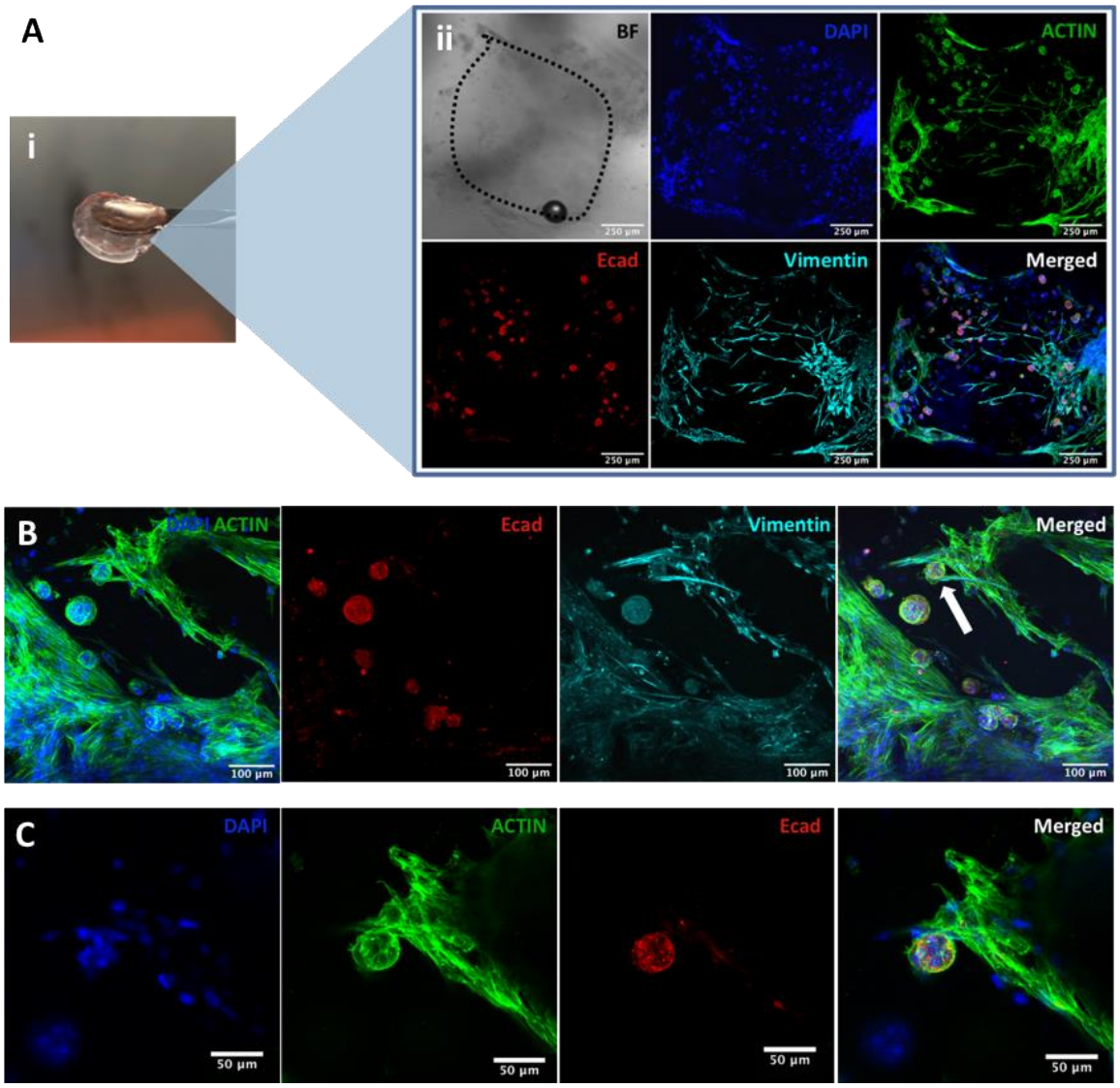

Figure 22 - hMF and MCF10A co-culture in alginate scaffolds. A) Representative image of the whole-mounted alginate scaffolds i), and CLSM images of alginate scaffolds seeded with $3.25x10^5$ hMFs and $4.0x10^5$ MCF10A - **Aii)**, **B)**, and **C)**. **Aii)** hMF migration towards central regions of pores was demonstrated at day 14 of culture, while epithelial cells were shown to be distributed throughout the pores, by F-actin (green), DAPI (blue), E-cadherin (red), and vimentin (cyan) stainings. Alginate-filled pore details are shown in BF images (black-dashed lines indicate pore periphery). **B)** hMF were able to migrate and establish juxtracrine interactions with multicellular MCF10A spheroids (white arrow), as demonstrated through F-actin (green), DAPI (blue), vimentin (cyan) E-cadherin (red) stainings, and from a **C)** detailed view (zoomed-in) of the corresponding area. Scale bars: 250 µm, 100 µm (10x, 30x and 60x magnification, respectively).

3.5. Separation of hMF and MCF10A cell populations from the alginate/ECM matrices after co-culture

After establishing the proposed 3D *in vitro* breast tissue model integrating both stromal and parenchymal compartments, we further explored the model as an *in vitro* platform for characterizing stromal-epithelial interactions. Besides microscopy techniques, such platform should also allow for more specific characterization of both cell types, namely at gene and protein

expression levels, following heterotypic interactions. Therefore, it should enable easy and mild retrieving of cells from constructs, for subsequent sorting and/or downstream analysis of distinct populations. For this, the possibility of reverting ionic crosslinks in alginate hydrogels, via treatment with chelating agents (EDTA or sodium citrate) that dissolve the hydrogel, is quite alluring, and it was one of the main reasons for having selected alginate to build the model. In addition to the use of chelating agents, alginate hydrogels can also be treated with naturally occurring enzymes, such as alginate lyase, that are capable of degrading alginate polymer chains through cleavage of glycosidic bonds [144]. Notably, after removing the cells from the dissolved hydrogel solution, we decided to analyse also the solution, in an attempt to identify secreted ECM components that had be retained within the polymeric network.

Herein, cell retrieval was promoted after 7 days of co-culture, by treating the alginate whole mounted constructs with alginate lyase, calcium chelating agents, and trypsin, in order to promote the dissolution of alginate hydrogels, and also disrupt cell-cell and cell-matrix interactions. Afterwards, cells were analysed/sorted by flow cytometry, to discriminate epithelial and fibroblastic cell populations, whereas the solution was further processed for proteomic analysis (**Figure S 5**).

3.5.1. Sorting of hMF and MCF10A populations

Flow cytometry analysis was performed using antibodies for CD90 (Thy-1) and E-cadherin markers to selectively stain hMF and MCF10A cells, respectively (**Figure 23**). CD90 consists in a glycosylphosphatidylinositol (GPI)-anchored outer membrane leaflet glycoprotein, that is found to be expressed in several cellular populations, such as fibroblasts [145]. Herein, stained and unstained 3D monocultures of each cell population were employed as positive and negative controls, respectively. In addition, unstained 3D co-cultures were also used as negative controls (**Figure S 6**).

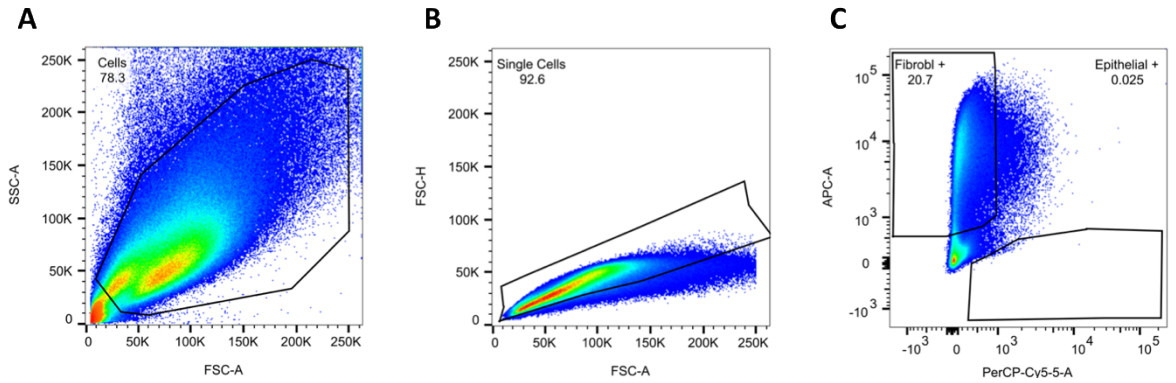

Figure 23. Representative gating strategy for immunophenotypic FC analysis of cells retrieved from the hybrid system. (A) Cells were first gated in an FSC-A vs. SSC-A plot, according to their size (SSC- side scatter) and granularity (FSC—forward scatter), **(B)** followed by debris and doublet exclusion on an FSC-A vs. FSC-H plot. **(C)** Dot plot of PerP-Cy-5-A (E-Cadherin) vs. APC (CD90) showing separation of epithelial-like and fibroblastic-like populations.

In our previous study [130], an anti E-cadherin antibody presenting a binding site within the intracellular domain of E-cadherin was used for the staining of epithelial cells in FC experiments. Hence, a prior cell permeabilization step was required in the FC preparation protocol, which could promote overall cell death along the staining process, resulting in a diminished number of cells obtained after sorting, hindering downstream analysis of isolated cells. To circumvent this limitation, we sought to employ a different anti E-cadherin antibody, presenting a binding site within the extracellular domain of E-cadherin, discarding the need for cell permeabilization. As seen in **Figure 23**, 20.7% of the events could be considered $CD90^{+}Ecad^{-}$, thus relating to hMF, which represents the successful isolation of a sufficient number of cells from this population. However, only 0.025% of the events were $CD90^{-}Ecad^{+}$, corresponding to MCF10A epithelial cells, which was insufficient for subsequent analysis. Given that the whole-mounted scaffolds were seeded with an approximate hMF/MCF10A ratio of 1:1, and taking into account the low efficiency of hMF-seeding and the high MCF10A proliferation rates (spheroids are formed by clonal proliferation [114]), we were expecting to isolate a greater proportion of epithelial vs. fibroblastic cells, as observed in our previous work [130]. Still, we do not know how both cells types actually proliferate in the present system, and it is possible that the protease-sensitive alginate hydrogels may favor fibroblasts proliferation and colonization of the pores, as compared to hMF cultures within protease-insensitive alginate [130]. On the other hand, the low number of $C90^{-}Ecad^{+}$ events may result from inadequate staining, namely due to internalization of E-cadherin adhesion molecules by MCF10A, upon being subjected to the FC preparation protocol. It has been shown that the intracellular pool of E-cadherin undergoing endocytosis is rapidly increased in response to destabilized cell-cell contacts and a depletion of extracellular Ca^{2+} [146]. Hence, the treatment of epithelial cells with trypsin and calcium chelating agents may have prompt the E-cadherin endocytosis, limiting MCF10A staining. In future experiments, this could be solved by resorting to other epithelial-specific markers, as EpCAM, a Ca^{2+}-independent transmembrane glycoprotein polypeptide that mediates homotypic cell-cell adhesion [147], [148].

Following sorting, the hMF population was analyzed by rt-PCR analysis for the expression of collagen type I and III, and α-smooth muscle actin (αSMA), as compared with data obtained from hMF 3D monocultures (**Figure 24**). αSMA is a well-studied fibroblastic marker, that is found to be associated with the acquisition of contractile phenotypes, being typically up-regulated upon malignant transition to CAF [37]. These results provide a proof-of-concept that our model allows for the effective isolation of fibroblasts and downstream evaluation of the impact of the fibroblast-epithelial crosstalk on cell expression. There were no significant differences between the expression of the selected genes by fibroblasts cultured in the presence or absence of epithelial cells, but more genes should be evaluated in future studies. Nevertheless, it remains urgent to proper refine the FACS preparation protocol, namely through the improvement of staining procedures, so that both cell populations under study may be adequately sorted through FACS and subsequently analyzed.

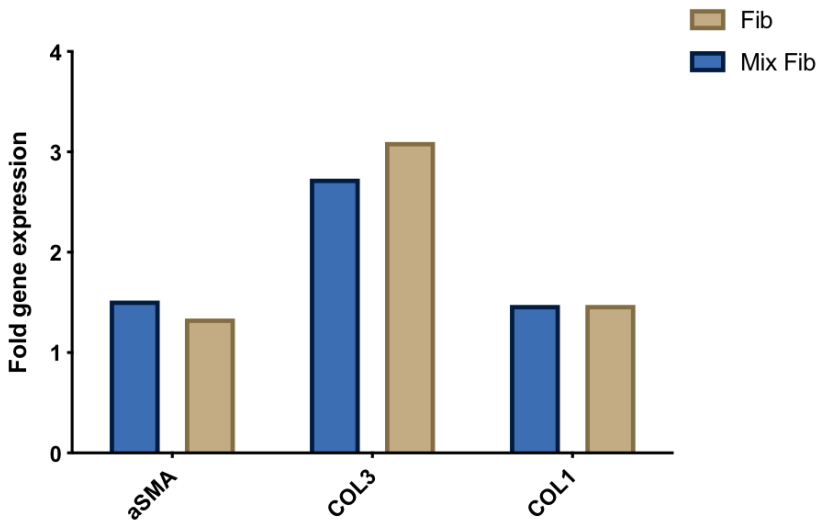

Figure 24. rt-PCR analysis of hMF following 1 week of 3D co-culture. The hMF expression of α-smooth muscle actin, collagen type I and III, was analysed after a 1-week culture with MCF10A cells (Mix Fib) and a 2-week 3D monoculture setting. Results are normalized for the housekeeping gene GAPDH.

3.5.2. Analysis of cell-derived extracellular proteins

Through proteomic analysis of the processed extracellular solution, following co-culture, several relevant extracellular proteins were detected and identified (**Figure 25**). These included either core-matrisome and matrisome-associated proteins, which play prominent roles regarding ECM maintenance and remodeling. Core-matrisome comprises a list of almost 300 ECM-proteins/glycans (including 43 collagen subunits, ca. 46 proteoglycans and 200 glycoproteins), identified through the analysis of both human and mouse genome [149]. In contrast, matrisome-associated proteins comprise an array of proteins that interact with ECM proteins but are not considered as ECM-proteins. This group can be further categorized into ECM-regulator proteins (as MMPs or crosslinking enzymes), ECM-affiliated proteins (as secreted C-type lectins), and soluble factors (as growth factors and cytokines) [149]. Herein, the presence of various types of proteins/glycans on the extracellular compartment of our model was identified, at different confidence levels. Some of the main identified core-matrisome proteins included: collagen type I, VI, and XII; fibronectin and laminin (glycoproteins); heparan sulfate (proteoglycans). Regarding some of the main matrisome-associated proteins, these included: plasminogen activator inhibitor-1 (ECM regulators); TGF- ß (soluble factors). Although this was a preliminary assay, the results demonstrate that during 3D co-culture different types of ECM-related compounds became retained in the alginate matrix, which can be easily recovered for analysis. Nevertheless, it is important to take into account the possible presence of contaminant proteins in the alginate-based extracellular solution that may be detected in this analysis. Such proteins could stem from the alginate itself (since the alginate purification process may be insufficient to completely extract all impurities), the cell media (even if the hydrogel was washed before being dissolved), and from cell-derived

contamination. Thus, in future experiments, it will be important to use cell-free alginate constructs as controls. All in all, these results further demonstrate the relevance of our model as an *in vitro* platform for dissecting stromal-epithelial crosstalk in breast tissue, allowing to elegantly assess alterations in the extracellular milieu, which should provide a key contribution for the for study of cell-matrix interactions.

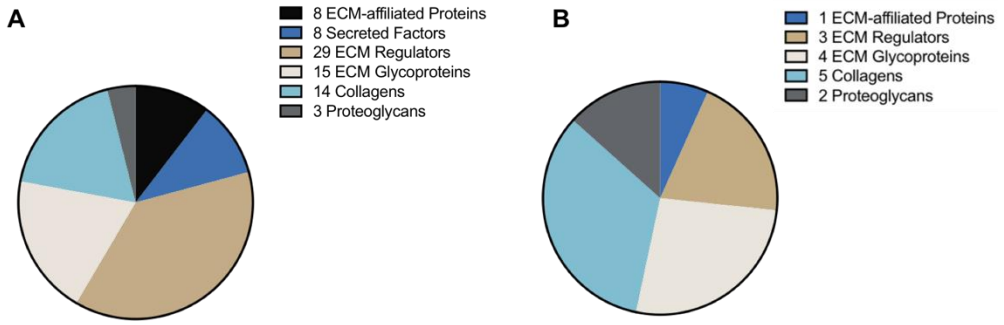

Figure 25. Proteomic analysis of co-culture-derived extracellular milieu after 7 days of co-culture. Through lower levels of confidence 77 ECM-associated proteins were identified **A)**, while through higher levels of confidence 15 ECM-associated proteins were identified **B)**.

3.6. Decellularization of scaffolds to study interactions between hMF-derived ECM and epithelial cells

Aside from the establishment of fibroblast-epithelial cell co-cultures, other variations of the 3D model proposed herein, may also be employed. For instance, before the addition of the epithelial cell-laden hydrogel, the stromal compartment of the hMF-seeded scaffolds could be decellularized, to obtain ECM-coated alginate scaffolds. This approach would allow isolating the effect of the fibroblast-derived ECM on epithelial cells from heterotypic cell-cell interactions. For such, it is necessary to promote the efficient removal of cells and cellular remnants from the scaffold, while ensuring that the ultrastructure and biochemical/biomechanical properties of the fibroblast-derived ECM are well preserved. For this goal, hMF-seeded scaffolds were subjected to a decellularization protocol based on Triton-X detergent with NH_4OH, adapted from previous optimizations performed in our lab (**Figure 26**).

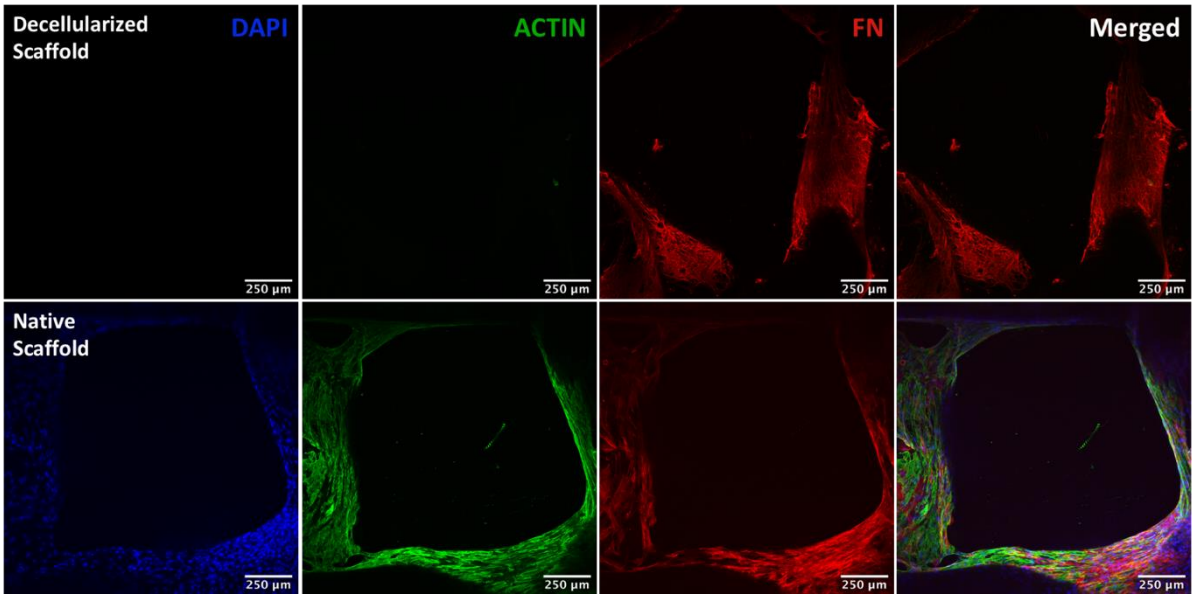

Figure 26. Decellularization preliminary results on 20 day-cultured hMFs. Representative CLSM images suggest that the decellularization protocol was successfully applied, leading to the apparent attainment of fibronectin-coated scaffolds, with no traces of F-actin or DAPI. CLSM images of native scaffolds, which did not undergo through the decellularization protocol, taken under the same conditions, served as controls.

Figure 26A suggests that the selected decellularization protocol was sufficient for removing all cellular traces, as decellularized scaffolds did not stain for F-actin (cell cytoskeleton) nor DAPI (cell nuclei), in contrast to non-decellularized scaffolds (**Figure 26B**) cultured for the same period of time. On the other hand, decellularized scaffolds stained for FN, suggesting that the ECM remained at the surface of the scaffolds retaining integrity to a great extent. However, despite such promising results, in future experiments it would be relevant to establish an adequate methodology to characterize the ECM, before and after decellularization, in order to demonstrate the maintenance of matrix composition, ultrastructure, and biomechanical performance after treatment. For instance, such ECM properties could be assessed through mass spectrometry-based proteomics, scanning electron microscopy (SEM), and microindentation respectively.

3.7. Microidentation of the whole-mounted scaffolds

As previously stated, it is well-known that cells are capable of sensing and processing mechanical signaling cues provided by their extracellular environment, that influence relevant physiological processes, as breast epithelial morphogenesis and disease progression. This is a result of mechanotransduction phenomena, in which the interactions established between the cells' cytoskeleton and their surrounding ECM trigger important intracellular signaling cascades that are pivotal for determining cell fate.

Within the 3D model proposed in this work, fibroblasts are expected to effectively migrate and colonize the scaffold's pores, while degrading the surrounding alginate and depositing endogenous ECM, leading to considerable alterations of the construct's stiffness along culture. Also, analyzing the stiffness throughout culture would be key to better understand the stromal-epithelial cross-talk, especially when using this model to recapitulate breast tumors, where matrix stiffness can be significantly altered. It is well-known that upon malignant transition to CAF, as a result of heterotypic interactions with tumour cells, the surrounding ECM undergoes changes mediated by malignant remodeling processes that typically lead to an increase of its stiffness. These changes in the ECM properties will, in turn, further influence epithelial cell behaviour. Hence, it would be highly relevant to be able to assess the stiffness of the constructs, at different culture timepoints. For this reason, preliminary assessments of the construct's stiffness were performed, through microindentation, to further validate our model as a valuable platform for studying breast tissue, under both healthy and diseased settings (**Figure 27**). Mechanical evaluation through such tests is quite alluring, since it allows the probing of local gradients and heterogeneities in natural materials, as well as, the examination of their hierarchical and multiscale organization, while dismissing extensive sample preparation [150].

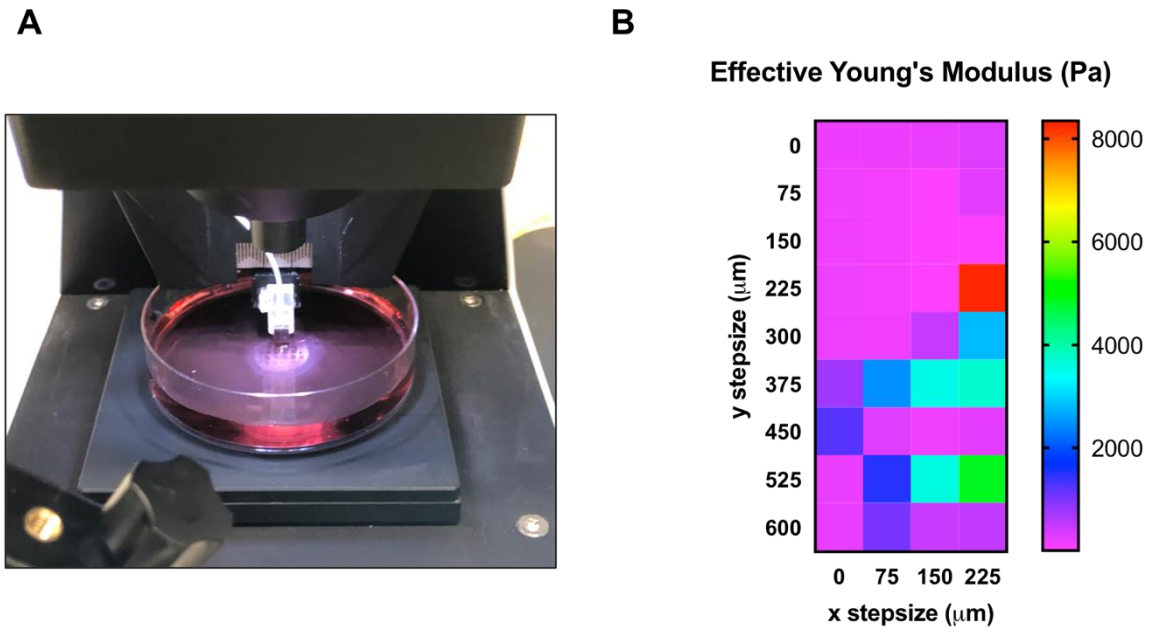

Figure 27. Microidentation of whole-mounted scaffolds. A) Representative image of the experimental setup. **B)** Heatmap of the effective Young's modulus measured through microindentation analysis of the whole-mounted scaffolds, after 1 day of co-culture. Young's modulus was measured throughout and 9x4 array, with a stepsize of 75μm.

Figure 27 depicts the different stiffnesses of a whole-mounted scaffold, measured throughout a 9x4 array, with a stepsize of 75 μm, after 1 day of co-culture. Through the observation of the obtained data, it is possible to denote that most of the analyzed construct's surface behaviour is quite soft (ca. 1000 Pa), with smaller regions of higher stiffnesses (in the range of 2 to >8 kPa).

These stiffer regions presumably correspondent to the 3D printed scaffold fibers, of higher alginate concentration (4 wt.%). While further optimizations are certainly needed to match the quantifications with images of the actual spatial region being analyzed, these preliminary results were important to show that this type of analysis can effectively be done in our system and is sensitive enough to detect regional differences in stiffness.

4. Concluding Remarks and future Perspectives

The breast is a highly heterogeneous and dynamic tissue, which undergoes extensive functional and structural changes throughout the different stages of the female reproductive cycle, or during disease. The mammary glands are surrounded by stromal tissue, characterized by the presence of several cell types, including fibroblasts, and a complex ECM network. **Epithelial-stromal interactions are of uttermost importance for breast tissue development, homeostasis, and disease, but they are still poorly understood, demanding further research**.

In this regard, 2D monolayer cultures on plastic have been largely employed to study normal and pathological breast tissue. These simplistic models are advantageous since they offer high control over the experimental variables, in contrast to *in vivo* animal models, but they poorly resemble the structure and function of the mammary tissue. Hence, in the past few years, there has been an incremental **interest to develop more advanced 3D *in vitro* models** which provide a good compromise between the simplicity of *in vitro* 2D models and the complexity of *in vivo* animal models. In this context, the fields of biomaterials and tissue engineering have been rapidly evolving, and thus, the engineering of human-representative 3D breast models is becoming a reality. Nonetheless, advanced 3D *in vitro* breast models, suitable for studying heterotypic cell-cell and cell-matrix interaction, are still lacking.

The goal of this work was to develop an integrative 3D *in vitro* model of breast tissue, combining fibroblasts and their ECM with epithelial cells, for the study of healthy and pathological processes. A previous work from our lab [130] reported the development of a 3D *in vitro* model of breast tissue, combining fibroblasts with epithelial cells in hybrid alginate scaffolds. 3D printed square-shaped RGD-alginate scaffolds were colonized with human mammary fibroblasts, which were able to adhere, spread and produce ECM. On a second stage, an RGD-alginate pre-gel with mammary epithelial cells was used to fill the scaffold's pores, forming a hydrogel *in situ* by ionic crosslinking. Throughout time, epithelial cells formed acini-like structures, in close proximity with fibroblasts and their ECM. Although this hybrid 3D system successfully recreated some key features of both stromal and parenchymal compartments of breast tissue, and promoted heterotypic cell-cell crosstalk, **it presented some limitations in terms of scaffolds' properties.** In particular, scaffolds: i) were produced with non-purified alginate, with less defined composition; ii) were square-shaped, and so did not fit adequately into the wells of standard tissue culture plates, and iii) had to be produced shortly before being used. Importantly, the hydrogel used for epithelial culture was not permissive to fibroblasts proteolytic invasion, hindering direct stromal-epithelial cell-to-cell contact.

To address those limitations, the key goal of this thesis was to further improve the model, by: A) refining the design of the 3D printed scaffolds, namely via Ai) the use of purified alginate

(instead of raw alginate), the Aii) production of disc-shaped scaffolds (instead of square-shaped), and iii. the production of ready-to-use lyophilized scaffolds; **and B) using a protease-degradable hydrogel for the epithelial cultures**, to promote fibroblast invasion and heterotypic cell-cell communication. In addition, we **C) tested the ability to decellularize fibroblast-colonized 3D printed scaffolds**.

In a first step, we have demonstrated the capability of printing 11mm-diameter circular scaffolds, that tightly fit to 48 multi-well plates, improving retention of seeded cells in the scaffold, while using purified alginate, instead of raw alginate. This allowed us to produce alginate scaffolds with lower level of impurities, which are often present within raw alginate and may impact cell behaviour and compromise experimental reproducibility [105]. Furthermore, preliminary scaffold lyophilization experiments were also performed, showing that the lyophilization process did not impair scaffold overall structure, and preserved both their circular-shape and macroporous structure. Notably, upon rehydration, scaffolds regained their original dimensions, and thus perfectly readapted to the 48 multi-well plates.

Optimized scaffolds were seeded with human mammary fibroblasts (hMF) and the effect of different parameters, such as RGD concentration, scaffold design, and cell seeding density/regimen were tested. We demonstrated the successful establishment of a mammary stromal compartment, through static seeding of hMF suspensions onto the 3D printed structures. This was characterized by the presence of spread fibroblasts distributed throughout the scaffolds' fibres, which were capable of producing several ECM components, such as fibronectin, collagen type I and IV, that organized into fibrillar networks. The same was obtained using a lyophilized scaffold, in a preliminary experiment, where rehydration was promoted simultaneously to seeding. These were promising results, but the experiments should be repeated in the future, to ensure statically significant results that support findings discussed herein. As for the lyophilised scaffolds, a more detailed assessment of the impact of freeze-drying steps on scaffold structural stability is also needed. Importantly, although proper scaffold colonization required a second seeding step, the process was still substantially improved, as compared to that reported in the previous work from our lab, which required higher cell seeding densities and longer culture times [130]. Still, the efficiency of this strategy can be further increased, by optimization of different parameters. For example, in future experiments, alginate scaffolds could be coated with common cell-adhesive substrates, such as poly-lysine, which is positively charged and would thus electrostatically interact with the negatively charged polymer and also with the seeded cells, potential improving adhesion and overall retention [134], [151]. Furthermore, a dynamic seeding approach, for example with shaking during the initial incubation period, could eventually be tested as a way to improve the seeding efficiency [134]–[136].

To assess the effect of protease sensitive hydrogel on the behavior of stromal and parenchymal cells, fibroblasts and epithelial cells were embedded in oxi-PVGLIG-modified alginate pre-gel solution and mono-cultured in 3D. Fibroblasts were shown to retain high viability (similar to that

of blank alginate hydrogel), while being able to spread and establish intricate cellular networks, in contrast with unmodified hydrogel where they remained round. In turn, epithelial cells were able to assemble and undergo epithelial morphogenesis, leading to generation of multicellular spheroids, with dimensions similar to the control alginate hydrogels and as previously documented [114]. In parallel experiments, rheological analysis of these monocultures showed that hydrogel stiffness was similar to that of native mammary tissue. These analyses were only conducted at the first day of culture, due to the ability of fibroblasts to contract and remodel the surrounding 3D network along culture, which significantly decreased the diameter of the samples and precluded analysis by oscillation rheometry. However, in future experiments, it will be important to analyze the evolution of rheological properties along culture, to ensure that the presented stiffness remains similar to that of the mammary tissue throughout time. Also, it will be important to analyze the control hydrogels, to be able to discriminate between mechanical and biochemical effects of the different hydrogel formulations on cell response.

Following monoculture characterization, the epithelial-laden solution was used to fill the pores of the printed scaffolds, forming a hydrogel *in situ*. Besides paracrine interactions mediated through the secretion of soluble factors, which can diffuse through the highly hydrated hydrogel network, this model was also able to support a much more expressive establishment of direct heterotypic cell-cell contacts, in comparison to our previous model, providing a closer environment to that of the *in vivo* setting. Nonetheless, in future studies, more attention should be focused on understanding the extent to which fibroblasts are able to establish ECM-derived networks throughout these hydrogels, as well as, the related kinetics of PVGLIG degradation, mediated by cells, through enzymatic degradation assays.

To further demonstrate the potential of the model proposed herein, we sought to retrieve cells cultured within the construct, after hydrogel dissolution, and discriminate them into different populations by FC followed by PCR analysis of phenotypic markers. Furthermore, after removing the cells from the dissolved hydrogel solution, we also decided to analyse the obtained solution by proteomic analysis, in an attempt to identify secreted ECM components that could be retained within the polymeric network. Although both processes are far from being optimized, especially the sorting of sufficient amounts of well-discriminated cell populations, the possibility of retrieving both the cells and the cell-derived extracellular components from the construct is of major relevance. In future studies, it will certainly allow a truly integrative analysis of cell-cell and cell-matrix interactions. Indeed, in a proof-of-concept experiment we have shown to be able to assess expression of a few genes (αSMA, collagen type I and III) in the isolated fibroblast population, but many others can be studied. Notably, from the proteomic analysis of the obtained solution, several relevant ECM-associated could detected and identified. However, alginate used herein may also include extrinsic proteins that may be eventually detected in this analysis, along with other media- or cell-derived contaminants, hence, in future experiments alginate-only controls should be used.

Additionally, decellularized scaffolds were successfully obtained, following fibroblast culture. In the future, this will allow the creation of an alternative type of model, which would not include coculturing fibroblasts, but only their matrix, as a cell-derived matrix where epithelial cells could be cultured and, cell-ECM interactions could be studied on an isolated fashion.

Finally, assessments of the construct's stiffness were performed through microindentation. In this experiment, we were able to measure different values of stiffness throughout the whole-mounted scaffold's surface, where most of its surface was quite soft (ca. 1000 Pa), while smaller regions were clearly stiffer (in the range of 2 to >8 kPa), the latter regions probably corresponding to the alginate printed fibers, whit more concentrated alginate. While further optimizations are certainly needed, these results further validate our model as a valuable platform for studying breast tissue, demonstrating that regional stiffness can be analyzed in a highly sensitive manner.

Collectively, along this work we were able to demonstrate that the developed model, where fibroblasts and epithelial cells were co-cultured in the same 3D microenvironment, recapitulates key aspects of stromal-parenchymal interactions in breast tissue. Thus, **such 3D model is expected to provide a versatile bioengineered platform to study, *in vitro*, the dynamics of breast tissue alterations, both at cellular and matrix levels, under healthy and pathological conditions**. Importantly, this model could incorporate additional cell types, or be adapted for mimicking other tissues. For personalized medicine approaches, patient-derived cells could also be used, to reflect person-specific traits.

References

[1] "WHO | Top 10 causes of death," *WHO*, 2019. [Online]. Available: https://www.who.int/gho/mortality_burden_disease/causes_death/top_10/en/. [Accessed: 24-Apr-2020].

[2] "WHO | Breast cancer," *WHO*, 2018. [Online]. Available: https://www.who.int/cancer/prevention/diagnosis-screening/breast-cancer/en/. [Accessed: 24-Apr-2020].

[3] X. Dai *et al.*, "Breast cancer intrinsic subtype classification, clinical use and future trends," *American Journal of Cancer Research*, vol. 5, no. 10. E-Century Publishing Corporation, pp. 2929–2943, 2015.

[4] G. Gambar, M. Gaeble, U. Keilhol, C. R. A. Regenbrecht, and A. Silvestri, "From chemotherapy to combined targeted therapeutics: In vitro and in vivo models to decipher intra-tumor heterogeneity," *Frontiers in Pharmacology*, vol. 9, no. FEB. Frontiers Media S.A., 14-Feb-2018.

[5] S. Cleator, W. Heller, and R. C. Coombes, "Triple-negative breast cancer: therapeutic options," *Lancet Oncology*, vol. 8, no. 3. pp. 235–244, Mar-2007.

[6] C. Toniatti, P. Jones, H. Graham, B. Pagliara, and G. Draetta, "Oncology drug discovery: Planning a turnaround," *Cancer Discov.*, vol. 4, no. 4, pp. 397–404, Apr. 2014.

[7] X. Wang, L. Sun, M. V. Maffini, A. Soto, C. Sonnenschein, and D. L. Kaplan, "A complex 3D human tissue culture system based on mammary stromal cells and silk scaffolds for modeling breast morphogenesis and function," *Biomaterials*, vol. 31, no. 14, pp. 3920–3929, May 2010.

[8] M. M. Morgan, L. A. Schuler, J. C. Ciciliano, B. P. Johnson, E. T. Alarid, and D. J. Beebe, "Modeling chemical effects on breast cancer: the importance of the microenvironment in vitro," *Integr. Biol.*, vol. 12, no. 2, pp. 21–33, Mar. 2020.

[9] M. C. Regier, E. T. Alarid, and D. J. Beebe, "Progress towards understanding heterotypic interactions in multi-culture models of breast cancer," *Integrative Biology (United Kingdom)*, vol. 8, no. 6. Royal Society of Chemistry, pp. 684–692, 01-Jun-2016.

[10] N. K. Paschos, W. E. Brown, R. Eswaramoorthy, J. C. Hu, and K. A. Athanasiou, "Advances in tissue engineering through stem cell-based co-culture," *Journal of Tissue Engineering and Regenerative Medicine*, vol. 9, no. 5. John Wiley and Sons Ltd, pp. 488–503, 01-May-2015.

[11] J. Radhakrishnan, S. Varadaraj, S. K. Dash, A. Sharma, and R. S. Verma, "Organotypic cancer tissue models for drug screening: 3D constructs, bioprinting and microfluidic chips," *Drug Discovery Today*. Elsevier Ltd, 09-Mar-2020.

[12] S. Krause, M. V. Maffini, A. M. Soto, and C. Sonnenschein, "A novel 3D in vitro culture model to study stromal-epithelial interactions in the mammary gland," *Tissue Eng. - Part C Methods*, vol. 14, no. 3, pp. 261–271, Sep. 2008.

[13] X. Yin, B. E. Mead, H. Safaee, R. Langer, J. M. Karp, and O. Levy, "Engineering Stem Cell Organoids," *Cell Stem Cell*, vol. 18, no. 1. Cell Press, pp. 25–38, 07-Jan-2016.

[14] E. R. Shamir and A. J. Ewald, "Three-dimensional organotypic culture: Experimental models of mammalian biology and disease," *Nature Reviews Molecular Cell Biology*, vol. 15, no. 10. Nature Publishing Group, pp. 647–664, 01-Jan-2014.

[15] F. Hirschhaeuser, H. Menne, C. Dittfeld, J. West, W. Mueller-Klieser, and L. A. Kunz-Schughart, "Multicellular tumor spheroids: An underestimated tool is catching up again," *J. Biotechnol.*, vol. 148, no. 1, pp. 3–15, Jul. 2010.

[16] G. Bahcecioglu, G. Basara, B. W. Ellis, X. Ren, and P. Zorlutuna, "Breast cancer models: Engineering the tumor microenvironment," *Acta Biomaterialia*, vol. 106. Acta Materialia Inc, pp. 1–21, 01-Apr-2020.

[17] I. D. Premaratne, Y. Toyoda, K.-B. Celie, K. A. Brown, and J. A. Spector, "Tissue Engineering Models for the Study of Breast Neoplastic Disease and the Tumor Microenvironment," *Tissue Eng. Part B Rev.*, Feb. 2020.

[18] K. Ling *et al.*, "Bioprinting-Based High-Throughput Fabrication of Three-Dimensional MCF-

7 Human Breast Cancer Cellular Spheroids," *Engineering*, vol. 1, no. 2, pp. 269–274, Jun. 2015.

[19] A. Boussommier-Calleja, "In vitro models of cancer," in *Bioengineering Innovative Solutions for Cancer*, Elsevier, 2020, pp. 273–325.

[20] J. M. Guinebretière, E. Menet, A. Tardivon, P. Cherel, and D. Vanel, "Normal and pathological breast, the histological basis," *Eur. J. Radiol.*, vol. 54, no. 1, pp. 6–14, 2005.

[21] H. Ellis and V. Mahadevan, "Anatomy and physiology of the breast," *Surgery (United Kingdom)*, vol. 31, no. 1. Elsevier Ltd, pp. 11–14, 01-Jan-2013.

[22] J. L. McManaman and M. C. Neville, "Mammary physiology and milk secretion," *Advanced Drug Delivery Reviews*, vol. 55, no. 5. Elsevier, pp. 629–641, 29-Apr-2003.

[23] L. Kass, J. T. Erler, M. Dembo, and V. M. Weaver, "Mammary epithelial cell: Influence of extracellular matrix composition and organization during development and tumorigenesis," *International Journal of Biochemistry and Cell Biology*, vol. 39, no. 11. pp. 1987–1994, 2007.

[24] C. Frantz, K. M. Stewart, and V. M. Weaver, "The extracellular matrix at a glance," *Journal of Cell Science*, vol. 123, no. 24. Company of Biologists, pp. 4195–4200, 15-Dec-2010.

[25] American Cancer Society, "Breast Density and Your Mammogram Report," 25-Oct-2020. [Online]. Available: https://www.cancer.org/cancer/breast-cancer/screening-tests-and-early-detection/mammograms/breast-density-and-your-mammogram-report.html#written_by. [Accessed: 29-Oct-2020].

[26] M. A. Cichon, A. C. Degnim, D. W. Visscher, and D. C. Radisky, "Microenvironmental influences that drive progression from benign breast disease to invasive breast cancer," *Journal of Mammary Gland Biology and Neoplasia*, vol. 15, no. 4. Springer, pp. 389–397, Dec-2010.

[27] "A Medium Corporation (2018) , Breast Cancer : Invasive Ductal Carcinoma (IDC)." [Online]. Available: https://medium.com/@indianflagco/breast-cancer-invasive-ductal-carcinoma-idc-19fc57e3743d. [Accessed: 29-Oct-2020].

[28] B. Yue, "Biology of the extracellular matrix: An overview," *Journal of Glaucoma*, vol. 23, no. 8. Lippincott Williams and Wilkins, pp. S20–S23, 10-Dec-2014.

[29] A. D. Theocharis, S. S. Skandalis, C. Gialeli, and N. K. Karamanos, "Extracellular matrix structure," *Advanced Drug Delivery Reviews*, vol. 97. Elsevier B.V., pp. 4–27, 01-Feb-2016.

[30] A. S. Dias, C. R. Almeida, L. A. Helguero, and I. F. Duarte, "Metabolic crosstalk in the breast cancer microenvironment," *European Journal of Cancer*, vol. 121. Elsevier Ltd, pp. 154–171, 01-Nov-2019.

[31] A. Birbrair, *Tumor microenvironment : non-hematopoietic cells*. Springer, 2020.

[32] J. Makki, "Diversity of breast carcinoma: Histological subtypes and clinical relevance," *Clin. Med. Insights Pathol.*, vol. 8, no. 1, pp. 23–31, 2015.

[33] A. C. Bateman and E. C. Shaw, "Breast pathology," *Surgery (United Kingdom)*, vol. 34, no. 1. Elsevier Ltd, pp. 1–7, 01-Jan-2016.

[34] X. J. Ma, S. Dahiya, E. Richardson, M. Erlander, and D. C. Sgroi, "Gene expression profiling of the tumor microenvironment during breast cancer progression," *Breast Cancer Res.*, vol. 11, no. 1, Feb. 2009.

[35] E. J. Brock, K. Ji, S. Shah, R. R. Mattingly, and B. F. Sloane, "In Vitro Models for Studying Invasive Transitions of Ductal Carcinoma In Situ," *Journal of Mammary Gland Biology and Neoplasia*, vol. 24, no. 1. Springer New York LLC, 15-Mar-2019.

[36] M. Nurmik, P. Ullmann, F. Rodriguez, S. Haan, and E. Letellier, "In search of definitions: Cancer-associated fibroblasts and their markers," *Int. J. Cancer*, vol. 146, no. 4, pp. 895–905, Feb. 2020.

[37] E. Sahai *et al.*, "A framework for advancing our understanding of cancer-associated fibroblasts," *Nature Reviews Cancer*, vol. 20, no. 3. Nature Research, pp. 174–186, 01-Mar-2020.

[38] J. Felipe Lima, S. Nofech-Mozes, J. Bayani, and J. Bartlett, "EMT in Breast Carcinoma—A Review," *J. Clin. Med.*, vol. 5, no. 7, p. 65, Jul. 2016.

[39] M. Fedele, L. Cerchia, and G. Chiappetta, "The epithelial-to-mesenchymal transition in breast cancer: Focus on basal-like carcinomas," *Cancers*, vol. 9, no. 10. MDPI AG, 01-Oct-2017.

[40] S. D. Soysal, A. Tzankov, and S. E. Muenst, "Role of the Tumor Microenvironment in Breast Cancer," *Pathobiology*, vol. 82, no. 3–4. S. Karger AG, pp. 142–152, 23-Sep-2015.

[41] Y. Miki, K. Ono, S. Hata, T. Suzuki, H. Kumamoto, and H. Sasano, “The advantages of co-culture over mono cell culture in simulating in vivo environment,” *Journal of Steroid Biochemistry and Molecular Biology*, vol. 131, no. 3–5. pp. 68–75, Sep-2012.

[42] J. T. Camp *et al.*, “Interactions with fibroblasts are distinct in basal-like and luminal breast cancers,” *Mol. Cancer Res.*, vol. 9, no. 1, pp. 3–13, Jan. 2011.

[43] U. E. Martinez-Outschoorn *et al.*, “Tumor cells induce the cancer associated fibroblast phenotype via caveolin-1 degradation: Implications for breast cancer and DCIS therapy with autophagy inhibitors,” *Cell Cycle*, vol. 9, no. 12, pp. 2423–2433, Jun. 2010.

[44] M. Q. Gao *et al.*, “Stromal fibroblasts from the interface zone of human breast carcinomas induce an epithelial-mesenchymal transition-like state in breast cancer cells in vitro,” *J. Cell Sci.*, vol. 123, no. 20, pp. 3507–3514, Oct. 2010.

[45] J. T. Emerman and D. R. Pitelka, “Maintenance and induction of morphological differentiation in dissociated mammary epithelium on floating collagen membranes,” *In Vitro*, vol. 13, no. 5, pp. 316–328, May 1977.

[46] E. Y. H. Lee, G. Parry, and M. J. Bissell, “Modulation of secreted proteins of mouse mammary epithelial cells by the collagenous substrata,” *J. Cell Biol.*, vol. 98, no. 1, pp. 146–155, 1984.

[47] E. Y. H. P. Lee, W. H. Lee, C. S. Kaetzel, G. Parry, and M. J. Bissell, “Interaction of mouse mammary epithelial cells with collagen substrata: Regulation of casein gene expression and secretion,” *Proc. Natl. Acad. Sci. U. S. A.*, vol. 82, no. 5, pp. 1419–1423, 1985.

[48] N. Boudreau, C. Myers, and M. J. Bissell, “From laminin to lamin: regulation of tissue-specific gene expression by the ECM,” *Trends Cell Biol.*, vol. 5, no. 1, pp. 1–4, Jan. 1995.

[49] C. H. Streuli and M. J. Bissell, “Expression of extracellular matrix components is regulated by substratum,” *J. Cell Biol.*, vol. 110, no. 4, pp. 1405–1415, 1990.

[50] H. G. Hall, D. A. Farson, and M. J. Bissell, “Lumen formation by epithelial cell lines in response to collagen overlay: a morphogenetic model in culture.,” *Proc. Natl. Acad. Sci. U. S. A.*, vol. 79, no. 15, pp. 4672–4676, 1982.

[51] T. Gudjonsson, L. Rønnov-Jessen, R. Villadsen, F. Rank, M. J. Bissell, and O. W. Petersen, “Normal and tumor-derived myoepithelial cells differ in their ability to interact with luminal breast epithelial cells for polarity and basement membrane deposition,” *J. Cell Sci.*, vol. 115, no. 1, pp. 39–50, 2002.

[52] S. A. Lelièvre *et al.*, “Tissue phenotype depends on reciprocal interactions between the extracellular matrix and the structural organization of the nucleus,” *Proc. Natl. Acad. Sci. U. S. A.*, vol. 95, no. 25, pp. 14711–14716, Dec. 1998.

[53] O. W. Petersen, L. Ronnov-Jessen, A. R. Howlett, and M. J. Bissell, “Interaction with basement membrane serves to rapidly distinguish growth and differentiation pattern of normal and malignant human breast epithelial cells,” *Proc. Natl. Acad. Sci. U. S. A.*, vol. 89, no. 19, pp. 9064–9068, 1992.

[54] B. Weigelt and M. J. Bissell, “Unraveling the microenvironmental influences on the normal mammary gland and breast cancer,” *Seminars in Cancer Biology*, vol. 18, no. 5. NIH Public Access, pp. 311–321, Oct-2008.

[55] P. A. Kenny *et al.*, “The morphologies of breast cancer cell lines in three-dimensional assays correlate with their profiles of gene expression,” *Mol. Oncol.*, vol. 1, no. 1, pp. 84–96, Jun. 2007.

[56] B. K. Jong, R. Stein, and M. J. O’Hare, “Three-dimensional in vitro tissue culture models of breast cancer - A review,” *Breast Cancer Research and Treatment*, vol. 85, no. 3. pp. 281–291, Jun-2004.

[57] K. J. Cheung, E. Gabrielson, Z. Werb, and A. J. Ewald, “Collective invasion in breast cancer requires a conserved basal epithelial program,” *Cell*, vol. 155, no. 7, pp. 1639–1651, Dec. 2013.

[58] K. R. Levental *et al.*, “Matrix Crosslinking Forces Tumor Progression by Enhancing Integrin Signaling,” *Cell*, vol. 139, no. 5, pp. 891–906, Nov. 2009.

[59] N. R. Lang *et al.*, “Biphasic response of cell invasion to matrix stiffness in three-dimensional biopolymer networks,” *Acta Biomater.*, vol. 13, pp. 61–67, Feb. 2015.

[60] K. E. Sung, X. Su, E. Berthier, C. Pehlke, A. Friedl, and D. J. Beebe, “Understanding the Impact of 2D and 3D Fibroblast Cultures on In Vitro Breast Cancer Models,” *PLoS One*, vol. 8, no. 10, Oct. 2013.

[61] H. Jaganathan *et al.*, “Three-dimensional in vitro co-culture model of breast tumor using

magnetic levitation," *Sci. Rep.*, vol. 4, no. 1, pp. 1–9, Oct. 2014.
[62] F. Keller, R. Rudolf, and M. Hafner, "Towards optimized breast cancer 3D spheroid mono- and co-culture models for pharmacological research and screening," *J. Cell. Biotechnol.*, vol. 5, no. 2, pp. 89–101, Jan. 2019.
[63] E. L. S. Fong, D. A. Harrington, M. C. Farach-Carson, and H. Yu, "Heralding a new paradigm in 3D tumor modeling," *Biomaterials*, vol. 108. Elsevier Ltd, pp. 197–213, 01-Nov-2016.
[64] S. L. Ham, R. Joshi, P. S. Thakuri, and H. Tavana, "Liquid-based three-dimensional tumor models for cancer research and drug discovery," *Exp. Biol. Med.*, vol. 241, no. 9, pp. 939–954, 2016.
[65] S. L. Ham *et al.*, "Three-dimensional tumor model mimics stromal - breast cancer cells signaling," *Oncotarget*, vol. 9, no. 1, pp. 249–267, 2018.
[66] N. Anastasov *et al.*, "A 3D-microtissue-based phenotypic screening of radiation resistant tumor cells with synchronized chemotherapeutic treatment," *BMC Cancer*, vol. 15, no. 1, Dec. 2015.
[67] L. A. Kunz-Schughart, P. Heyder, J. Schroeder, and R. Knuechel, "A heterologous 3-D coculture model of breast tumor cells and fibroblasts to study tumor-associated fibroblast differentiation," *Exp. Cell Res.*, vol. 266, no. 1, pp. 74–86, May 2001.
[68] M. Majety, L. P. Pradel, M. Gies, and C. H. Ries, "Fibroblasts Influence Survival and Therapeutic Response in a 3D Co-Culture Model," *PLoS One*, vol. 10, no. 6, p. e0127948, Jun. 2015.
[69] D. L. Priwitaningrum *et al.*, "Tumor stroma-containing 3D spheroid arrays: A tool to study nanoparticle penetration," *J. Control. Release*, vol. 244, pp. 257–268, Dec. 2016.
[70] V. Brancato, F. Gioiella, G. Imparato, D. Guarnieri, F. Urciuolo, and P. A. Netti, "3D breast cancer microtissue reveals the role of tumor microenvironment on the transport and efficacy of free-doxorubicin in vitro," *Acta Biomater.*, vol. 75, pp. 200–212, Jul. 2018.
[71] V. Brancato *et al.*, "3D is not enough: Building up a cell instructive microenvironment for tumoral stroma microtissues," *Acta Biomater.*, vol. 47, pp. 1–13, Jan. 2017.
[72] T. Andersen, P. Auk-Emblem, and M. Dornish, "3D Cell Culture in Alginate Hydrogels," *Microarrays*, vol. 4, no. 2, pp. 133–161, Mar. 2015.
[73] J. W. Haycock, "3D cell culture: a review of current approaches and techniques.," *Methods in molecular biology (Clifton, N.J.)*, vol. 695. Methods Mol Biol, pp. 1–15, 2011.
[74] M. Bahram, N. Mohseni, and M. Moghtader, "An Introduction to Hydrogels and Some Recent Applications," in *Emerging Concepts in Analysis and Applications of Hydrogels*, InTech, 2016.
[75] B. Amsden, "Solute diffusion within hydrogels. Mechanisms and models," *Macromolecules*, vol. 31, no. 23, pp. 8382–8395, Nov. 1998.
[76] A. D. Augst, H. J. Kong, and D. J. Mooney, "Alginate hydrogels as biomaterials," *Macromol. Biosci.*, vol. 6, no. 8, pp. 623–633, Aug. 2006.
[77] E. Jabbari, J. Leijten, Q. Xu, and A. Khademhosseini, "The matrix reloaded: The evolution of regenerative hydrogels," *Materials Today*, vol. 19, no. 4. Elsevier B.V., pp. 190–196, 01-May-2016.
[78] C. D. Spicer, "Hydrogel scaffolds for tissue engineering: The importance of polymer choice," *Polymer Chemistry*, vol. 11, no. 2. Royal Society of Chemistry, pp. 184–219, 14-Jan-2020.
[79] A. Parak, P. Pradeep, L. C. du Toit, P. Kumar, Y. E. Choonara, and V. Pillay, "Functionalizing bioinks for 3D bioprinting applications," *Drug Discov. Today*, vol. 24, no. 1, pp. 198–205, Jan. 2019.
[80] M. C. Catoira, L. Fusaro, D. Di Francesco, M. Ramella, and F. Boccafoschi, "Overview of natural hydrogels for regenerative medicine applications," *J. Mater. Sci. Mater. Med.*, vol. 30, no. 10, pp. 1–10, Oct. 2019.
[81] B. Weigelt, C. M. Ghajar, and M. J. Bissell, "The need for complex 3D culture models to unravel novel pathways and identify accurate biomarkers in breast cancer," *Advanced Drug Delivery Reviews*, vol. 69–70. Elsevier, pp. 42–51, 2014.
[82] M. Hospodiuk, M. Dey, D. Sosnoski, and I. T. Ozbolat, "The bioink: A comprehensive review on bioprintable materials," *Biotechnol. Adv.*, vol. 35, no. 2, pp. 217–239, Mar. 2017.
[83] W. . Hennink and C. . van Nostrum, "Novel crosslinking methods to design hydrogels," *Adv. Drug Deliv. Rev.*, vol. 54, no. 1, pp. 13–36, Jan. 2002.
[84] H. Jung *et al.*, "Molecular tandem repeat strategy for elucidating mechanical properties of

high-strength proteins.," *Proc. Natl. Acad. Sci. U. S. A.*, vol. 113, no. 23, pp. 6478–83, Jun. 2016.

[85] B. Jeong, S. W. Kim, and Y. H. Bae, "Thermosensitive sol–gel reversible hydrogels," *Adv. Drug Deliv. Rev.*, vol. 64, pp. 154–162, Dec. 2012.

[86] F. Dolati, Y. Yu, Y. Zhang, A. M. De Jesus, E. A. Sander, and I. T. Ozbolat, "In vitro evaluation of carbon-nanotube-reinforced bioprintable vascular conduits.," *Nanotechnology*, vol. 25, no. 14, p. 145101, Apr. 2014.

[87] Z. Wang, R. Abdulla, B. Parker, R. Samanipour, S. Ghosh, and K. Kim, "A simple and high-resolution stereolithography-based 3D bioprinting system using visible light crosslinkable bioinks," *Biofabrication*, vol. 7, no. 4, p. 045009, Dec. 2015.

[88] S. A. Irvine *et al.*, "Printing cell-laden gelatin constructs by free-form fabrication and enzymatic protein crosslinking," *Biomed. Microdevices*, vol. 17, no. 1, p. 16, Feb. 2015.

[89] L. S. Moreira Teixeira, J. Feijen, C. A. van Blitterswijk, P. J. Dijkstra, and M. Karperien, "Enzyme-catalyzed crosslinkable hydrogels: Emerging strategies for tissue engineering," *Biomaterials*, vol. 33, no. 5, pp. 1281–1290, Feb. 2012.

[90] A. Bigi, G. Cojazzi, S. Panzavolta, N. Roveri, and K. Rubini, "Stabilization of gelatin films by crosslinking with genipin," *Biomaterials*, vol. 23, no. 24, pp. 4827–4832, Dec. 2002.

[91] A. Parak, P. Pradeep, L. C. du Toit, P. Kumar, Y. E. Choonara, and V. Pillay, "Functionalizing bioinks for 3D bioprinting applications," *Drug Discovery Today*, vol. 24, no. 1. Elsevier Ltd, pp. 198–205, 01-Jan-2019.

[92] J. H. Y. Chung *et al.*, "Bio-ink properties and printability for extrusion printing living cells," *Biomater. Sci.*, vol. 1, no. 7, p. 763, Jun. 2013.

[93] T. Pan, W. Song, and X. Cao, "3D Bioplotting of Gelatin/Alginate Scaffolds for Tissue Engineering: Influence of Crosslinking Degree and Pore Architecture on Physicochemical Properties," *J. Mater. Sci. Technol.*, vol. 32, no. 9, pp. 889–900, Sep. 2016.

[94] C. J. Olsen, J. Moreira, E. M. Lukanidin, and N. S. Ambartsumian, "Human mammary fibroblasts stimulate invasion of breast cancer cells in a three-dimensional culture and increase stroma development in mouse xenografts.," *BMC Cancer*, vol. 10, no. 1, p. 444, Dec. 2010.

[95] K. Xu and R. J. Buchsbaum, "Isolation of mammary epithelial cells from three-dimensional mixed-cell spheroid co-culture," *J. Vis. Exp.*, no. 62, p. 3760, Apr. 2012.

[96] I. Lühr *et al.*, "Mammary fibroblasts regulate morphogenesis of normal and tumorigenic breast epithelial cells by mechanical and paracrine signals," *Cancer Lett.*, vol. 325, no. 2, pp. 175–188, Dec. 2012.

[97] J. S. McLane and L. A. Ligon, "Stiffened Extracellular Matrix and Signaling from Stromal Fibroblasts via Osteoprotegerin Regulate Tumor Cell Invasion in a 3-D Tumor in Situ Model," *Cancer Microenviron.*, vol. 9, no. 2–3, pp. 127–139, Dec. 2016.

[98] Z. Koledova, "3D coculture of mammary organoids with fibrospheres: A model for studying epithelial–stromal interactions during mammary branching morphogenesis," in *Methods in Molecular Biology*, vol. 1612, Humana Press Inc., 2017, pp. 107–124.

[99] E. Dondajewska, W. Juzwa, A. Mackiewicz, and H. Dams-Kozlowska, "Heterotypic breast cancer model based on a silk fibroin scaffold to study the tumor microenvironment," *Oncotarget*, vol. 9, no. 4, pp. 4935–4950, 2018.

[100] X. Wang, L. Sun, M. V. Maffini, A. Soto, C. Sonnenschein, and D. L. Kaplan, "A complex 3D human tissue culture system based on mammary stromal cells and silk scaffolds for modeling breast morphogenesis and function," *Biomaterials*, vol. 31, no. 14, pp. 3920–3929, May 2010.

[101] G. Zhang *et al.*, "A simple 3D cryogel co-culture system used to study the role of CAFs in EMT of MDA-MB-231 cells," *RSC Adv.*, vol. 7, no. 28, pp. 17208–17216, Mar. 2017.

[102] M. F. Estrada *et al.*, "Modelling the tumour microenvironment in long-term microencapsulated 3D co-cultures recapitulates phenotypic features of disease progression," *Biomaterials*, vol. 78, pp. 50–61, Feb. 2016.

[103] M. K. Koch *et al.*, "Stromal fibroblasts regulate microvascular-like network architecture in a bioengineered breast tumour angiogenesis model," *Acta Biomater.*, vol. 114, pp. 256–269, Sep. 2020.

[104] K. Y. Lee and D. J. Mooney, "Alginate: Properties and biomedical applications," *Progress in Polymer Science (Oxford)*, vol. 37, no. 1. Elsevier Ltd, pp. 106–126, 01-Jan-2012.

[105] G. Orive, S. Ponce, R. M. Hernández, A. R. Gascón, M. Igartua, and J. L. Pedraz,

"Biocompatibility of microcapsules for cell immobilization elaborated with different type of alginates," *Biomaterials*, vol. 23, no. 18, pp. 3825–3831, Sep. 2002.

[106] L. Szabó, S. Gerber-Lemaire, and C. Wandrey, "Strategies to functionalize the anionic biopolymer na-alginate without restricting its polyelectrolyte properties," *Polymers*, vol. 12, no. 4. MDPI AG, p. 919, 01-Apr-2020.

[107] A. D. Augst, H. J. Kong, and D. J. Mooney, "Alginate hydrogels as biomaterials," *Macromol. Biosci.*, vol. 6, no. 8, pp. 623–633, Aug. 2006.

[108] H. J. Kong, M. K. Smith, and D. J. Mooney, "Designing alginate hydrogels to maintain viability of immobilized cells," *Biomaterials*, vol. 24, no. 22, pp. 4023–4029, 2003.

[109] L. W. Chan, H. Y. Lee, and P. W. S. Heng, "Mechanisms of external and internal gelation and their impact on the functions of alginate as a coat and delivery system," *Carbohydr. Polym.*, vol. 63, no. 2, pp. 176–187, Feb. 2006.

[110] S. J. Bidarra, C. C. Barrias, K. B. Fonseca, M. A. Barbosa, R. A. Soares, and P. L. Granja, "Injectable in situ crosslinkable RGD-modified alginate matrix for endothelial cells delivery," *Biomaterials*, vol. 32, no. 31, pp. 7897–7904, Nov. 2011.

[111] J. A. Rowley, G. Madlambayan, and D. J. Mooney, "Alginate hydrogels as synthetic extracellular matrix materials," *Biomaterials*, vol. 20, no. 1, pp. 45–53, Jan. 1999.

[112] M. Farokhi, F. Jonidi Shariatzadeh, A. Solouk, and H. Mirzadeh, "Alginate Based Scaffolds for Cartilage Tissue Engineering: A Review," *Int. J. Polym. Mater. Polym. Biomater.*, vol. 69, no. 4, pp. 230–247, Mar. 2020.

[113] S. I. Jeong, M. D. Krebs, C. A. Bonino, S. A. Khan, and E. Alsberg, "Electrospun alginate nanofibers with controlled cell adhesion for tissue engineering," *Macromol. Biosci.*, vol. 10, no. 8, pp. 934–943, Aug. 2010.

[114] S. J. Bidarra, P. Oliveira, S. Rocha, D. P. Saraiva, C. Oliveira, and C. C. Barrias, "A 3D in vitro model to explore the inter-conversion between epithelial and mesenchymal states during EMT and its reversion," *Sci. Rep.*, vol. 6, no. 1, pp. 1–14, Jun. 2016.

[115] F. R. Maia, K. B. Fonseca, G. Rodrigues, P. L. Granja, and C. C. Barrias, "Matrix-driven formation of mesenchymal stem cell-extracellular matrix microtissues on soft alginate hydrogels," *Acta Biomater.*, vol. 10, no. 7, pp. 3197–3208, 2014.

[116] Y. Chau *et al.*, "Incorporation of a matrix metalloproteinase-sensitive substrate into self-assembling peptides - A model for biofunctional scaffolds," *Biomaterials*, vol. 29, no. 11, pp. 1713–1719, Apr. 2008.

[117] K. B. Fonseca, S. J. Bidarra, M. J. Oliveira, P. L. Granja, and C. C. Barrias, "Molecularly designed alginate hydrogels susceptible to local proteolysis as three-dimensional cellular microenvironments," *Acta Biomater.*, vol. 7, no. 4, pp. 1674–1682, Apr. 2011.

[118] O. Jeon, D. S. Alt, S. M. Ahmed, and E. Alsberg, "The effect of oxidation on the degradation of photocrosslinkable alginate hydrogels," *Biomaterials*, vol. 33, no. 13, pp. 3503–3514, May 2012.

[119] X. Du, "3D Bio-Printing Review," in *IOP Conference Series: Materials Science and Engineering*, 2018, vol. 301, no. 1.

[120] J. W. Higgins *et al.*, "Bioprinted pluripotent stem cell-derived kidney organoids provide opportunities for high content screening," *bioRxiv*, p. 505396, Dec. 2018.

[121] S. V Murphy and A. Atala, "3D bioprinting of tissues and organs," *Nat. Biotechnol.*, vol. 32, no. 8, pp. 773–785, Aug. 2014.

[122] E. Garreta *et al.*, "Tissue engineering by decellularization and 3D bioprinting," *Mater. Today*, vol. 20, no. 4, pp. 166–178, May 2017.

[123] C. Mandrycky, Z. Wang, K. Kim, and D.-H. Kim, "3D bioprinting for engineering complex tissues," *Biotechnol. Adv.*, vol. 34, no. 4, pp. 422–434, Jul. 2016.

[124] W. L. Ng, J. M. Lee, W. Y. Yeong, and M. Win Naing, "Microvalve-based bioprinting - process, bio-inks and applications.," *Biomater. Sci.*, vol. 5, no. 4, pp. 632–647, Mar. 2017.

[125] B. Guillotin *et al.*, "Laser-Assisted Bioprinting for Tissue Engineering," *Biofabrication*, pp. 95–118, Jan. 2013.

[126] J. A. Belgodere, C. T. King, J. B. Bursavich, M. E. Burow, E. C. Martin, and J. P. Jung, "Engineering breast cancer microenvironments and 3D bioprinting," *Frontiers in Bioengineering and Biotechnology*, vol. 6, no. MAY. Frontiers Media S.A., 24-May-2018.

[127] Y. Wang *et al.*, "3D Bioprinting of Breast Cancer Models for Drug Resistance Study," *ACS Biomater. Sci. Eng.*, vol. 4, no. 12, pp. 4401–4411, Dec. 2018.

[128] T. Jiang *et al.*, "Directing the Self-Assembly of Tumour Spheroids by Bioprinting Cellular

Heterogeneous Models within Alginate/Gelatin Hydrogels," *Sci. Rep.*, vol. 7, no. 1, pp. 1–9, Dec. 2017.

[129] E. M. Langer *et al.*, "Modeling Tumor Phenotypes In Vitro with Three-Dimensional Bioprinting," *Cell Rep.*, vol. 26, no. 3, pp. 608-623.e6, Jan. 2019.

[130] P. Barros da Silva, M. Coelho, S. J. Bidarra, S. C. Neves, and C. C. Barrias, "Reshaping in vitro Models of Breast Tissue: Integration of Stromal and Parenchymal Compartments in 3D Printed Hydrogels," *Front. Bioeng. Biotechnol.*, vol. 8, p. 494, Jun. 2020.

[131] C. T. Rueden *et al.*, "ImageJ2: ImageJ for the next generation of scientific image data," *BMC Bioinformatics*, vol. 18, no. 1, p. 529, Nov. 2017.

[132] J. Caldeira *et al.*, "Matrisome Profiling during Intervertebral Disc Development and Ageing," *Sci. Rep.*, vol. 7, no. 1, Dec. 2017.

[133] S. Wang, T. Goecke, C. Meixner, A. Haverich, A. Hilfiker, and W. F. Wolkers, "Freeze-dried heart valve scaffolds," *Tissue Eng. - Part C Methods*, vol. 18, no. 7, pp. 517–525, Jul. 2012.

[134] G. A. Villalona *et al.*, "Cell-Seeding Techniques in Vascular Tissue Engineering."

[135] M. Vitacolonna, D. Belharazem, P. Hohenberger, and E. D. Roessner, "Effect of static seeding methods on the distribution of fibroblasts within human acellular dermis Equal contributors," 2013.

[136] L. Tan, Y. Ren, and R. Kuijer, "A 1-min method for homogenous cell seeding in porous scaffolds," *J. Biomater. Appl.*, vol. 26, no. 7, pp. 877–889, Mar. 2012.

[137] Z. Fereshteh, "Freeze-drying technologies for 3D scaffold engineering," in *Functional 3D Tissue Engineering Scaffolds: Materials, Technologies, and Applications*, Elsevier, 2018, pp. 151–174.

[138] Y. Zhang, C. Wang, W. Jiang, W. Zuo, and G. Han, "Influence of Stage Cooling Method on Pore Architecture of Biomimetic Alginate Scaffolds," *Sci. Rep.*, vol. 7, no. 1, pp. 1–8, Dec. 2017.

[139] J. Insua-Rodríguez and T. Oskarsson, "The extracellular matrix in breast cancer," *Advanced Drug Delivery Reviews*, vol. 97. Elsevier B.V., pp. 41–55, 01-Feb-2016.

[140] M. Kumar Jena, J. Janjanam, and A. R. Craig Canada, "Role of extracellular matrix in breast cancer development: a brief update [version 2; referees: 2 approved, 1 not approved] Referee Status: Invited Referees version 2 , Queen's University," 2018.

[141] K. B. Fonseca *et al.*, "Enzymatic, physicochemical and biological properties of MMP-sensitive alginate hydrogels," *Soft Matter*, vol. 9, no. 12, pp. 3283–3292, Mar. 2013.

[142] M. Muhammad, C. Willems, J. Rodríguez-Fernández, G. Gallego-Ferrer, and T. Groth, "Synthesis and Characterization of Oxidized Polysaccharides for In Situ Forming Hydrogels," *Biomolecules*, vol. 10, no. 8, p. 1185, Aug. 2020.

[143] I. Levental, P. C. Georges, and P. A. Janmey, "Soft biological materials and their impact on cell function," *Soft Matter*, vol. 3, no. 3. Royal Society of Chemistry, pp. 299–306, 14-Feb-2007.

[144] A. Inoue and T. Ojima, "Functional identification of alginate lyase from the brown alga Saccharina japonica," *Sci. Rep.*, vol. 9, no. 1, pp. 1–11, Dec. 2019.

[145] D. A. Moraes *et al.*, "A reduction in CD90 (THY-1) expression results in increased differentiation of mesenchymal stromal cells," *Stem Cell Res. Ther.*, vol. 7, no. 1, p. 97, Jul. 2016.

[146] T. L. Le, A. S. Yap, and J. L. Stow, "Recycling of E-Cadherin: A Potential Mechanism for Regulating Cadherin Dynamics," 1999.

[147] L. Keller, S. Werner, and K. Pantel, "Biology and clinical relevance of EpCAM," *Cell Stress*, vol. 3, no. 6. Shared Science Publishers OG, pp. 165–180, 01-Jun-2019.

[148] Y. Qu *et al.*, "Evaluation of MCF10A as a Reliable Model for Normal Human Mammary Epithelial Cells," 2015.

[149] R. O. Hynes and A. Naba, "Overview of the Matrisome-An Inventory of Extracellular Matrix Constituents and Functions."

[150] M. L. Oyen and R. F. Cook, "A practical guide for analysis of nanoindentation data," *J. Mech. Behav. Biomed. Mater.*, vol. 2, no. 4, pp. 396–407, Aug. 2009.

[151] J. Taylor, "The Use of Poly-L-lysine as an Adhesive in Scanning Electron Microscopy," *Micros. Today*, vol. 16, no. 6, pp. 52–53, Nov. 2008.

Supplementary Information

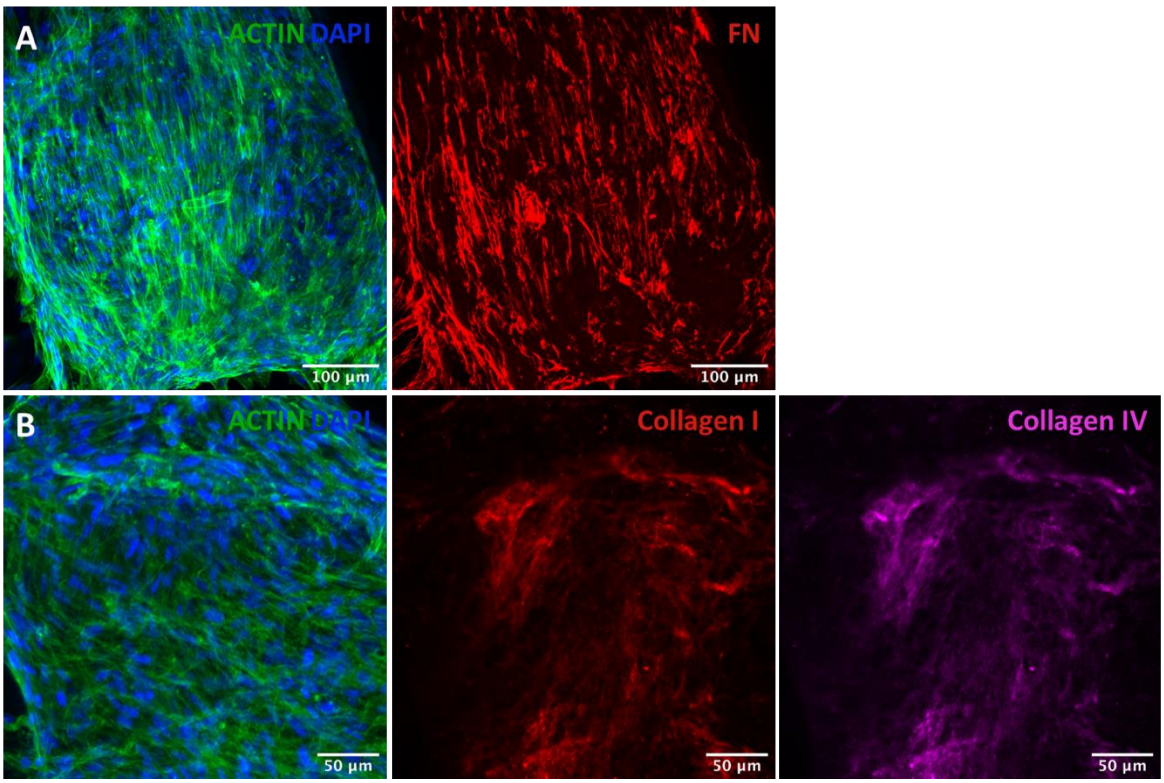

Figure S1. Close-up characterization of hMF-produced ECM. Representative CLSM images of alginate scaffolds seeded with $2.25x10^5$ hMFs. Fibroblasts grown on the scaffolds for 7-10 days were able to spread (F-actin, green) and secrete/accumulate an organized fibrillar ECM, rich in A) fibronectin (red), B) collagen I (red) and collagen IV (magenta), where the latter components were found co-localized. Scale bar: 100 and 50 µm (30x and 50x magnification, respectively).

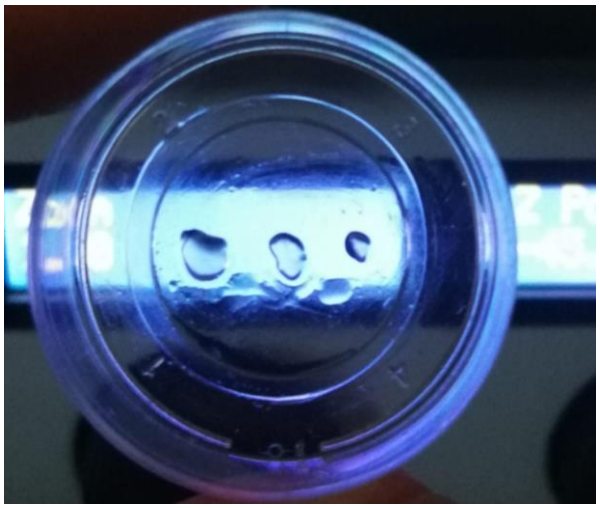

Figure S2. hMF embedded within oxidized PVGLIG-alginate throughout a 1-week culture. Alginate discs progressively contracted and thus, diminished, along day 1 (left), day 3 (middle), and day 7 (right).

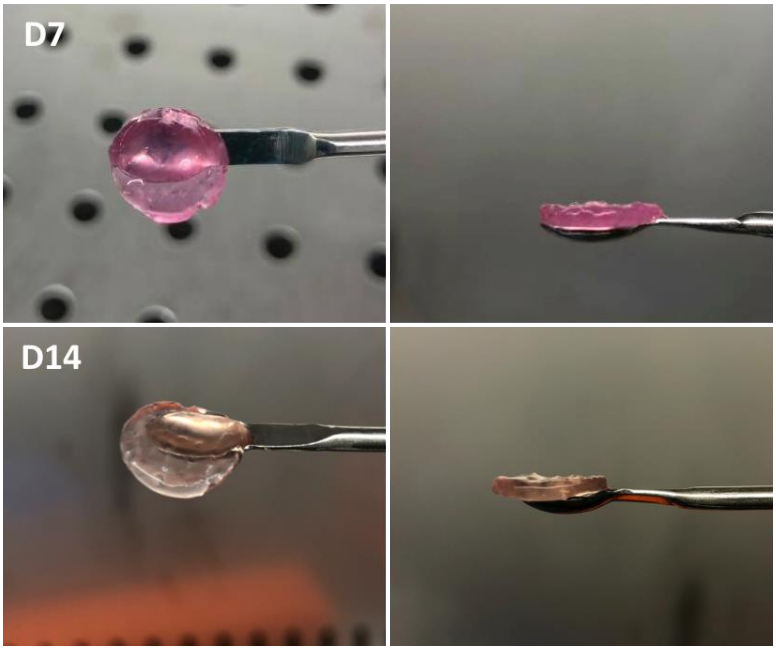

Figure S3. 3D whole mounted co-culture discs throughout 2 weeks of culture. Whole mounted discs were able to maintain their shape and structural integrity along 14 days of culture.

Figure S4. Representative CLSM images of MC10A epithelial cells assembling into multicellular spheroids, upon co-culture with hMF. Fibroblasts were able to migrate towards epithelial spheroids, seemingly undergoing lumenization, and establish heterotypic juxtracrine interactions. Scale bar: 20 µm

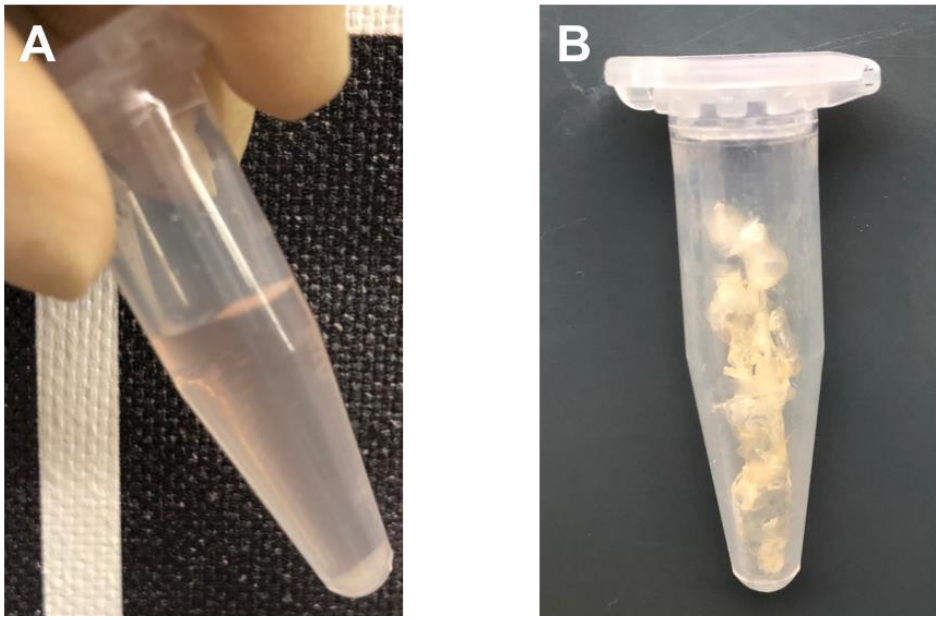

Figure S5. Extracellular solution supernatant obtained after cell extraction A), and after lyophilization

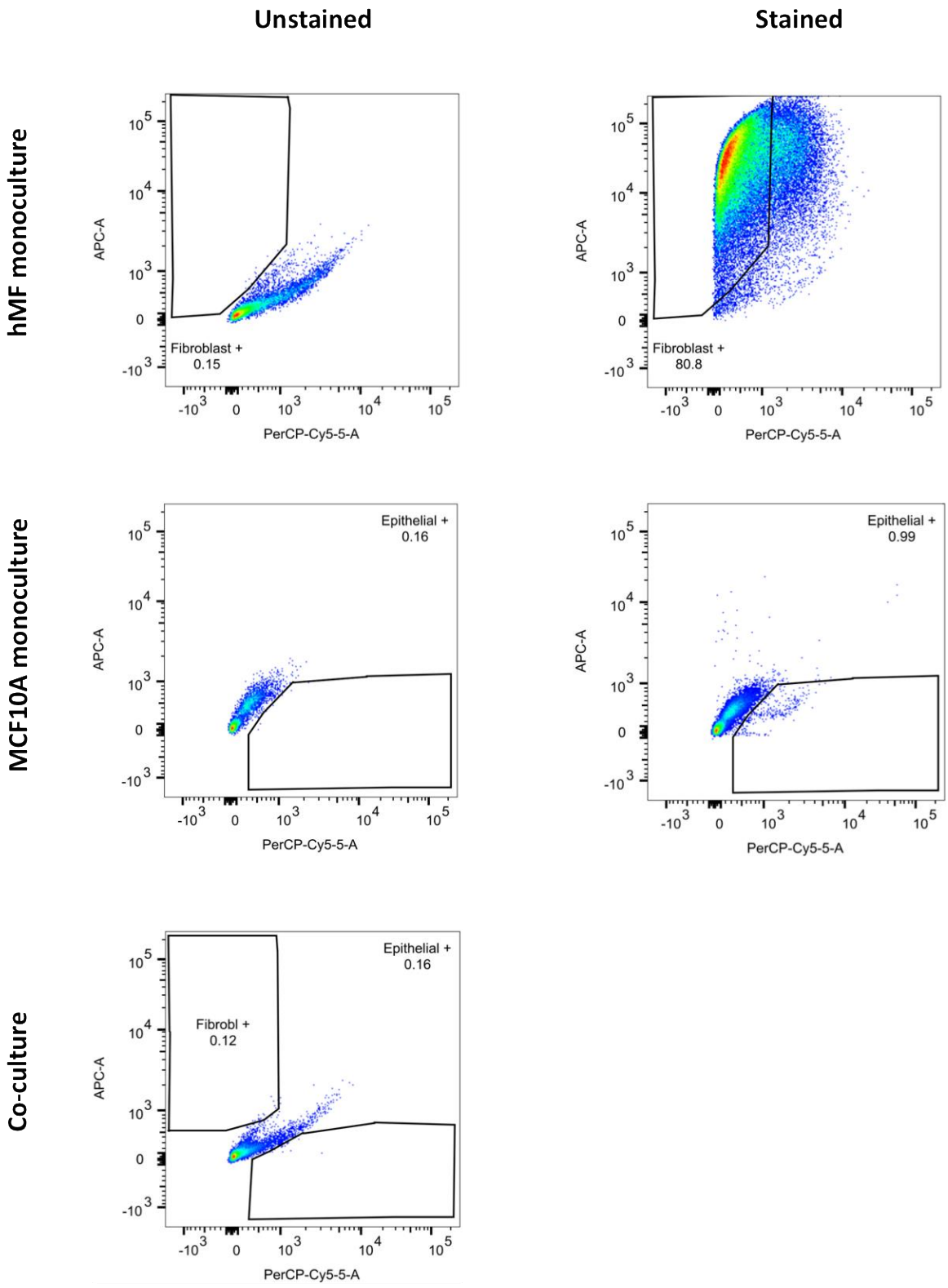

Figure S6. FACS gating strategy of hMFs (top plots), MCF10A (bottom plots) monocultures, and unstained co-cultures (bottom).